# Phosphorus cycling in anoxic sediments

**Dissertation**

Zur Erlangung des Doktorgrades
der Mathematisch-Naturwissenschaftlichen Fakultät
der Christian-Albrechts-Universität zu Kiel

vorgelegt von
Anna Noffke

Kiel, 2014

Referent: Prof. Dr. Klaus Wallmann
Koreferentin: Prof. Dr. Tina Treude

Tag der mündlichen Prüfung: 21.11.2014
Zum Druck genehmigt: 21.11.2014

gez. Prof. Dr. Wolfgang J. Duschl, Dekan

Hiermit erkläre ich, dass ich die vorliegende Doktorarbeit selbständig und ohne Zuhilfenahme unerlaubter Hilfsmittel erstellt habe. Weder diese noch eine ähnliche Arbeit wurde an einer anderen Abteilung oder Hochschule im Rahmen eines Prüfungsverfahrens vorgelegt, veröffentlicht oder zur Veröffentlichung vorgelegt. Ferner versichere ich, dass die Arbeit unter Einhaltung der Regeln guter wissenschaftlicher Praxis der Deutschen Forschungsgemeinschaft entstanden ist.

16. Januar 2014

Anna Noffke

# Abstract

Worldwide oxygen minimum zones (OMZs) as well as coastal oxygen-deficient regions have been shown to be expanding during recent decades. When such oxygen minima impinge on the sea floor, the retention capacity of sediments for phosphate ($TPO_4$), ferrous iron ($Fe^{2+}$), as well as ammonium ($NH_4^+$) is strongly reduced, resulting in high sea-bed release rates of these key nutrients into the bottom water. Despite the significance of the benthos exerting a major positive feedback on surface-water primary productivity and in turn maintenance of oxygen ($O_2$) deficiency, the nutrient release in OMZ and coastal $O_2$-deficient regions has hardly been quantified. The aim of this study was to investigate the benthic nutrient turnover in two different highly $O_2$-deficient systems: i. the intense OMZ off Peru and ii. the landlocked Gotland Basin, Baltic Sea, which suffers from anthropogenically induced eutrophication. The focus was on the phosphorus (P) cycle but associated cycles of iron (Fe) and nitrogen (N) were also included.

Off the coast of Peru, benthic fluxes of $TPO_4$ and $Fe^{2+}$ were quantified in situ using benthic landers and were calculated from pore-water profiles across a latitudinal depth transect at 11°S. This transect extended from 80 m to 1000 m water depth and covered anoxic to oxic bottom-water conditions. The working area was divided into three different zones: the shelf that is subjected to periodically fluctuating bottom-water $O_2$ conditions, the core of the OMZ where anoxia can be assumed to be permanent, and the depth range below 500 m where $O_2$ levels increased again. $TPO_4$ fluxes were high (maximum 292 mmol $m^{-2}$ $yr^{-1}$) throughout the shelf and in the core of the OMZ. In contrast, $Fe^{2+}$ fluxes were high on the shallow shelf (maximum 316 mmol $m^{-2}$ $yr^{-1}$) but moderately low (15.4 mmol $m^{-2}$ $yr^{-1}$) in water depths between 250 m and 600 m due to the continuous reduction of Fe oxides and Fe hydroxides (henceforth referred to as Fe oxyhydroxides). Below 600 m, where $O_2$ concentrations increased, $Fe^{2+}$ fluxes became negligible due to the precipitation of $Fe^{2+}$ in the oxic sediment surface. Ratios between organic carbon degradation and $TPO_4$ flux indicated an excess release of P over carbon (C) when compared to Redfield stoichiometry. This was most likely caused by preferential P release during organic matter degradation, dissolution of fish debris, and/or P release from sulfide-oxidizing microbial mat communities. Fe oxyhydroxides were relevant as a P source only on the shallow shelf. The benthic fluxes are among the highest reported

from similar $O_2$-deficient continental margin systems, and highlight the efficiency of OMZ sediments returning $TPO_4$ and $Fe^{2+}$ to the bottom water. The shelf region is particularly important in this regard since $O_2$ fluctuations likely trigger a complex biogeochemical reaction network of P, Fe and sulfur turnover resulting in transient, high $TPO_4$ and $Fe^{2+}$ release under anoxia.

Sources for P release were further constrained by combining P speciation data, based on sequential extraction of sediment samples, with a mass balance and benthic modeling. P speciation revealed that authigenic calcium phosphate (Ca-P; including carbonate fluorapatite, biogenic apatite from fish remains, and calcium carbonate-bound P), was the major fraction along the transect. It accounted for 35 to 47% of the depth-averaged total extracted P on the shelf and upper slope, but for > 70% below 300 m water depth. Further extraction of fish-P showed that below 259 m water depth this fraction dominated the authigenic Ca-P pool by 60 to 69%. Organic P was present in considerable amounts (18 to 37%) only at the shelf and the upper slope, whereas detrital P and P bound to Fe oxyhydroxides was generally of minor importance at all sites. Organic matter in surface sediments was highly depleted in P relative to Redfield stoichiometry with C:P ratios of up to 516. The benthic model found preferential P mineralization in the water column or, alternatively, preferential P release during organic matter degradation in the sediment surface as possible pathways explaining such high C:P ratios. Nevertheless, both model and mass balance calculations revealed that irrespective of which pathway prevails, organic P was only of minor importance for the benthic P budget of Peruvian OMZ sediments. According to the solid phase speciation, authigenic Ca-P, with a high contribution of fish debris, is a likely candidate for the missing source of P required to close the P budget. These sediments were identified as weak sinks for P, as more than 80% of the imported P was recycled back into the water column.

In the Gotland Basin, $TPO_4$ and DIN fluxes were quantified in situ across an oxic to anoxic depth-transect using benthic landers. A CTD-water sampling rosette was deployed to record the nutrient and $O_2$ distribution in the water column and thereby investigate the benthic-pelagic coupling because of its significance for the euthrophication state of the Baltic Proper. The study area was divided into three different zones: the oxic zone at 60 m to < 80 m water depth, the hypoxic transition zone between > 80 m and 120 m, and the deep anoxic and sulfidic basin at > 120 m. The hypoxic transition zone was

characterized by fluctuating $O_2$ levels as well as the occurrence of extended mats of sulfur bacteria. Beside the deep anoxic basin, the hypoxic transition zone was revealed as a major release site for $TPO_4$ and $NH_4^+$ with rates of up to 0.2 mmol $m^{-2}$ $d^{-1}$ and 1 mmol $m^{-2}$ $d^{-1}$, respectively. There are clear indications that the bacterial mats converted $NO_3$-/$NO_2^-$ into $NH_4^+$ during dissimilatory nitrate reduction to ammonium (DNRA), thereby retaining reactive N in the ecosystem. The transient release and uptake of $TPO_4$ during oscillating anoxic and oxic conditions by these bacteria, however, can only be speculated as the entire $TPO_4$ release from the sediment could be potentially covered by preferential P release during organic matter degradation. Extrapolation of benthic fluxes to the Baltic Proper resulted in internal $TPO_4$ and DIN loads of 109 kt $yr^{-1}$ and 295 kt $yr^{-1}$, respectively, which is significantly higher than external P and DIN loads. This up-scaling of fluxes revealed the importance of the hypoxic transition zone for the internal nutrient loading, which only covered 51% of the total considered area, but released as much as 70% of the total $TPO_4$ load. Likewise, 75% of the internal $NH_4^+$ load (200 kt $yr^{-1}$) was released from this particular environment; however, this $NH_4^+$ did not reach the surface mixed layer. This resulted in the supply of water with a low N:P ratio to the euphotic zone. In summertime, such low N:P ratios favor the development of $N_2$-fixing cyanobacterial blooms which, by different feedback processes, counteract the recovery of the Baltic Proper from eutrophication.

# Kurzfassung

Es wurde gezeigt, dass sich in den letzten Jahrzehnten weltweit Sauerstoffminimumzonen (SMZ) sowie küstennahe sauerstoffverarmte Bereiche ausdehnen. Treffen solche Sauerstoffminima auf den Meeresboden, ist die Rückhaltekapazität der Sedimente für Phosphat ($TPO_4$), Eisen ($Fe^{2+}$) und Ammonium ($NH_4^+$) stark herabgesetzt, was in hohen Freisetzungsraten dieser Schlüsselnährstoffe vom Meeresboden ins Bodenwasser resultiert. Trotz dieser Bedeutung des Benthos, der eine grundlegende positive Rückkopplung auf die Oberflächenprimärproduktivität und damit wiederum auf die Aufrechterhaltung des Sauerstoffmangels ausübt, ist die Nährstofffreisetzung in SMZs und küstennahen sauerstoffverarmten Regionen kaum quantifiziert worden. Das Ziel dieser Studie war, den Nährstoffumsatz in zwei verschiedenen, stark sauerstoffverarmten Systemen zu untersuchen: i) die ausgeprägte SMZ vor Peru und ii) das landumschlossene Gotlandbecken (Ostsee), das von anthropogen verursachter Eutrophierung betroffen ist. Der Schwerpunkt lag auf dem Phosphor (P)-Kreislauf, aber angegliederte Eisen (Fe)- und Stickstoff (N)-Kreisläufe wurden ebenfalls einbezogen.

Vor Peru wurden benthische Flüsse von $TPO_4$ und $Fe^{2+}$ in situ mittels benthischer Lander und anhand von Porenwasserprofilen über einen zonalen Tiefenschnitt bei 11°S quantifiziert. Dieser Tiefenschnitt erstreckte sich über Wassertiefen von 80 m bis 1000 m und deckte anoxische bis oxische Bodenwasserbedingungen ab. Das Arbeitsgebiet wurde in drei verschiedene Zonen unterteilt: der Schelf, der periodisch fluktuierenden Sauerstoffbedingungen ausgesetzt ist, der Kern der SMZ, wo beständige Anoxie angenommen werden kann, und der Tiefenbereich unterhalb von 500 m, wo der Sauerstoffgehalt wieder anstieg. Die $TPO_4$ Flüsse waren über den ganzen Schelf und den Kern der OMZ mit einem Maximum von 292 mmol $m^{-2}$ $yr^{-1}$ hoch. Dagegen waren die $Fe^{2+}$ Flüsse auf dem flachen Schelf (Maximum 316 mmol $m^{-2}$ $yr^{-1}$) hoch, jedoch in Wassertiefen zwischen 250 m und 600 m, verursacht durch die fortwährende Reduktion von Fe-Oxyhydroxiden, vergleichsweise gering (15.4 mmol $m^{-2}$ $yr^{-1}$). Unterhalb von 600 m wurden mit zunehmender Sauerstoffkonzentration die $Fe^{2+}$ Flüsse aufgrund der Fällung von $Fe^{2+}$ in der oxischen Sedimentoberfläche vernachlässigbar. Im Vergleich zur Redfield Stöchiometrie zeigten Verhältnisse zwischen Abbau von organischem Material und dem Phosphatfluss überschüssige Freisetzung von P gegenüber Kohlenstoff (C).

Höchstwahrscheinlich wurde dies durch die preferentielle Freisetzung von P beim Abbau von organischem Material, die Lösung von Fischüberresten und/oder P Freisetzung von sulfid-oxidierenden mikrobiellen Matten-Gemeinschaften verursacht. Fe-Oxyhydroxide waren als P Quelle nur auf dem flachen Schelf von Bedeutung. Die benthischen Flüsse sind unter den höchsten für vergleichbare sauerstoffverarmte Kontinentalrandsysteme und heben die Effizienz von SMZ Sedimenten für die Rückführung von $TPO_4$ und $Fe^{2+}$ ins Bodenwasser hervor. Die Schelfregion ist in dieser Hinsicht besonders bedeutend, da die $O_2$ Fluktuationen vermutlich ein komplexes biogeochemisches Reaktionsnetzwerk von P, Fe und Schwefelumsatz steuern, das unter anoxischen Bedingungen schubweise in hoher $TPO_4$ und $Fe^{2+}$ Freisetzung resultiert.

Die Quellen der Phosphatfreisetzung wurden weiter eingegrenzt, indem P Speziierungsdaten, basierend auf sequentieller Extraktion von Sedimentproben, mit einer Massenbilanz und benthischer Modellierung kombiniert wurden. Die P Speziierung zeigte, dass authigenes Ca-P (welches Carbonat-Fluorapatit, biogenen Apatit aus Fischüberresten und Calciumcarbonat-gebundenen P beinhaltet) die Hauptfraktion entlang des Tiefenschnitts war. Es machte 35 bis 47% des tiefengemittelten gesamtextrahierten P auf dem Schelf und oberen Hang, aber > 70% unterhalb von 300 m Wassertiefe aus. Weitergehende Extraktion von Fisch-P zeigte, dass diese Fraktion den authigenen Ca-P Pool mit 60 bis 69% dominierte. Organischer P war in erheblichen Mengen mit 18 bis 37% nur auf dem Schelf und oberen Hang vorhanden, wogegen detritischer P und an Fe-Oxyhydroxide gebundener P im Allgemeinen von untergeordneter Bedeutung an allen Stationen war. Das organische Material in Oberflächensedimenten war relativ zur Redfield Stöchiometrie mit C:P Verhältnissen bis zu 516 stark an P abgereichert. Das benthische Modell hat die preferentielle P Mineralisierung in der Wassersäule oder, alternativ, die preferentielle P Freisetzung während des Abbaus organischen Materials in der Sedimentoberfläche als mögliche Pfade, solch hohe C:P Verhätlnisse zu erklären, erkennen lassen. Dennoch zeigten sowohl Modell- als auch Massenbilanzrechnungen, dass, unabhängig welcher Pfad voherrscht, organischer P nur von untergeordneter Bedeutung für das benthische P-Budget Peruanischer OMZ Sedimente war. Gemäß der P Speziierung ist authigenes Ca-P, mit einem hohen Beitrag von Fischüberresten, ein wahrscheinlicher Kandidat für die fehlende P-Quelle um das P-Budget zu schließen. Diese Sedimente wurden als schwache Senken

für P identifiziert, da mehr als 80% des eingetragenen P ins Bodenwasser zurückgeführt wurden.

Im Gotlandbecken wurden $TPO_4$ und DIN ($NH_4^+$; Nitrat, $NO_3^-$; Nitrit, $NO_2^-$) Flüsse in situ mit benthischen Landern entlang eines oxisch-anoxischen Tiefenschnitts quantifiziert. Ein CTD-Kranzwasserschöpfer wurde eingesetzt, um die Nährstoff- und $O_2$-Verteilung in der Wassersäule zu erfassen und so die benthisch-pelagische Kopplung, aufgrund ihrer Bedeutung für den Eutrophierungstatus der zentralen Ostsee, zu untersuchen. Das Untersuchungsgebiet wurde in drei verschiedene Bereiche unterteilt: der oxische Bereich in 60 m bis < 80 m Wassertiefe, der hypoxische Übergangbereich zwischen > 80 m und 120 m, und das tiefe anoxische und sulfidische Becken in > 120 m. Der hypoxische Übergangsbereich war durch fluktuierende Sauerstoffgehalte sowie das Auftreten von ausgedehnten Matten von Schwefelbakterien charakterisiert. Neben dem tiefen anoxischen Becken wurde der hypoxische Übergangsbereich als eine bedeutende Zone für die Freisetzung von $TPO_4$ und $NH_4^+$, mit Raten von bis zu 0.2 mmol $m^{-2}$ $d^{-1}$ und 1 mmol $m^{-2}$ $d^{-1}$, aufgezeigt. Es gibt deutliche Hinweise, dass die Bakterienmatten während der dissimilatorischen Nitratreduktion zu Ammonium (DNRA) $NO_3^-/NO_2^-$ in $NH_4^+$ überführten, und so reaktiven Stickstoff im Ökosystem zurückhielten. Die alternierende Freisetzung und Aufnahme von $TPO_4$ in Folge oszillierender anoxischer und oxischer Bedingungen durch diese Bakterien kann jedoch nur spekuliert werden, da die gesamte Freisetzung von $TPO_4$ aus dem Sediment potentiell durch preferentielle P Freisetzung während des Abbaus von organischem Material gedeckt werden könnte. Die Extrapolation der benthischen Flüsse auf die zentrale Ostsee ergab interne $TPO_4$ und DIN Einträge von 109 kt $yr^{-1}$ und 295 kt $yr^{-1}$, was signifikant höher ist als externe P und DIN Einträge. Die Hochskalierung der Flüsse zeigte die Bedeutung der hypoxischen Übergangszone für den internen Nährstoffeintrag, die nur 51% der betrachteten Gesamtfläche ausmachte, aber 70% des gesamten $TPO_4$ freisetzte. Gleichermaßen wurden 75% (200 kt $yr^{-1}$) des gesamten $NH_4^+$ aus dieser besonderen Umgebung freigesetzt, gelangte jedoch nicht bis in die durchmischte Deckschicht. Dies resultierte in der Zufuhr von Wasser mit einem niedrigen N:P Verhältnis in die euphotische Zone. Im Sommer fördern solch niedrige N:P Verhältnisse die Entwicklung von $N_2$-fixierenden Cyanobacterienblüten, die über verschiedene Rückkopplungsprozesse der Erholung der zentralen Ostsee von der Eutrophierung entgegen wirken.

# Contents

# 1 General introduction

## 1.1 Benthic feedback on nutrient inventories in oxygen-deficient environments

Climate change projections predict a 4 to 7% decline of the dissolved oxygen ($O_2$) in the ocean until the end of this century (Joos et al. 2003). This is partly related to the warming of the ocean and associated lower solubility of $O_2$, but particularly to enhanced stratification and a decrease in ventilation of the ocean interior (Bopp et al. 2002; Keeling & Garcia 2002). This has severe implications for the major oxygen minimum zones (OMZs) which constitute a significant proportion of 8% of the world ocean area (Paulmier and Ruiz-Pino 2009). Although naturally formed by the interaction of upwelling fueling primary production and $O_2$ consumption during the export of organic matter, in combination with sluggish ventilation, OMZs have been shown to be expanding during recent decades (Stramma et al. 2009). Alterations of the redox state of the ocean and the sea floor, strongly affect bioavailability of marine nutrients (phosphorus, P; nitrogen, N; iron, Fe) and consequently oceanic primary productivity (Falkowski 1997; Falkowski et al. 1998, and references therein). Under $O_2$-deficient conditions the retention capacity of sediments for phosphate ($TPO_4$), ferrous iron ($Fe^{2+}$) as well as ammonium ($NH_4^+$) is strongly reduced, resulting in high sea-bed release rates of these key nutrients into the bottom water. When reaching the euphotic zone these solutes fuel surface-water primary productivity, which during its decay contributes to maintain or even increase the $O_2$ deficit, which in turn further promotes benthic nutrient release. Despite the significance of the benthos exerting a major positive feedback on surface-water primary productivity, still the nutrient release in OMZs has been hardly quantified.

In contrast to the above described OMZs, enclosed basins such as the Baltic Sea suffer from hypoxia that is caused from anthropogenically induced eutrophication (HELCOM 2009*a*, Conley et al. 2009). Although a reduction of the external nutrient input via the catchment area has been achieved by most of the Baltic Sea states, there has been no significant mitigation of eutrophication (HELCOM 2009*b*). It is assumed that in the open Baltic Sea nutrient sources are regulated by internal feedback mechanisms preventing recovery from eutrophication (Vahtera et al. 2007). This internal nutrient cycling is

sustained by N-limited production and sedimentation of phytoplankton during the spring bloom. Subsequent decay of this organic material leads to $O_2$ deficiency, resulting in the mobilization of nutrients from the sea floor. High fluxes of $TPO_4$ lower the N:P ratio, giving competitive advantage to P-limited diazotrophic cyanobacteria in summer. These $N_2$-fixing organisms restore water-column N levels that in the following spring support the N-limited phytoplankton. Via this vicious cycle a high organic load in combination with seasonally shifting nutrient levels is maintained, leading to hypoxia. Quantification of the benthic nutrient release is critical to understand this internal nutrient cycling. However, to date quantitative measurements on benthic nutrient release in the open Baltic Sea are scarce.

In this thesis, particularly the benthic P turnover has been addressed, hence in the following a more detailed description of the marine P cycle is provided, including the associated Fe and N cycles.

## 1.2 Phosphorus — an important element

Phosphorus is an essential element required for life on Earth. It occurs in many biomolecules and plays an important role in cell physiology and biochemistry. In natural systems P does not exist in elemental form, since it is highly reactive and readily combines with $O_2$ when exposed to air. When P is fully oxidized, the product is phosphate ($PO_4^{3-}$), in which P has the oxidation state +5.

At near neutral pH, as found in most natural waters and soils, free phosphate occurs as a mixture of the mono- and diprotonated species of orthophosphoric acid ($HPO_4^{2-}$ and $H_2PO_4^-$). As dissolved phosphate P is directly available for biological uptake and occurs in cells in both inorganic and organic forms in a multitude of structural and functional components. Phospholipids are the main component of cell wall membranes, the double helix strands of the genetic molecules deoxyribonucleic acid (DNA) and ribonucleic acid (RNA) are built by phosphodiester bridges, and, forming adenine nucleotides (adenosine triphosphate, ATP; adenosine diphosphate, ADP; adenosine monophosphate, AMP), P plays an important role in cellular energetics. In form of the mineral component hydroxylapatite, $Ca_{10}(PO_4)_6(OH)_2$, and its carbonate-fluoride substitutes P is incorporated in vertebrates' bones and teeth, respectively.

Although the majority of P compounds found in nature contain fully oxidized P, reduced

P compounds are also widely distributed in the environment, which may be either of natural origin or introduced by anthropogenic activities (fertilizers, industries) (Hanrahan et al. 2005; Ternan et al. 1998). This includes both reduced organic P compounds such as phosphonates (+3) and phosphinates (+1), and inorganic P compounds such as phosphite (+3), hypophosphite (+1), and phosphine (-3). A number of bacteria are specialized to use reduced P as alternative P source (Hanrahan et al. 2005; White and Metcalf 2007). Besides its utilization as a substrate for growth, first evidence for the use of reduced P in energy metabolism has been provided with the isolation of *Desulfotignum phosphitoxidans* (Schink and Friedrich 2000), an anaerobic bacterium that gains energy for growth by coupling the oxidation of phosphite to $PO_4^{3-}$ to sulfate reduction. The reverse to the oxidative pathway, the microbial respiratory reduction of $PO_4^{3-}$, is, however, a matter of debate, since it is energetically not favorable (e.g. Roels and Verstraete 2001).

P is a limiting nutrient for primary production and thus strongly influences other biogeochemical cycles, in particular those of carbon (C) and N. In marine ecosystems, P is often considered the "ultimate limiting nutrient" on geological time scales (Tyrell 1999; Bjerrum and Canfield 2002). Whereas phytoplankton N demand can be satisfied instantaneously from a vast pool of atmospheric N by $N_2$-fixing cyanobacteria (McCarthy and Carpenter 1983; Tyrell et al. 1999), P forms no stable gaseous phases, and its supply in bioavailable forms depends solely on external input following the slow process of chemical weathering (Filippelli 2002). Evidence has been demonstrated that P is also the limiting nutrient in many regions of the modern ocean, such as the eastern Mediterranean Sea (Krom et al. 1991; 2004), as well as the northern Atlantic and Pacific Oceans (Sañudo-Wilhelmy et al. 2001; Karl et al. 2001; Watkins-Brandt et al. 2011).

The characteristic of P not to form stable gaseous forms renders the marine P cycle unique amongst the major nutrient cycles, and P geochemistry is somewhat simplified by the lack of the atmospheric reservoir. Nevertheless, the marine P cycle still faces the complexity of significant P transformations occurring in both the water column and sediments, mediated not only by biological (metabolic) but also by abiotic (dissolution, precipitation) processes.

## 1.3 Marine phosphorus cycle

*1.3.1 Transport of phosphorus to the oceans*

The primary natural source of P to earth ecosystems is the weathering of continental material. The main P-bearing rock mineral is apatite, which contains over 95% of all naturally occurring P (Paytan and McLaughlin 2007). Whereas physical rock destruction liberates P mainly in inert forms, the chemical weathering of apatite releases dissolved, bioavailable phosphate into soil pore spaces (Filippelli 2002). From soil solution major amounts of phosphate are rapidly transformed to the solid phase into pools of different leachability and hence varying availability to plants (Filippelli 2002; Filippelli et al. 2008). P is mobilized and exported from soil systems by surface and subsurface runoff and erosion, and is delivered to the oceans in particulate and dissolved forms mainly with rivers. On the local scale contributions from dust supplied with aerosols or volcanogenic sources may become important (Benitez-Nelson 2000).

More than 95% of the riverine P flux is in particulate inorganic and organic forms (Compton 2000) that are mostly unavailable to biota, and a large part of it is rapidly deposited in near-shore areas. A maximum of ~ 30% of the total riverine P flux is considered to be potentially bioavailable (Compton et al. 2000). Besides the dissolved P fractions this includes inorganic P phases, such as P adsorbed to clay surfaces or bound to manganese and iron oxides and hydroxides (hereafter referred to as Mn and Fe oxyhydroxides), and P in particulate organic matter. However, a significant fraction of this potentially reactive P is trapped in estuaries or buried in continental margin sediments and thereby removed from the water column (Compton et al. 2000).

Riverine P input to the oceans has strongly increased due to anthropogenic influence. Nutrient discharge from agriculture, sewage and waste water, as well as that associated with the enhanced solubilization of P coupled to soil loss, has about doubled the estimated natural dissolved P fluxes to the oceans (Compton et al. 2000). Enhanced external nutrient loading can lead to eutrophication of coastal regions and associated hypoxia (Rabalais et al. 2010). A prominent case for such anthropogenic eutrophication is the Baltic Sea, as reflected by the occurrence of toxic cyanobacterial blooms and widespread hypoxic and anoxic bottom-water conditions (Conley et al. 2009). The eastern Gotland Basin, one of the Baltic Sea sub-regions severely affected by these adverse conditions is investigated for its P and N cycling in chapter 4 of this thesis.

*1.3.2 Phosphorus cycling in the water column*

Once entering the surface waters of the oceans, dissolved P is assimilated together with C and N by phytoplankton during photosynthesis and converted into organic matter (Fig. 1.1). P is taken up by phytoplankton mainly as orthophosphate (hereafter referred to as $TPO_4$), the most readily utilizable form of P in nature (Björkman and Karl 1994; Cembella et al. 1984). Nevertheless, under strong P depletion certain phytoplankton species can exploit dissolved organic matter to meet their P demand, since they possess specific enzyme systems capable to cleave organically bound P compounds through hydrolysis (Cembella et al. 1984; Karl and Björkmann 2002; Dhyrman and Ruttenberg 2006).

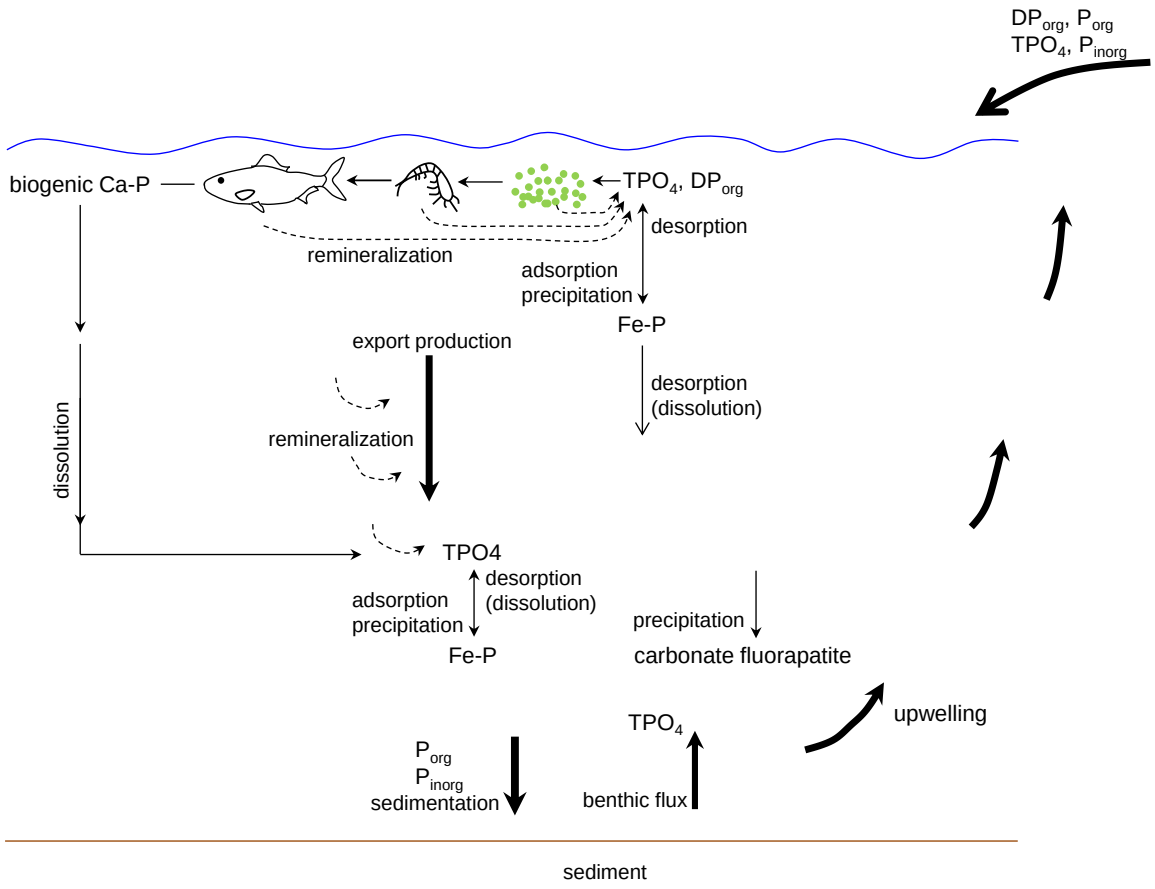


**Fig. 1.1:** Water-column marine P cycling. $P_{org}$ and $DP_{org}$: particulate and dissolved organic P; $P_{inorg}$ and $TPO_4$: particulate inorganic P and dissolved orthophosphate; Fe-P: Fe oxyhydroxide-bound P; biogenic Ca-P: biogenic apatite (hydroxylapatite). Land-derived flux of $P_{inorg}$ includes P in apatite, Fe oxyhydroxide-bound P and P adsorbed to particle surfaces. Sedimentation flux of $P_{inorg}$ additionally includes water column-derived Ca-P as well as biogenic Ca-P. Dissolution of Fe-P only occurs in anoxic water bodies.

A large proportion of productivity undergoes immediate biological oxidation within the euphotic zone. A fraction of the organic matter is exported to deeper water layers, mostly by sinking particles (dead organisms, fecal pellets). This process is termed the ocean's "biological pump". By locking carbon dioxide from the atmosphere into the ocean interior, the biological pump is a key factor controlling climate (Falkowski et al. 1998; Sabine et al. 2004). Yet, much of the downward particle flux is already remineralized within the "twilight" zone, the layer below the euphotic zone extending down to about 1000 m water depth (Buesseler et al. 2007), whereby organically bound nutrients are converted back into their inorganic forms and released into the water column. These recycled nutrients may be returned to the surface via mixing and upwelling and are thus made available for new primary production. Besides being incorporated into organic matter, P may also be transformed inorganically to the particulate phase during its transport through the water column. Such reactions include the precipitation of carbonate fluorapatite subsequent to organic P mineralization (Faul et al. 2005) or the scavenging of P by particulate Mn and Fe oxyhydroxides (Föllmi 1996; Delaney 1998). In reverse, the presence of anoxic conditions in the water column enables the reduction of such metal oxides (Landing and Bruland 1987; Lewis and Landing 1991; Lewis and Luther 2000; Moffet 2007) and concomitant release of P.

A certain fraction of the C fixed by primary producers escapes water-column degradation and reaches the sea floor. It is estimated that for coastal environments 25 to 50% of the fixed C sinks to the sediment surface (Wollast 1991). In contrast, in deep sea environments of > 1000 m water depth this fraction amounts to only about 1% (Jahnke et al. 1996). After deposition, organic matter becomes remineralized and a certain fraction is buried. In many settings degradation of organic matter is highly efficient, so that on average for marine sediments only ~ 10% of the organic matter reaching the sea floor is ultimately preserved (Hedges and Keil 1995). When organic matter is remineralized, dissolved $TPO_4$ becomes available for biological uptake (formation of biomass and energy storage), may be transferred to the solid phase (adsorption or precipitation), or be released to the water column (section 1.3.3).

Besides P from marine export production, further P will be delivered to the sediments with mineral phases of both terrestrial and oceanic origin (Mn and Fe oxyhydroxides, carbonate fluorapatites). Moreover, fish debris (scales, bones, teeth consisting of

hydroxylapatite) is a major marine P source to the sediments in highly productive upwelling regions, such as the Peruvian and Arabian Sea OMZs (Suess et al. 1981; Schenau and De Lange 2001). Like the organic P, part of the particulate inorganic P being deposited will be transformed into dissolved $TPO_4$ during early diagenesis (section 1.3.3.1) that eventually may be provided to the bottom water and thus escape burial. As will be outlined below, $TPO_4$ release is especially elevated in highly productive and/or environments with $O_2$-deficient bottom waters. The quantification of this reflux as well as the investigation of the underlying processes is the focus of this study. These were carried out in two highly $O_2$-deficient systems, with a major emphasis on the Peruvian upwelling region and the eastern Gotland Basin of the Baltic Sea as an additional example.

### *1.3.3 Phosphorus cycling in the sediment*

#### 1.3.3.1 Pathways of phosphorus release

This study focuses on the cycling of P in sediments underlying strong redox gradients. Therefore, in the following section a detailed description of P geochemistry under different redox conditions will be provided. Since in the marine environment the P and Fe cycles are strongly linked, important aspects of the Fe cycle are described which are necessary for the understanding of P dynamics. In the Gotland Basin, besides P cycling benthic N turnover has been investigated. It has been previously shown that benthic and pelagic N and P turnover strongly affect the water-column N:P ratio and in turn primary productivity, and thus play a major role in the eutrophication state of the Baltic Sea (Vahtera et al. 2007). The benthic N cycle will be briefly introduced in section 1.5.

Organic matter is commonly regarded as the major source of P to the sea floor (e.g. Delaney 1998). Hence, in many settings, its ongoing degradation in the surface sediments after deposition is the most important process that releases $TPO_4$ into the pore water and ultimately back into the water column. During microbial metabolism, organic matter sequentially undergoes reactions with different electron acceptors used in the order of decreasing free energy yield. $O_2$, whose reaction with organic matter is energetically most favorable, is used first, followed by nitrate, Mn oxyhydroxides, Fe oxyhydroxides, and sulfate (Froelich et al. 1979). This sequence of electron acceptors gives rise to a characteristic vertical zonation of the sediment, constituting oxic, suboxic (nitrogenous, manganous and ferruginous) and anoxic (sulfidic) layers. However, this sharp vertical

distribution of microbial respiration processes is only hypothetical, since there is often an overlap of the boundaries of aerobic and anaerobic reactions. For example, sulfate reduction can occur in oxic zones of the sediment, which has been explained by the existence of anoxic micro-niches within particles (Jørgensen 1977; Jahnke 1985). Vice versa, oxidized zones related to the burrowing activity of organisms may extend into anaerobic zones, allowing aerobic respiration to occur (Aller 1982). Furthermore, different Mn and Fe oxyhydroxides show different reactivities (Roden 1996, 2006; van der Zee and van Raaphorst 2004), and therefore there may be some change in the order of microbial Mn and Fe reduction.

By the release of reduced components during the individual mineralization reactions biogeochemical gradients are established, resulting in their upward directed diffusive transport and their potential release into the bottom water. However, oxidation of these solutes may occur with any of the electron acceptors in the crossed reaction zones. An internal sediment cycle may establish from the alternating reduction and reoxidation processes that allows an electron acceptor to be repeatedly used, thus maintaining elevated rates of reduction in the sediment. For example, according to Canfield et al. (1993) one Fe atom may be reduced and reoxidized up to 300 times before being ultimately buried.

The importance of the different mineralization pathways depends on the environmental conditions, such as organic matter rain rates, redox conditions of the bottom water or the local availability of Fe and Mn oxyhydroxides. Thus, in pelagic sediments where the supply of organic matter is generally smaller than that in the ocean margins, $O_2$ is by far the most important electron acceptor, accounting for well over 90% of organic matter oxidation (water depths > 1000 m; Archer et al. 2002). In contrast, in coastal regions where high amounts of particulate organic matter reach the sea floor or under low bottom-water $O_2$ conditions, $O_2$ is removed from pore waters within the upper few millimeters of the sediment. Here, organic matter is degraded via anaerobic pathways (Gundersen and Jørgensen 1990; Canfield et al. 1993). Furthermore, the combination of compressed redox zones and $O_2$ depletion leads to steeper gradients of reduced solutes and potentially greater fluxes.

$TPO_4$ is released during either of the individual organic matter degradation reactions, but is not redox-sensitive itself (see section 1.2). Nevertheless, its mobilization is strongly

influenced by redox conditions in the sediment (Fig. 1.2). During anoxic conditions, the pathway of Fe reduction will release additional $TPO_4$, initially bound to Fe oxyhydroxides (Sundby et al. 1992; Slomp et al. 1998). Besides, inorganic reductive dissolution of Fe oxyhydroxides by sulfide within the sulfate reduction zone (Canfield 1989; Krom et al. 2002; Poulton 2003) will also release $TPO_4$ into the pore water (Jensen et al. 1995). Similarly to Fe, Mn oxyhydroxides will release $TPO_4$ during their reductive dissolution. However, as compared to Fe oxyhydroxides, Mn oxyhydroxides have a reduced binding capacity for $TPO_4$ (Jensen and Thamdrup 1993) and, hence, are less important for its remobilization. Moreover, in highly $O_2$-deficient systems like the major OMZs, much of the Mn reduction can occur already in the water column (Martin and Knauer 1984; Landing and Bruland 1987; Böning et al. 2004). Under oxic bottom-water conditions, a large amount of the total dissolved $TPO_4$ in sediments will be scavenged in the surface by Fe oxyhydroxides, limiting the rate of $TPO_4$ release to the overlying water. Sometimes, this "iron trap" may be so efficient that $TPO_4$ will be taken up from the bottom water by the sediment (McManus et al. 1997). In contrast, under anoxic and hypoxic bottom-water conditions, Fe reduction occurs close to the surface, leaving only a limited amount of Fe oxyhydroxides that might scavenge $TPO_4$. This diminished retention capacity of the sediment together with the enhanced release of $TPO_4$ from reductive Fe dissolution leads to high rates of $TPO_4$ remobilization into the overlying bottom waters. Preferential release of organic P during organic matter degradation (Ingall et al. 1993; Van Cappellen and Ingall 1997; Jilbert et al. 2011; Steenbergh et al. 2011) further contributes to high $TPO_4$ mobilization from anoxic sediments, but the underlying mechanism for this phenomenon has not yet been found. Recently, Steenbergh et al. (2011) proposed that under conditions of C limitation both aerobically and anaerobically living bacteria use phosphatases to remove phosphate groups from organic matter and make it more easily degradable. Since anaerobic bacteria cannot retain this phosphate (Gächter and Wehrli 1998; Hupfer et al. 2004), it is released into the pore water. An additional source of P that can be ultimately mobilized into the water column is the dissolution of hydroxylapatite from fish debris, as has been shown to be of high importance for the Peruvian and Arabian Sea OMZs (Suess 1981; Froelich et al. 1988; Schenau and De Lange 2000).

A further mechanism affecting benthic P cycling is most pronounced under oscillating oxic and anoxic conditions, and refers to the redox-dependent storage and release of P

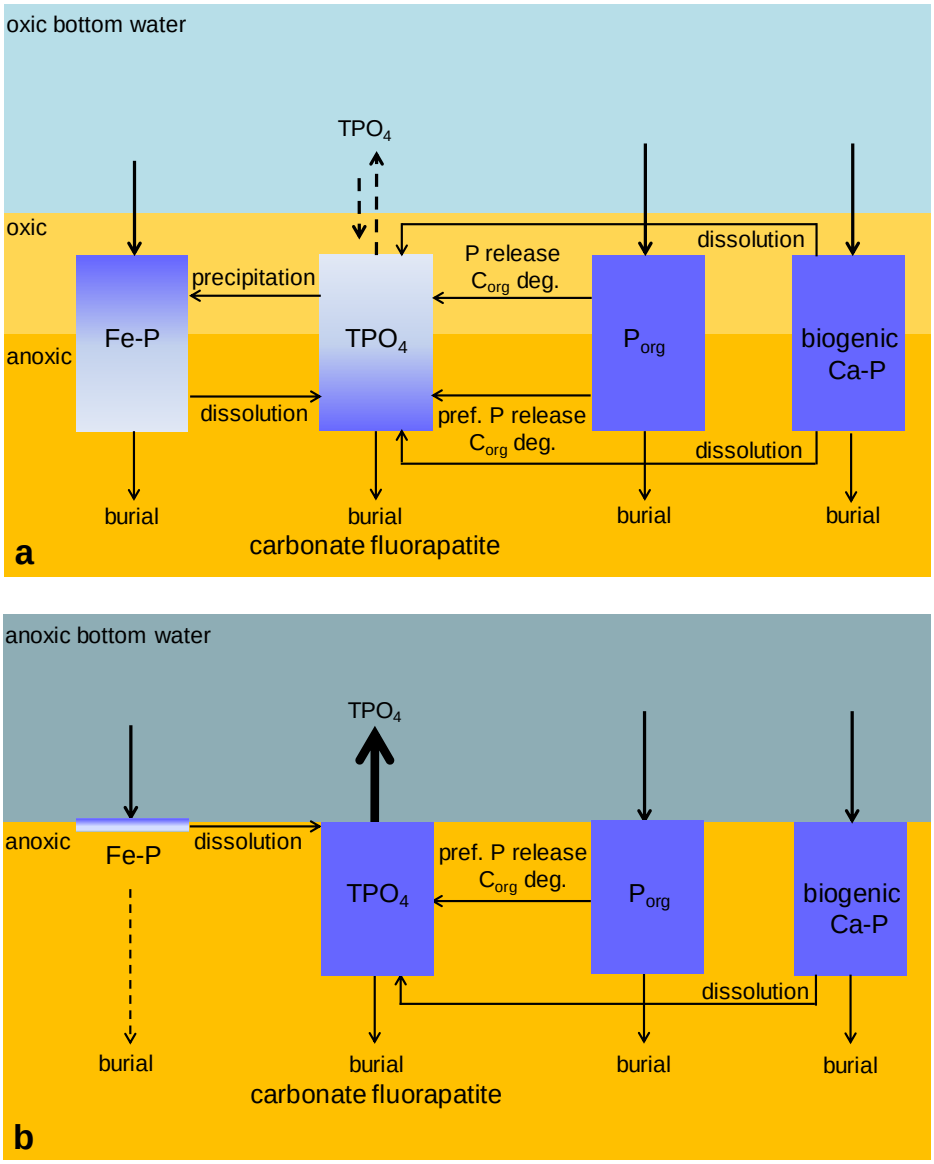


**Fig. 1.2:** Benthic P cycle under **a** oxic and **b** anoxic bottom-water conditions, considering the depositional fluxes of Fe oxyhydroxide-bound P (Fe-P), organic P ($P_{org}$) and biogenic calcium phosphate (biogenic Ca-P). Transformations (dissolution, precipitation, release) between the different P pools of the solid phase and dissolved P in the pore water ($TPO_4$) are indicated. Within the color graded Fe-P and $TPO_4$ pools, dark blue indicates higher concentrations of P. For anoxic conditions, only a small Fe-P pool is indicated at the sediment surface. Under oxic conditions, the presence of Fe oxyhdyroxides in the sediment surface impedes the benthic release of $TPO_4$ or even results in $TPO_4$ uptake from the bottom water (dashed arrows). In contrast, under anoxic conditions, the retention capacity is diminished, resulting in high $TPO_4$ fluxes (thick arrow). It was refrained from indicating the magnitude of input and burial fluxes, as well as transformation processes in the sediment. For details see text.

from certain bacteria and protozoa (Sannigrahi and Ingall 2005, and references therein). Under oxygenated conditions, these organisms store excess P in the form of polyphosphates, which, when the ambient bottom water becomes $O_2$-depleted, are degraded to gain energy. The large sulfide-oxidizing bacteria *Thiomargarita namibiensis* and *Beggiatoa* spp. that are ubiquitiously occurring in sediments below extensive upwelling regions from major OMZs worldwide (Schulz et al. 1999; Levin et al. 2003; Gutiérrez et al. 2008; Mosch et al. 2012) may be of particular importance in this regard (Schulz and Schulz 2005; Goldhammer et al. 2010; Brock and Schulz-Vogt 2011). In contrast, the genus *Thioploca* spp. that also is a prominent member of the microbial community particularly off Peru and Chile (Gallardo et al. 1977; Rosenberg et al. 1983; Jørgensen and Gallardo 1999) seems not to be capable for polyphosphate storage (Holmkvist et al. 2010). Occurrences of *Beggiatoa* spp. have also been reported for sediments from the Gotland Basin (Piker et al. 1998; Emeis et al. 2000).

Up to now, except for the study by Goldhammer et al. (2010), this special type of transient P metabolism in sulfide-oxidizing bacteria lacks direct evidence in upwelling environments. In general, quantitative information on the interaction of polyphosphate storing bacteria and pore waters is hardly available, and its importance in the global P cycle is still unresolved. These bacteria are further strongly involved in the benthic N and sulfur cycle, for details see section 1.5 “Benthic nitrogen cycle”.

#### 1.3.3.2 Precipitation reactions

Dissolved $TPO_4$ released during the above mentioned processes may be incorporated into the solid phase instead of being liberated into the bottom water. One such process, as already mentioned, is the redox dependent precipitation of $TPO_4$ coupled to the reoxidation of reduced manganese and iron. Secondly, P precipitation as carbonate fluorapatite (francolite) is generally favored under high $TPO_4$ pore-water concentrations (e.g. Föllmi 1996), and is an important step in the formation of modern phosphorite deposits. The chemical composition of francolite is quite complex, since it has multiple sites for possible substitution, but can be approximated by the formula:

$Ca_{10-a-b}Na_aMg_b(PO_4)_{6-x}(CO_3)_{x-y-z}$ x $(CO_3{*}F)_y(SO_4)_zF_2$.

There are two general modes of precipitation that depend on the initial level of supersaturation of pore waters with respect to francolite (Föllmi 1996, and references

therein). When these show high levels of supersaturation, precipitation proceeds rapidly within hours to days forming phosphatic pellets. This process involves the formation of metastable intermediates, thereafter used as substrate for francolite precipitation, and is the form that takes place in modern coastal upwelling regions. At lower levels of supersaturation, francolite precipitation proceeds directly but much slower on the timescales of months to years. This mode results in the formation of dispersed authigenic phosphate minerals, and commonly occurs in non-upwelling continental margin systems and/or rapidly accumulating sediments. The identification of dispersed carbonate fluorapatites has been only made possible by the development and application of special sediment extraction techniques (Ruttenberg 1993; Fillippelli and Delaney 1996; see section 1.4). With the increased number of identified deposits, global burial estimates for authigenic carbonate fluorapatite have greatly increased, resulting in this mineral phase being the most important sink of P in the modern ocean (e.g. Berner et al. 1993; see also Delaney 1998, her Table 3; Föllmi 1996, his Table 1).

All areas of modern phosphorite formation have two important factors in common, these are i. high primary productivity in overlying surface waters, resulting in high $TPO_4$ pore-water concentrations, and ii. intense sediment-reworking related to strong bottom current systems. In combination, these allow for strong $TPO_4$ enrichment in pore waters, its precipitation and the subsequent concentration of phosphatic minerals into deposits (Föllmi 1996). Phosphogenesis generally takes place close to the sediment surface, whereas below it is impeded by rising alkalinity during organic carbon degradation (Glenn and Arthur 1988). The presence of carbonate in pore waters results in its substitution for phosphate, in effect limiting apatite crystallization.

Redox conditions in the sediment have also been suggested to play a role in carbonate fluorapatite formation. In this regard, in particular the oxidation-reduction cycling of Fe oxyhydroxides is of importance (Ruttenberg and Berner 1993). $TPO_4$ that is first scavenged at the sediment surface will afterwards be released at greater sediment depths and thus result in a concentration effect of pore-water $TPO_4$.

Besides, the close association in the occurrences of modern phosphorites and dense mats of large sulfur bacteria (Schulz and Schulz 2005) as well as the occurrence of microfossils resembling sulfur bacteria in ancient phosphorite deposits (Williams and Reimers 1983; Bailey et al. 2007) has led to the suggestion that these might be involved in P

sequestration. The exact formation factors of authigenic phosphorites, however, remain largely unconstrained.

## 1.4 Methodological aspects - Phosphorus extraction

The profound understanding of the sedimentary P cycle of aquatic systems requires not only the quantification of the total $TPO_4$ release by (in situ) flux measurements but also the identification of the underlying biogeochemical processes. These can be only marginally approached by flux measurements. Also, pore-water profiles that are frequently measured in parallel often cannot be unambiguously interpreted. To identify the processes that give rise to the pore-water composition, a characterization of sedimentary P phases in addition is therefore helpful. This is commonly done by the application of sequential extraction procedures, extracting individual P phases according to their leachability in solutions of increasing severity (acidity or reducing strength). Since sequential extraction procedures are operationally defined, they generally have to be regarded as qualitative in identifying discrete sedimentary P pools.

The most frequently used extraction procedure today is the one by Ruttenberg (1992) as well as several modifications of it. This method has been especially developed for its use in marine sediments. It is able to detect small concentrations of P compounds that would be difficult to analyze with other methods, and has been a valuable tool in the identification of phosphorite burial rates in the marine environment. Ruttenberg's SEDEX (sedimentary extraction) procedure separates five sedimentary P components: loosely bound or exchangeable P; ferric Fe-bound P; authigenic calcium phosphate (authigenic Ca-P; including authigenic carbonate fluorapatite, biogenic apatite and calcium carbonate-associated P); detrital apatite P and organic P.

In this thesis, a modified version by Anderson and Delaney (2001) was used for the extraction of sediments from the Peruvian OMZ (Fig. 1.3). Its major alteration is that the five-step procedure was changed into a four-step procedure in that the authors combined the adsorbed and the oxide-associated fractions to a new "sorbed" fraction (referred to as Fe-bound P in Fig. 1.3).

This change finds its justification based on two reasons:

i. under sea-water conditions the amount of phosphate anions adsorbed to clays can be considered to be negligible as compared to that adsorbed to oxide surfaces; ii. most of the

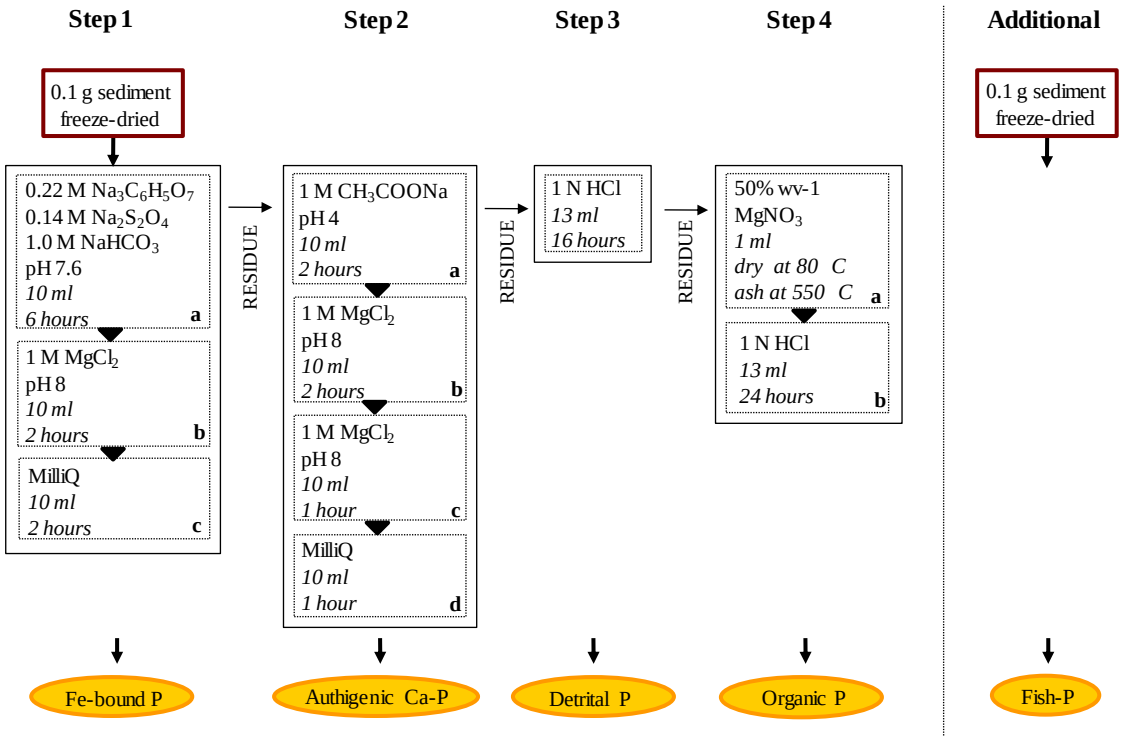


**Fig. 1.3:** Sequential phosphorus extraction scheme applied during this thesis. Steps 1-4 are according to Anderson and Delaney (2001), the additional $NH_4Cl$ extraction step is from Schenau and De Lange (2000).

phosphate seems to be adsorbed on the internal surfaces of oxide precipitates rather than being incorporated into their crystal lattices, leaving the distinction between adsorbed and oxide-associated somewhat arbitrary. In addition, a $NH_4Cl$ extraction (Schenau and De Lange 2000) was applied independently from the above extraction scheme (Fig. 1.3), to differentiate biogenic apatite (hydroxylapatite from fish debris) from the total pool of apatite phases (biogenic plus authigenic) extracted during its second step. This separation is possible due to the higher solubility of hydroxylapatite in comparison to carbonate fluorapatite, and was done since we expected to find high amounts of fish debris in the sediments underlying the highly productive Peruvian upwelling system (Suess et al. 1981).

## 1.5 Benthic nitrogen cycle

The nitrogen cycle is highly complicated, since marine organisms can alter the redox state of N, ranging from the fully oxidized nitrate ($NO_3^-$; +V) to the completely reduced ammonium ($NH_4^+$; -III), and add or remove available N from the oceanic/sedimentary

pool. A recent overview of the N cycle is provided by Capone et al. (2008). Nitrogen is highly abundant in the ocean and atmosphere, however it becomes only available for heterotrophic and phototrophic organisms in its fixed form.

Besides riverine- and atmospheric input fixation of gaseous $N_2$ into $NH_4^+$ by diazotrophs constitutes the major source for bio-available N in the oceans. Biological $N_2$-fixation providing reactive N to the marine environment has been mostly recognized in pelagic environments. However, recently benthic $N_2$-fixation has been reported to occur in a variety of benthic habitats including anoxic cold seep environments as well as coastal sediments (Fulweiler et al. 2007; Dekas et al. 2009; Bertics et al. 2010).

Under $O_2$-deficient bottom-water conditions ($O_2 < 5$ $\mu$mol $L^{-1}$; Devol 2008, and references therein) particulate organic matter on the sea floor can be decomposed using $NO_3^-$ as terminal electron acceptor. This process of dissimilatory $NO_3^-$ reduction, commonly referred to as heterotrophic denitrification, has been considered as a major sink for fixed N, releasing $N_2$ into the environment (Gruber & Sarmiento 1997). During denitrification microbes reduce $NO_3^-$ via a series of intermediates to $N_2$, with each step making use of different enzyme systems (Devol et al. 2008) (Fig. 1.4). Recently, it has been shown that $NH_4^+$ can be oxidized anaerobically in the water column as well as in anoxic sediments (Dalsgaard et al. 2005, and references therein). This process, which is referred to as anammox (anaerobic ammonium oxidation), also produces $N_2$ and together with denitrification causes a loss of fixed N, which represents a self-cleaning process for the ecosystem.

In oxic environments, nitrification is opposing this N loss. During this process, $NH_4^+$ that is released during the degradation of organic matter (ammonification) is sequentially oxidized to $NO_3^-$ (Fig. 1.4). In habitats, where there are sharp oxic to anoxic gradients, denitrification can be closely coupled to nitrification. Coupled denitrification to nitrification has been observed in a variety of different habitats, playing a significant role in N removal (Seitzinger 1988; Devol and Christensen 1993). Since nitrification is suppressed in $O_2$-deficient sediments, large amounts of $NH_4^+$, both from organic matter degradation and dissimilatory nitrate reduction to ammonium (DNRA), may reach the water column.

DNRA represents an important process, since it, similarly to nitrification, counteracts N loss from the sediment (Fig. 1.4). During DNRA sulfide is oxidized using $NO_3^-$ instead of

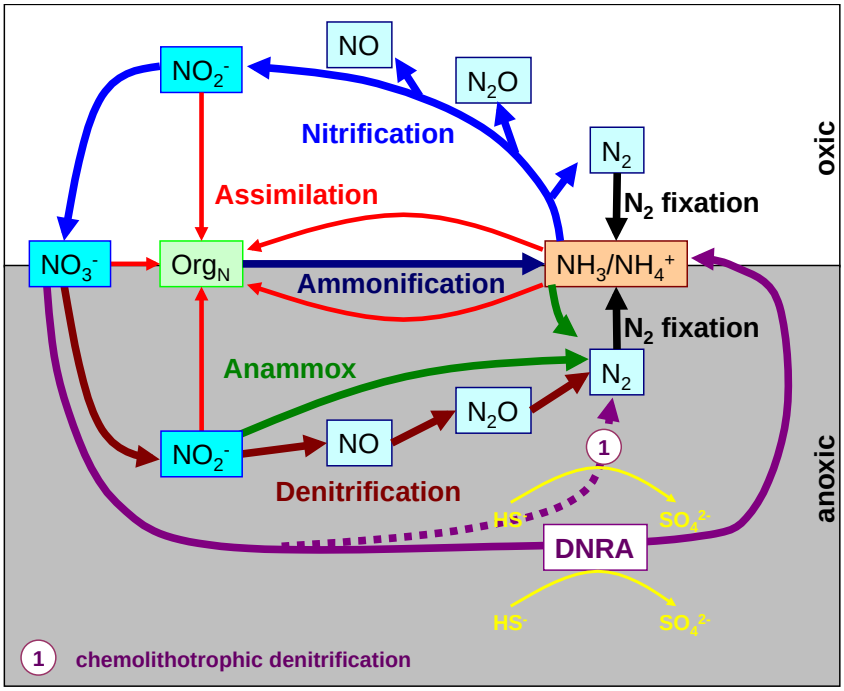


**Fig. 1.4:** Simplified scheme of the marine N cycle, including aerobic and anaerobic N transformations (redrawn after Kuypers 2007).

$O_2$, releasing $NH_4^+$ into the environment. DNRA is mediated by sulfide-oxidizing bacteria, such as *Thiomargarita* spp. or filamentous *Beggiatoa* spp. and *Thioploca* spp., which have often have been observed to form extended microbial mats on the surface of organic–rich sediments in OMZs (e.g. Gallardo 1977; Schmaljohann et al. 2001; Gutiérrez et al. 2008; Mosch et al. 2012). DNRA has been shown to occur in different organically enriched and/or $O_2$-deficient habitats, such as the Bay of Concepción (Graco et al. 2001), fish-farms (Christensen et al. 2000) or the shelf and upper slope of the Peruvian OMZ (Bohlen et al. 2011). However, it is discussed that instead of DNRA there is the potential alternative pathway of chemolithotrophic denitrification, where $NO_3$- is channeled into $N_2$ (Mußmann et al. 2000; Brüchert et al. 2003). To the best of my knowledge, there is still no concluding evidence to what extent this process proceeds in natural environments. Based on thermodynamical considerations, it has been concluded that DNRA should be more relevant (Jørgensen & Nelson 2004). DNRA as a recycling process is of high ecological impact, as it retains dissolved inorganic N in the ecosystem and may contribute to sustain high rates of primary production, if the $NH_4^+$ is transported to the euphotic zone.

## 1.6 Aims and thesis outline

Major aim of this thesis was to decipher the functionality of the sediments to act as sink or source for nutrients in different $O_2$-deficient environments, and thereby to constrain benthic feedbacks contributing to maintain or even promote $O_2$-deficiency. This thesis contributes to close the gap of missing flux studies by having quantified benthic release rates of predominantly P, but also to a certain extent of Fe and N, using benthic landers as well as pore-water gradients. Furthermore, major processes involved in the benthic nutrient release were addressed using mass balance calculations. This study encompassed two major working areas, i. the intense OMZ off Peru at 11°S and ii. the Gotland Basin in the Baltic Sea. In either working area, measurements were made along depth transects covering oxic to anoxic conditions as well as different organic C contents in the surface sediments.

In the following chapters the results of benthic P and associated Fe and N cycling in these two regions are presented.

Chapter 2 presents sea-bed fluxes of $TPO_4$ and $Fe^{2+}$ that were quantified during in situ benthic chamber incubations and calculated from pore-water profiles along an anoxic to oxic latitudinal depth transect traversing the OMZ off Peru. To the best of my knowledge, this is the first dataset on benthic release of this redox-sensitive couple in the eastern South Pacific upwelling region. This comprehensive dataset is of major importance for our quantitative understanding of how $TPO_4$ and $Fe^{2+}$ release from sediments underlying $O_2$-deficient bottom water via positive feedback loops potentially contribute towards the maintenance or even further spreading of this OMZ. Release rates of $TPO_4$ and $Fe^{2+}$ are explained in relation to redox conditions, and potential sedimentary sources for $TPO_4$ release are discussed. Release rates of $TPO_4$ and $Fe^{2+}$ are set into context with other OMZs worldwide. This chapter has been published in the journal Limnology and Oceanography in 2012.

Chapter 3 directly extends on the benthic flux results presented in Chapter 2, which indicate that, in contrast to the common assertion that input of $P_{org}$ is the major P source for the benthos, this source was not sufficient to support the high $TPO_4$ release rates measured in the Peruvian OMZ sediments. In this chapter it is investigated from a mass balance perspective in combination with solid phase P speciation measurements to what extent different sedimentary P sources contribute to sustain these high $TPO_4$ release rates.

In addition to $P_{org}$, input of Fe-bound P and an authigenic Ca-P pool (consisting of carbonate fluorapatite, calcium carbonate-bound P, and biogenic apatite (fish debris)) is considered in the mass balance. Furthermore, for one site inside the anoxic core of the OMZ a benthic P model is used to explore the validity of different scenarios of organic matter C:P composition and associated P release. It constrains organic P turnover by opposing i. organic matter degradation following Redfield stoichiometry, ii. preferential P release during organic matter degradation, and iii. mineralization of highly P-depleted organic matter settling on the sea floor. This chapter is close to submission to Geochimica Cosmochimica Acta.

Chapter 4 focuses on P and N cycling along an oxic to anoxic gradient in the eastern Gotland Basin, Baltic Sea. Despite great efforts to mitigate external anthropogenic nutrient load, this region still suffers from eutrophication and associated deoxygenation. Benthic fluxes of dissolved inorganic N (DIN = $NH_4^+$ + $NO_3^-$ + $NO_2^-$) as well as $TPO_4$ were quantified in situ using benthic landers and complemented by water-column nutrient measurements. The biogeochemical mechanisms underlying the benthic nutrient release are discussed. Special emphasis is on a hypoxic transition zone at water depths between about 80 m and 120 m that was extensively covered with mats of sulfide-oxidizing bacteria and further characterized by highly variable bottom-water $O_2$ concentrations on different time scales. In previous studies this transition zone has not been acknowledged for its importance for the benthic nutrient release in the Baltic Proper. By extrapolation of the measured flux rates, internal DIN and $TPO_4$ load estimates for the Baltic Proper are provided, excluding the Arkona Basin as well as shallow sandy sediments < 60 m water depth, where no measurements were taken. Using mass balances, capabilities for the Gotland Basin sediments to potentially recover from eutrophication are investigated. This chapter is close to submission to Limnology and Oceanography.

Chapter 5 gives a summary of the major findings of this thesis and an outlook on possible research questions for the future.

Beyond the above articles I was co-author of the following manuscripts:

Bohlen, L., A. W. Dale, S. Sommer, T. Mosch, C. Hensen, **A. Noffke**, F. Scholz, and K. Wallmann. 2011. Benthic nitrogen cycling traversing the Peruvian oxygen minimum zone. Geochim. Cosmochim. Acta **75:** 6094-6111.

Scholz, F., C. Hensen, **A. Noffke**, A. Rohde, V. Liebetrau, and K. Wallmann. 2011. Early diagenesis of redox-sensitive trace metals in the Peruvian upwelling region — response to ENSO related oxygen fluctuations in the water column. Geochim. Cosmochim. Acta **75:** 7257-7267.

Mosch, T., S. Sommer, M. Dengler, **A. Noffke**, L. Bohlen, O. Pfannkuche, V. Liebetrau, and K. Wallmann. 2012. Factors influencing the distribution of epibenthic megafauna across the Peruvian oxygen minimum zone. Deep- Sea Res. I **68:** 123-135.

Dale, A. W., S. Sommer, E. Ryabenko, **A. Noffke**, L. Bohlen, K. Wallmann, K. Stolpovsky, and O. Pfannkuche. Benthic nitrogen fluxes and fractionation of nitrate in the Mauritanian oxygen minimum zone (Eastern Tropical North Atlantic). Geochim. Cosmochim. Acta (in revision).

## References

Aller, R. C. 1982. The effects of macrobenthos on chemical characteristics of marine sediments and overlying waters, p. 53-102. *In* P. L. McCall and M. J. S. Tevesz [eds.], Animal-sediment relations: The biogenic alteration of sediments. Plenum Press.

Anderson, L. D., and M. L. Delaney. 2001. Sequential extraction and analysis of phosphorus in marine sediments: Streamlining of the SEDEX procedure. Limnol. Oceanogr. **45:** 509-515.

Archer, D. E., J. L. Morford, and S. R. Emerson. 2002. A model of suboxic sedimentary diagenesis suitable for automatic tuning and gridded global domains. Glob. Biogeochem. Cycles **16:** 17-1 - 17-21.

Bailey, J. V., S. B. Joye, K. M. Kalanetra, B. E. Flood, and F. A. Corsetti. 2007. Evidence of giant sulphur bacteria in Neoproterozoic phosphorites. Nature **445:** 198-201.

Benitez-Nelson, C. R. 2000. The biogeochemical cycling of phosphorus in marine systems. Earth Sci. Rev. **51:** 109-135.

Bjerrum, C. J., and D. E. Canfield. 2002. Ocean productivity before about 1.9 Gyr ago limited by phosphorus adsorption onto iron oxides. Nature **417:** 159-162.

Björkman, K., and D. Karl. 1994. Bioavailability of organic and inorganic phosphorus compounds to natural assemblages of microorganisms in Hawaiian coastal waters. Mar. Ecol. Prog. Ser. **111:** 365-372.

Berner, R., K. C. Ruttenberg, E. D. Ingall, and J.-L. Rao. 1993. The nature of phosphorus burial in modern marine sediments, p. 365-378. *In* R. Wollast, F. T. McKenzie and L. Chou [eds.], Interactions of C, N, P and S biogeochemical cycles and global change. NATO ASI Series Vol. 14.

Bertics, V. J., J. A. Sohm, T. Treude, C.-E. T. Chow, D. G. Capone, J. A. Fuhrmann, and W. Ziebis. 2010. Burrowing deeper into benthic nitrogen cycling: The impact of bioturbation on nitrogen fixation coupled to sulfate reduction. Mar. Ecol. Prog. Ser. **409:** 1-15.

Bohlen, L., A. W. Dale, S. Sommer, T. Mosch, C. Hensen, A. Noffke, F. Scholz, and K. Wallmann. 2011. Benthic nitrogen cycling traversing the Peruvian oxygen minimum zone. Geochim. Cosmochim. Acta **75:** 6094-6111.

Böning, P., H.-J. Brumsack, M. E. Böttcher, B. Schnetger, C. Kriete, J. Kallmeyer, and S. L. Borchers. 2004. Geochemistry of Peruvian near-surface sediments. Geochim.Cosmochim. Acta **68:** 4429-4451.

Bopp, L., C. Le Quéré, M. Heimann, A. C. Manning, and P. Monfray. 2002. Climate-induced oceanic oxygen fluxes: Implications for the contemporary carbon budget. Glob. Biogeochem. Cycles **16:** 1022, doi: 10.1029/2001GB001445

Buesseler, K. O., C. H. Lamborg, P. W. Boyd, P. J. Lam, T. W. Trull, R. R. Bidigare, J. K. B. Bishop, K. L. Casciotti, F. Dehairs, M. Elskens, M. Honda, D. M. Karl, D. A. Siegel, M. W. Silver, D. K. Steinberg, J. Valdes, B. Van Mooy, and S. Wilson. 2007. Revisiting carbon flux through the ocean's twilight zone. Science **316:** 567-570.

Brock, J., and H. N. Schulz-Vogt. 2011. Sulfide induces phosphate release from polyphosphate in cultures of a marine *Beggiatoa* strain. ISME J. **5:** 497-506.

Brüchert, V., B. B. Jørgensen, K. Neumann, D. Riechmann, M. Schlösser, and H. Schulz. 2003. Regulation of bacterial sulfate reduction and hydrogen sulfide fluxes in the central Namibian upwelling system. Geochim. Cosmochim Acta **67:** 1505-1518.

Canfield, D. E. 1989. Reactive iron in marine sediments. Geochim Cosmochim Acta **53:** 619-632.

Canfield, D. E., B. B. Jørgensen, H. Fossing, R. Glud, J. Gundersen, N. B. Ramsing, B. Thamdrup, J. W. Hansen, L. P. Nielsen, and P. O. J. Hall. 1993. Pathways of organic carbon oxidation in three continental margin sediments. Mar. Geol. **113:** 27-40.

Capone, D. G., D. A. Bronk, M. R. Mulholland, and E. J. Carpenter. 2008. Nitrogen in the marine environment. 2nd ed., Elsevier Science.

Cembella, A. D., N. J. Antia, and P. J. Harrison. 1984. The utilization of inorganic and organic phosphorus compounds as nutrients by eukaryotic microalgae: A multidisciplinary perspective. Part I. CRC Crit. Rev. Microbiol. **10:** 317-389.

Christensen, P. B., S. Rysgaard, N. P. Sloth, T. Dalsgaard, and S. Schwærter. 2000. Sediment mineralization, nutrient fluxes, denitrification and dissimilatory nitrate reduction to ammonium in an estuarine fjord with sea cage trout farms. Aquat. Microb. Ecol. **21:** 73-84.

Compton, J., D. Mallinson, C. R. Glenn, G. Filippelli, K. Föllmi, G. Shields, and Y. Zanin. 2000. Variations in the global phosphorus cycle, p. 21-33. *In* C. R. Glenn, L. Prévôt-Lucas and J. Lucas [eds.], Marine authigenesis: From global to microbial. SEPM Spec. Publ. No. 66.

Conley, D. J., S. Björck, E. Bonsdorff, J. Carstensen, G. Destouni, B. G. Gustafsson, S. Hietanen, M. Kortekaas, H. Kuosa, H. E. M. Meier, B. Müller-Karulis, K. Nordberg, A. Norkko, G. Nürnberg, H. Pitkänen, N. N. Rabalais, R. Rosenberg, O. P. Savchuk, C. P. Slomp, M. Voss, F. Wulff, and L. Zillén. 2009. Hypoxia related processes in the Baltic Sea. Environ. Sci. Technol. **43:** 3412-3420.

Dalsgaard, T., B. Thamdrup, and D. E. Canfield. 2005. Anaerobic ammonium oxidation (anammox) in the marine environment. Res. Microbiol. **156:** 457-464.

Delaney, M. L. 1998. Phosphorus accumulation in marine sediments and the oceanic phosphorus cycle. Glob. Biogeochem. Cycles **12:** 563-572.

Dekas, A. E., R. S. Poretsky, and V. J. Orphan. 2009. Deep-sea archaea fix and share nitrogen in methane consuming microbial consortia. Science **326:** 422-426.

Devol, A. H., and J. P Christensen. 1993. Benthic fluxes and nitrogen cycling in sediments of the continental margin of the eastern North Pacific. J. Mar. Res. **51:** 345-372.

Devol, A. H. 2008. Denitrification including anammox, p. 263-301. *In* D. G. Capone, D. A. Bronk, M. R. Mulholland and E. J. Carpenter [eds.], Nitrogen in the marine environment. 2nd ed., Elsevier Science.

Dhyrman, S. T., and K. C. Ruttenberg. 2006. Presence and regulation in alkaline phosphatase activity in eukaryotic phytoplankton from the coastal ocean: Implications for dissolved organic phosphorus remineralization. Limnol. Oceanogr. **51:** 1381-1390.

Emeis, K.-C., U. Struck, T. Leipe, F. Pohllehne, H. Kunzendorf, and C. Christiansen. 2000. Changes in the C, N, P burial rates in some Baltic Sea sediments over the last 150 years — relevance for P regeneration rates and the phosphorus cycle. Mar. Geol. **167:** 43-59.

Falkowski, P. G. 1997. Evolution of the nitrogen cycle and its influence in the biological sequestration of $CO_2$ in the ocean. Nature **387:** 272-274.

Falkowski, P. G., R. T. Barber, and V. Smetacek. 1998. Biochemical controls and feedbacks on ocean primary production. Science **281:** 200-206.

Faul, K. L., A. Paytan, and M. L. Delaney. 2005. Phosphorus distribution in sinking oceanic particulate matter. Mar. Chem. **97:** 307-333.

Filippelli, G. M., and M. L. Delaney. 1996. Phosphorus geochemistry of equatorial Pacific sediments. Geochim. Cosmochim. Acta **60:** 1479-1489.

Filippelli, G. 2002. The global phosphorus cycle. Rev. Mineral. Geochem. **48:** 391-425.

Filippelli, G. M. 2008. The global phosphorus cycle: Past, present, and future. Elements **4:** 89-95.

Föllmi, K.B. 1996. The phosphorus cycle, phosphogenesis and marine phosphate-rich deposits. Earth Sci. Rev. **40:** 55-124.

Froelich, P. N., G. P. Klinkhammer, M. L. Bender, N. A. Luedtke, G. R. Heath, D. Cullen, and P. Dauphin. 1979. Early oxidation of organic matter in pelagic sediments of the eastern equatorial Atlantic: Suboxic diagenesis. Geochim. Cosmochim. Acta **43:** 1075-1090.

Froelich, P. N., M. A. Arthur, W. C. Burnett, M. Deakin, V. Hensley, R. Jahnke. L. Kaul, K.-H. Kim, R. Roe, A. Soutar, and C. Vathakanon. 1988. Early diagenesis of organic matter in Peru continental margin sediments: Phosphorite precipitation. Mar. Geol. **80:** 309-343.

Fulweiler, R. W., S. W. Nixon, B. A. Buckley, and S. L. Granger. 2007. Reversal of the net dinitrogen gas flux in coastal marine sediments. Nature **448:** 180-182.

Gächter, R., and B. Wehrli. 1998. Ten years of artificial mixing and oxygenation: no effect on the internal nutrient loading of two eutrophic lakes. Environm. Sci. Technol. **32:** 3659-3665.

Gallardo, V. A. 1977. Large benthic microbial communities in sulfide biota under Peru-Chile subsurface countercurrent. Nature **268:** 331-332.

Glenn, C. R., and M. A. Arthur. 1988. Petrology and major element geochemistry of Peru margin phosphorites and associated diagenetic minerals: Authigenesis in modern organic-rich sediments. Mar. Geol. **80:** 231-267.

Goldhammer, T., V. Brüchert, T. G. Ferdelman, and M. Zabel. 2010. Microbial sequestration of phosphorus in anoxic upwelling sediments. Nat. Geosci. **3:** 557-561.

Graco, M., L. Farías, V. Molina, D. Gutiérrez, and L. P. Nielsen. 2001. Massive developments of microbial mats following phytoplankton blooms in a naturally eutrophic bay: Implications for nitrogen cycling. Limnol. Oceanogr. **46:** 821-832.

Gruber, N., and J. L. Sarmiento. 1997. Global patterns of marine nitrogen fixation and denitrification. Glob. Biogeochem. Cycles **11:** 235-266.

Gundersen, J. K., and B. B. Jørgensen. 1990. Microstructure of diffusive boundary layers and the oxygen uptake of the sea floor. Nature **345:** 604-607.

Gutiérrez, D., E. Enríquez, S. Purca, L. Quipúzcoa, R. Marquina, G. Flores, and M. Graco. 2008. Oxygenation episodes on the continental shelf of central Peru: Remote forcing and benthic ecosystem response. Prog. Oceanogr. **79:** 177-189.

Hanrahan, G., T. M. Salmassi, C. S. Khachikian, and K. L. Foster. Reduced inorganic phosphorus in the natural environment: significance, speciation and determination. Talanta **66:** 435-444.

Hedges, J. I., and R. G. Keil. 1995. Sedimentary organic matter preservation: an assessment and speculative synthesis. Mar. Chem. **49:** 81-115.

HELCOM. 2009*a*. Eutrophication in the Baltic Sea — an integrated thematic assessment of the effects of nutrient enrichment in the Baltic Sea region: Executive summary. Balt. Sea Environ. Proc., no. 115A. Helsinki Comission.

HELCOM. 2009*b*. Eutrophication in the Baltic Sea — an integrated thematic assessment of the effects of nutrient enrichment and eutrophication in the Baltic Sea region. Balt. Sea Environ. Proc., no. 115B. Helsinki Comission.

Holmkvist, L., E. T. Arning, K. Küster-Heins, V. Vandieken, J. Peckmann, M. Zabel, and B. B. Jørgensen. 2010. Phosphate geochemistry, mineralization processes and *Thioploca* distribution in shelf sediments off central Chile. Mar. Geol. **277:** 61-72.

Hupfer, M., B. Rübe, and P. Schmieder. 2004. Origin and diagenesis of polyphosphates in lake sediments: A $^{31}$P-NMR study. Limnol. Oceanogr. **49:** 1-10.

Ingall, E. D., R. M. Bustin, and P. Van Cappellen. 1993. Influence of water column anoxia on the burial and preservation of carbon and phosphorus in marine shales. Geochim. Cosmochim. Acta **57:** 303-316.

Jahnke, R. A. 1996. The global ocean flux of particulate organic carbon. Areal distribution and magnitude. Glob. Biogeochem. Cycles **10:** 71-88.

Jahnke, R. 1985. A model of microenvironments in deep-sea sediments: Formation and effects on pore water profiles. Limnol. Oceanogr. **30:** 956-965.

Jensen, H. S., and B. Thamdrup. 1993. Iron-bound phosphorus in marine sediments as measured by bicarbonate-dithionite extraction. Hydrobiologia. **253:** 47-59.

Jensen, H. S., P. B. Mortensen, F. Ø. Andersen, E. Rasmussen, and A. Jensen. 1995. Phosphorus cycling in a coastal marine sediment, Aarhus Bay, Denmark. Limnol. Oceanogr. **40:** 908-917.

Jilbert, T., C. P. Slomp, B. G. Gustafsson, and W. Boer. 2011. Beyond the Fe-P redox connection: Preferential regeneration of phosphorus from organic matter as a key control on Baltic Sea nutrient cycles. Biogeosciences. **8:** 1699-1720.

Joos, F., G.-A. Plattner, T. F. Stocker, A. Körtzinger, and D. W. R. Wallace. 2003. Trends in marine dissolved oxygen: implications for ocean circulation changes and the carbon budget. Eos **84:** 197-201.

Jørgensen, B. B. 1977. Distribution of colorless sulfur bacteria (*Beggiatoa* spp.) in a coastal marine sediment. Mar. Biol. **41:** 19-28.

Jørgensen, B. B., and V. A. Gallardo. 1999. *Thioploca* spp.: filamentous sulfur bacteria with nitrate vacuoles. FEMS Microb. Ecol. **28:** 301-313.

Jørgensen, B. B., and D. C. Nelson. 2004. Sulfide oxidation in marine sediments: Geochemistry meets microbiology. GSA Spec. Pap. **379:** 63-81.

Karl, D. M., R. R. Bidigare, and R. M. Letelier. 2001. Long term changes in plankton community structure and productivity in the North Pacific Subtropical Gyre: The domain shift hypothesis. Deep-Sea Res. II **48:** 1449-1470.

Karl, D. M., and K. M. Björkman. 2002. Dynamics of DOP, p. 249-366. *In* D. A. Hansell and C. A. Carlson [eds.], Biogeochemistry of Marine Dissolved Organic Matter. Elsevier Science.

Keeling, R. F., and H. E. Garcia. 2002. The change in oceanic $O_2$ inventory associated with recent global warming. PNAS **12:** 7848-7853.

Krom, M. D., N. Kress, S. Brenner, and L. I. Gordon. 1991. Phosphorus limitation of primary productivity in the eastern Mediterranean Sea. Limnol. Oceanogr. **36:** 424-432.

Krom, M. D., R. J. G. Mortimer, S. W. Poulton, P. Hayes, I. M. Davies, W. Davison, and H. Zhang. 2002. In-situ determination of dissolved iron production in marine sediments. Aquat. Sci. **64:** 282-291.

Krom, M. D., B. Herut, and R. F. C. Mantoura. 2004. Nutrient budget for the Eastern Mediterranean: Implications for phosphorus limitation. Limnol Oceanogr. **49:** 1582-1592.

Kuypers, M. M. M. 2007. Der Stickstoffzyklus des Ozeans. Forschungsbericht 2007. Max-Planck Gesellschaft.

Landing, W. M., and K. W. Bruland. 1987. The contrasting biogeochemistry of iron and manganese in the Pacific Ocean. Geochim. Cosmochim. Acta **51:** 29-43.

Levin, L. A. 2003. Oxygen minimum zone benthos: adaptation and community response to hypoxia. Oceanogr. Mar. Biol. Ann. Rev. **41:** 1-45.

Lewis, B. L., and W. M. Landing. 1991. The investigation of dissolved and suspended-particulate trace metal fractionation in the Black Sea. Mar. Chem. **40:** 105-141.

Lewis, B. L., and G. W. Luther III. 2000. Processes controlling the distribution and cycling of manganese in the oxygen minimum zone of the Arabian Sea. Deep-Sea Res. II **47:** 1541-1561.

Martin, J. H., and G. A. Knauer. 1987. VERTEX: manganese transport through oxygen minima. Earth Plan. Sci. Lett. **67:** 35-47.

McCarthy, J. J., and E. J. Carpenter. 1983. Nitrogen cycling in near-surface waters of the open ocean, p. 487-512. *In* E. J. Carpenter and D. G. Capone [eds.], Nitrogen in the marine environment. 1st ed., Academic Press.

McManus, J., W. M. Berelson, K. H. Coale, K. S. Johnson, and T. E. Kilgore. 1997. Phosphorus regeneration in continental margin sediments. Geochim. Cosmochim. Acta **61:** 2891-2907.

Moffet, J. W., T. J. Goepfert, S. W. A. Naqvi. 2007. Reduced iron associated with secondary nitrite maxima in the Arabian Sea. Deep-Sea Res. I **54:** 1341-1349.

Mosch, T., S. Sommer, M. Dengler, A. Noffke, L. Bohlen, O. Pfannkuche, V. Liebetrau, and K. Wallmann. 2012. Factors influencing the distribution of epibenthic megafauna across the Peruvian oxygen minimum zone. Deep-Sea Res. I **68:** 123-135.

Mußmann, M., F. Z. Hu, M. Richter, D. de Beer, A. Preisler, B. B. Jørgensen, M. Huntermann, F. O. Glöckner, R. Amann, W. J. H. Koopman, R. S. Lasken, B. Janto, J. Hogg, P. Stoodley, R. Boissy, and G. D. Ehrlich. Insights into the genome of large sulfur bacteria revealed by analysis of single filaments. PLoS Biol. **5:** 1923-1973.

Paulmier, A., and D. Ruiz-Pino. 2009. Oxygen minimum zones (OMZs) in the modern ocean. Prog. Oceanogr. **80:** 113-128.

Paytan, A., and K. McLaughlin. 2007. The oceanic phosphorus cycle. Chem. Rev. **107:** 563-578.

Piker, L., R. Schmaljohann, and J. F. Imhoff. 1998. Dissimilatory sulfate reduction and methane production in Gotland deep sediments (Baltic Sea) during a transition period from oxic to anoxic bottom water (1993-1996). Aquat. Microb. Ecol. **14:** 183-193.

Poulton, S. W. 2003. Sulfide oxidation and iron dissolution kinetics during the reaction of dissolved sulfide with ferrihydrite. Chem. Geol. **202:** 79-94.

Rabalais, N. N., R. J. Diaz, L. A. Levin, R. E. Turner, D. Gilbert, and J. Zhang. 2010. Dynamics and distribution of natural and human-induced hypoxia. Biogeosciences **7:** 585-619.

Roels, J., and W. Verstraete. 2011. Biological formation of volatile phosphorus compounds. Biores. Technol. **79:** 243-250.

Roden. E. E., and J. M. Zachara. 1996. Microbial reduction of crystalline iron(III) oxides: Influence of oxide surface area and potential for cell growth. Environm. Sci. Technol. **30:** 1618-1628.

Roden, E. E. 2006. Geochemical and microbiological controls on dissimilatory iron reduction. C. R. Geosci. **338:** 456-467.

Rosenberg, R., W. E. Arntz, E. Chumán de Flores, L. A. Flores, G. Carbajal, I. Finger, and J. Tarazona. 1983. Benthos biomass and oxygen deficiency in the upwelling system off Peru. J. Mar. Res. **41:** 263-279.

Ruttenberg, K. C. 1992. Development of a sequential extraction method for different forms of phosphorus in marine sediments. Limnol. Oceanogr. **37:** 1460-1482.

Ruttenberg, K. C. 1993. Reassessment of the oceanic residence time of phosphorus. Chem. Geol. **107:** 405-409.

Ruttenberg, K. C., and R. A. Berner. 1993. Authigenic apatite formation and burial in sediments from non-upwelling continental margin environments. Geochim. Cosmochim. Acta **57:** 991-1007.

Sabine, C. L., R. A. Feely, N. Gruber, R. M. Key, K. Lee, J. L. Bullister, R. Wanninkhof, C. S. Wong, D. W. R. Wallace, B. Tilbrook, F. J. Millero, T.-H. Peng, A. Kozyr, T. Ono, and A. F. Rios. 2004. The oceanic sink for anthropgenic $CO_2$. Science **305:** 367-371.

Sannigrahi, P., and E. Ingall. 2005. Polyphosphates as a source of enhanced P fluxes in marine sediments overlain by anoxic water: Evidence from $^{31}$P NMR. Geochem. Trans. **6:** 52-59.

Sañudo-Wilhelmy, S. A., A. B. Kustka, C. J. Gobler, D. A. Hutchins, M. Yang, K. Lwiza, J. Burns, D. G. Capone, J. A. Raven, and E. J. Carpenter. 2001. Phosphorus limitation of nitrogen fixation by *Trichodesmium* in the central Atlantic Ocean. Nature **411:** 66-69.

Schenau S. J., and G. J. De Lange. 2000. A novel chemical method to quantify fish debris in marine sediments. Limnol. Oceanogr. **45:** 963-971.

Schenau, S. J., and G. J. De Lange. 2001. Phosphorus regeneration vs. burial in sediments of the Arabian Sea. Mar. Chem. **75:** 201-217.

Schink, B., and M. Friedrich. Phosphite oxidation by sulphate reduction. Nature 406: 37.

Schmaljohann, R., M. Drews, S. Walter, P. Linke, U. von Rad, and J. F. Imhoff. 2001. Oxygen minimum zone sediments in the northeastern Arabian Sea off Pakistan: A habitat for the bacterium *Thioploca*. Mar. Ecol. Prog. Ser. **211:** 27-42.

Schulz, H. N., T. Brinkhoff, T. G. Ferdelman, M. Hernández-Mariné, A. Teske, B. B. Jørgensen. 1999. Dense population of a giant sulfur bacterium in Namibian shelf sediments. Science **284:** 493-495.

Schulz, H. N., and H. D. Schulz. 2005. Large sulfur bacteria and the formation of phosphorite.Science **21:** 416-418.

Seitzinger, S. P. 1988. Denitrification in freshwater and coastal marine ecosystems: Ecological and geochemical significance. Limnol. Oceanogr. **33:** 702-724.

Slomp, C. P., J. F. P. Malschaert, and W. Van Raaphorst. 1998. The role of adsorption in sediment-water exchange of phosphate in North Sea continental margin sediments. Limnol. Oceanogr. **43:** 832-846.

Steenberg, A. K., P. L. E. Bodelier, H. L. Hoogveld, C. P. Slomp, and H. J. Laanbroek. 2011. Phosphatases relieve carbon limitation of microbial activity in Baltic Sea sediments along a redox-gradient. Limnol. Oceanogr. **56:** 2018-2026.

Stramma, L., G. C. Johnson, J. Sprintall, and V. Mohrholz. 2008. Expanding oxygen-minimum zones in the tropical oceans. Science **320:** 655-658.

Suess, E. 1981. Phosphate regeneration from sediments of the Peru continental margin by dissolution of fish debris. Geochim. Cosmochim. Acta **45:** 577-588.

Sundby, B., C. Gobeil, N. Silverberg, and A. Mucci. 1992. The phosphorus cycle in coastal marine sediments. Limnol. Oceanogr. **37:** 1129-1145.

Ternan, N. G., J. W. Mc Grath, G. Mc Mullan, and J. P. Quinn. 1998. Organophosphonates: occurrence, synthesis and biodegradation by microorganisms. W. J Microbiol. Biotechnol. **14:** 635-647.

Tyrell, T. 1999. The relative influence of nitrogen and phosphorus on oceanic primary production. Nature **400:** 525-531.

Vahtera, E., D. J. Conley, B. G. Gustafsson, H. Kuosa, H. Pitkänen, O. P. Savchuk, T. Tamminen, M. Viitasalo, M. Voss, N. Wasmund, and F. Wulff. 2007. Internal ecosystem feedbacks enhance nitrogen-fixing cyanobacteria blooms and complicate management in the Baltic Sea. Ambio **36:** 186-194.

Watkins-Brandt, K. S., R. M. Letelier, Y. H. Spitz, M. J. Church, D. J. Böttcher, and A. E. White. 2011. Addition of inorganic or organic phosphorus enhances nitrogen and carbon fixation in the oligotrophic North Pacific. Mar. Ecol. Prog. Ser. **432:** 17-29.

White, A. K., and W. M. Metcalf. 2007. Microbial metabolism of reduced phosphorus compounds. Ann. Rev. Microbiol. **61:** 379-400.

Williams, L. A., and C. Reimers. 1983. Role of bacterial mats in oxygen-deficient marine basins and coastal upwelling systems: Preliminary report. Geology **11:** 267-269.

Wollast, R. 1991. The coastal organic carbon cycle: fluxes, sources and sinks, p. 365-381. *In* R. F. C. Mantoura, J. M. Martin and R. Wollast [eds.], Ocean margin processes in global change. Wiley.

Van Cappellen, P., and E. D. Ingall 1997. Response to comment "Redox stabilization of the atmosphere and oceans and marine productivity" by Colman et al. 1997. Science **475:** 407-408.

Van der Zee, C., and W. van Raaphorst. 2004. Manganese oxide reactivity in North Sea sediments. J. of Sea Res. **52:** 73-8.

# 2 Benthic iron and phosphorus fluxes across the Peruvian oxygen minimum zone

A. Noffke[a,*], C. Hensen,[a] S. Sommer,[a] F. Scholz,[a] L. Bohlen,[a] T. Mosch,[a] M. Graco,[b] and K. Wallmann[a]

[a]Helmholtz-Zentrum für Ozeanforschung Kiel, Kiel, Germany

[b]Instituto del Mar del Perú, Callao, Peru

[*]author for correspondence: anoffke@geomar.de

Published in 2012 in Limnology and Oceanography **57:** 851-867

## Abstract

Benthic fluxes of dissolved ferrous iron ($Fe^{2+}$) and phosphate ($TPO_4$) were quantified by in situ benthic chamber incubations and pore-water profiles along a depth transect (11°S, 80 m to 1000 m) across the Peruvian oxygen minimum zone (OMZ). Bottom-water $O_2$ levels were $< 2$ $\mu$mol $L^{-1}$ down to 500 m water depth, and increased to ~ 40 $\mu$mol $L^{-1}$ at 1000 m. $Fe^{2+}$ fluxes were highest on the shallow shelf (maximum 316 mmol $m^{-2}$ $yr^{-1}$), moderate (15.4 mmol $m^{-2}$ $yr^{-1}$) between 250 m and 600 m, and negligible at deeper stations. In the persistent OMZ core continuous reduction of Fe oxyhydroxides results in depletion of sedimentary Fe:Al ratios. $TPO_4$ fluxes were high (maximum 292 mmol $m^{-2}$ $yr^{-1}$) throughout the shelf and the OMZ core in association with high organic carbon degradation rates. Ratios between organic carbon degradation and $TPO_4$ flux indicate excess release of P over C when compared to Redfield stochiometry. Most likely, this is caused by preferential P-release from organic matter, dissolution of fish debris, and/or P-release from microbial mat communities, while Fe oxyhydroxides can only be inferred as a major P-source on the shallow shelf. The benthic fluxes presented here are among the highest reported from similar, oxygen-depleted environments, and highlight the importance of sediments underlying anoxic water bodies as nutrient sources to the ocean. The shelf is particularly important as the periodic passage of coastal trapped

waves and associated bottom-water oxygenation events can be expected to induce a transient biogeochemical environment with highly variable release of $Fe^{2+}$ and $TPO_4$.

## 2.1 Introduction

Oxygen minimum zones (OMZ), water layers with oxygen concentrations < 20 $\mu$mol $L^{-1}$, are persistent hydrographic features in large parts of the ocean, in particular the eastern Pacific, the northern Indian Ocean, and the eastern Atlantic off southwest Africa (Helly and Levin 2004). One of the most extended and intense OMZs (dropping to oxygen concentrations close to anoxia in core regions, Stramma et al. 2008) is located in the eastern South Pacific, underneath the productive coastal waters of the Humboldt Current System. This OMZ stretches from 37°S, Chile**,** to the equatorial belt (0-5°S) and reaches its greatest extension off Peru between 5 and 13°S, with > 600 m thickness to about 1000 km offshore (Fuenzalida et al. 2009).

The complex maintenance mechanisms and dynamics of OMZs still have not been sufficiently resolved. However, the principal factors leading to their formation are intense oxygen consumption in response to high surface productivity, sustained by high amounts of upwelled nutrients, and sluggish ventilation due to the hydrographic regime (Wyrtki 1962). Climate models predict an overall decline of dissolved oxygen in the ocean interior to emerge from global warming (Matear and Hirst 2003). For the tropical oxygen minimum zones this decline was recently confirmed by 50 year time series analyses of $O_2$ data (collected since 1960, Stramma et al. 2008).

In response to the expansion of the hypoxic water masses, major changes in nutrient cycling could occur and affect the marine carbon, nitrogen, phosphorus, and iron cycles via various feedback mechanisms. Thus, improving current knowledge on the key biogeochemical and physical processes governing today's OMZs by quantitative approaches remains critical to estimating the ocean's responses to global warming and becomes a future research challenge.

Oxygen depletion substantially affects the biogeochemical reactions of redox-sensitive elements. This in particular applies to iron (Fe) and phosphorus (P), whose individual cycles are strongly linked in the marine environment. A number of previous studies have resulted in the observation that under oxygen-deficient bottom-water conditions dissolved ferrous iron ($Fe^{2+}$) and phosphate ($TPO_4$) are preferentially released into the pore fluids

and overlying bottom water (Sundby et al. 1986; Ingall and Jahnke 1997; McManus et al. 1997). Particulate ferric iron oxides and hydroxides (hereafter referred to as iron oxyhydroxides) scavenge phosphate, and oxygen deficiency promotes their reduction to soluble states by microbial induced dissolution and the concomitant liberation of metal-oxide-bound phosphate (Sundby et al. 1992). Phosphate release from iron oxyhydroxides may further be enhanced through reductive dissolution by hydrogen sulfide (Jensen et al. 1995). Furthermore, in addition to these metal oxide interactions, growing evidence has been presented that phosphate is preferentially regenerated from P-bearing organic matter (as compared to C) under hypoxic and anoxic bottom-water conditions (Ingall et al. 1993).

Despite the obvious biogeochemical significance of organic rich sediments underlying productive upwelling systems for global element cycles and related feedbacks on ocean-climate interactions, relatively few systematic in situ studies on benthic nutrient turnover have been conducted to date. Phosphate fluxes derived from benthic chamber incubations are available for the continental margins off Washington State (Devol and Christensen 1993; Hartnett and Devol 2003), Central California (Ingall and Jahnke 1997; McManus et al. 1997; Berelson et al. 2003), and Northwest Mexico (Hartnett and Devol 2003), as well as the California borderland basins (Ingall and Jahnke 1997; McManus et al. 1997; Hammond et al. 2004). Measurements in the Arabian Sea (Woulds et al. 2009) have recently complemented the existing data pool. With regard to iron, the knowledge on benthic release rates is even smaller. This can mainly be ascribed to the fact that generally aeolian dust deposition (Jickells et al. 2005) has been assumed to be the major supply pathway of iron to the open ocean, and it was only recently that the potential contribution of a sedimentary iron source has begun to be considered (Moore and Braucher 2008). Much of the work done in continental margin upwelling settings focused on iron inventories and turnover in the water column. However, a number of these studies highlight the role of sediments supplying iron to the water column by mechanisms of resuspension (Hutchins et al. 1998) and reductive mobilization (Johnson et al. 1999). Direct measurements with benthic chambers revealed that reductive mobilization can be significant in such sedimentary settings (McManus et al. 1997; Elrod et al. 2004; Severmann et al. 2010).

In this paper we report sea-bed fluxes of dissolved phosphate and iron for the OMZ off

Peru. To our knowledge, this represents the first detailed investigation on benthic release of this redox-sensitive couple in the Eastern South Pacific upwelling region. Benthic fluxes were derived from time series of in situ incubations with benthic landers and calculations from pore-water gradients. Sampling was conducted along a latitudinal transect (11°S) at water depths from 80 m to 1000 m, affected by regionally varying environmental influences (redox conditions, hydrodynamics and organic carbon availability). This enabled us to directly link magnitudes of nutrient release with potential controlling parameters.

## 2.2 Methods

### *2.2.1 Regional setting*

The Peruvian coast is part of the most productive marine ecosystem in the world. High primary productivity of up to 3.6 g C $m^{-2}$ $d^{-1}$ (Pennington et al. 2006) is sustained by coastal upwelling that transports cold, oxygen-poor but nutrient-rich water to the well-mixed surface layer. Upwelling off Peru is perennial, favored by almost constant alongshore oriented winds which drive an offshore Ekman transport of surface waters (Strub et al. 1998). Upwelled waters are predominantly fed by Equatorial Subsurface Water, which is transported poleward with the Peru Chile Undercurrent (Strub et al. 1998). Intensity of the coastal upwelling changes seasonally due to varying wind strength with maximum wind speed and coastal upwelling occurring in austral winter and spring (Pennington et al. 2006). The OMZ that develops from intense degradation of organic matter and associated oxygen consumption extends roughly from < 100 m to 700 m (oxycline of 22 $\mu$mol $L^{-1}$ defined by Fuenzalida et al. 2009). Seasonal changes in upwelling intensity typically result in variable mixed surface layer depths of 10 m to 40 m (Bakun 1985). However, periodic oxygenation events of the bottom waters may reach down to about 100 m water depth as observed off Callao at 12°S (Gutiérrez et al. 2008). According to this study, the vertical position of the upper boundary of the OMZ (defined as the 22 $\mu$mol $L^{-1}$ isopleth) fluctuated between 10 m and 90 m water depth (mean depth: 52 m) over a period of 13 years (1992-2005). Such oxygenation events are strongly associated with the passage of coastal trapped waves that occur more frequently during positive El Niño Southern Oscillation (ENSO) periods (Gutiérrez et al. 2008) and are associated with a significant deepening of the thermo- and oxycline. Most intense

oxygenation events have been reported for the strong El Niño periods in 1982-1983 and 1997-1998 during which the upper boundary of the OMZ deepened to almost 300 m (Levin et al. 2002; Fuenzalida et al. 2009).

Between 11°S and 15°S, underneath the region of most intense primary productivity (Pennington et al. 2006), organic rich (>> 5 wt%), diatomaceous muds accumulate at water depths between 50 m and 500 m (Suess et al. 1987). A distinct feature of this region is a thick lens-shaped deposit that extends between 10.5°S and 13.6°S from outer shelf to upper slope depths (Krissek et al. 1980). Preservation and burial within this deposit is due to high bulk sedimentation rates, which are favored by reduced bottom velocities in the poleward directed undercurrent (Suess et al. 1987). At greater water depths, increasing fluctuations in the velocity and direction of bottom currents result in lower sedimentation rates (Reimers and Suess 1983), winnowing, and the accumulation of phosphorite crusts and nodules (Reimers and Suess 1983; Glenn and Arthur 1988).

### *2.2.2 Sediment sampling and in situ flux measurements*

Sediment samples were taken during the R/V *Meteor* cruise M77-1/2 in October-December 2008, using a video-guided multiple corer (MUC) and two benthic landers (Biogeochemical Observatories — BIGO and BIGO-T) along a latitudinal depth transect at 11°S (Fig. 2.1; Table 2.1). Bottom-water $O_2$ levels of < 2 $\mu$mol $L^{-1}$ extended from ~ 50 m to ~ 500 m water depth (Fig. 2.2), hitherto referred to as OMZ. During the time of sampling, the shallow shelf Sta. 543 and 568 at 78 m and 85 m water depth, respectively, also displayed bottom-water $O_2$ levels < 2 $\mu$mol $L^{-1}$. However, these sites might experience periodic oxygenation events similar to those observed at a 94 m deep site off Callao (Gutiérrez et al. 2008). As with increasing water depth oxygenation events can be assumed to occur more rarely, we henceforth refer to the core of the OMZ as the depth range between 250 m down to its lower boundary at ~ 500 m.

Sediment cores (inner diameter: 10 cm) retrieved by MUC were immediately transferred into a cold room which was kept at in situ temperature (4°C). Core processing was performed within 1-2 h upon retrieval. Two parallel cores were processed for all MUC stations. The overlying bottom water was sampled and filtered through 0.2 $\mu$m cellulose acetate (CA) syringe filters, and the remaining water was siphoned off and discarded. The first one of the two parallel cores was vertically sectioned within a glove bag under an

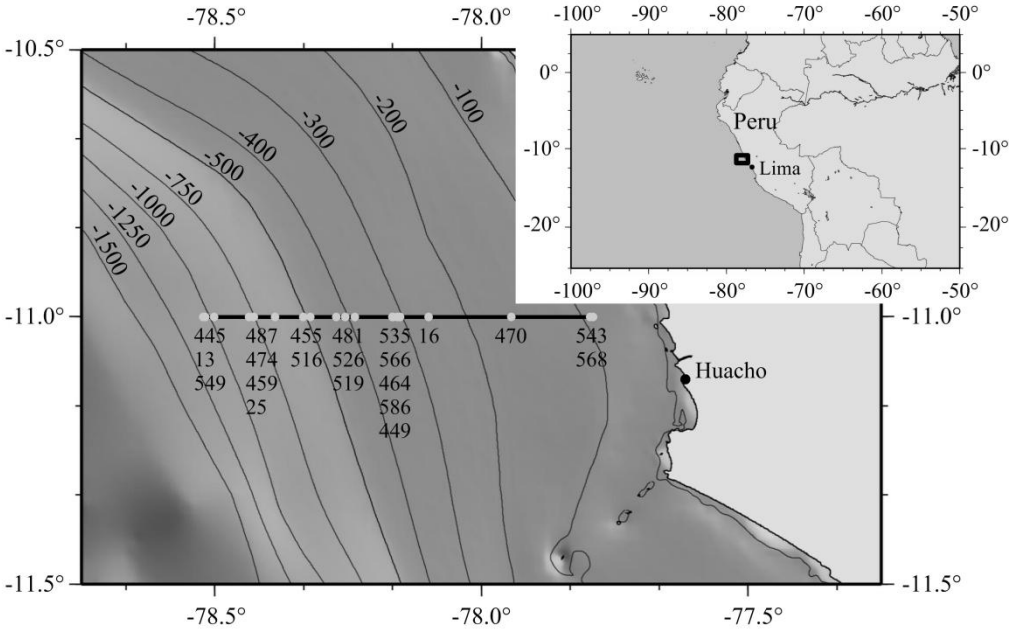


**Fig. 2.1:** Location map showing the Peruvian continental margin (bathymetry based on the Earth Topography Five Minute Grid (ETOPO5)). The sampling stations on the latitudinal transect at 11°S (horizontal line) are indicated by the gray dots. Where stations were close together, station names were listed in descending order in accordance with increasing water depth.

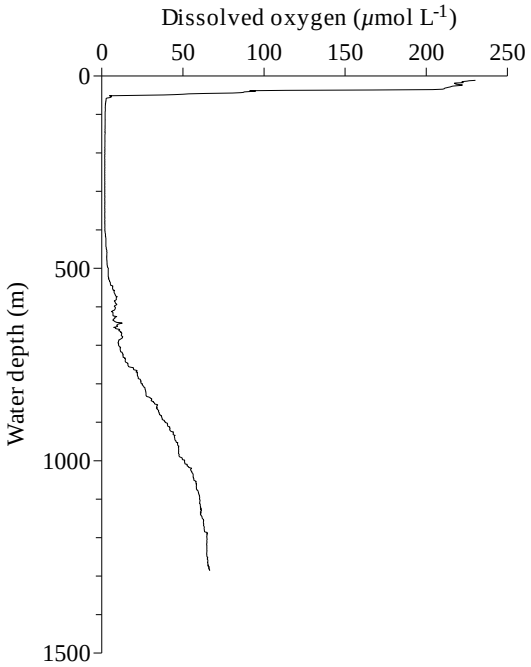


**Fig. 2.2:** Representative profile of dissolved oxygen (438 CTD-RO 16, position shown in Table 2.1) through the OMZ at 11°S during October – December 2008.

**Table 2.1:** Location, bottom-water oxygen concentration (BW $O_2$), and solid phase geochemical data (TOC, TOC:$P_{excess}$, reactive Fe, and Fe:Al, each for 0-1 cm sediment depth) of the study sites during the R/V *Meteor* cruise M77/ 1-2. Further included are positions of CTD deployments for water-column $O_2$ (representative profile shown in Fig. 2.2) and water-column nutrients. Empty cells indicate that the parameter was not measured.

| Station | Device | Cruise leg | Latitude (S) | Longitude (W) | Depth (m) | BW $O_2$ ($\mu$mol $L^{-1}$) | TOC (wt%) | TOC:$P_{excess}$ | highly reactive Fe (wt%) | Fe:Al* |
|---|---|---|---|---|---|---|---|---|---|---|
| 543 | MUC 52 | 1 | 10°59.99’ | 77°47.40’ | 78 | <2 | 3.50 | 181 | | 0.46 |
| 568 | BIGO 5 | 1 | 11°00.02’ | 77°47.72’ | 85 | <2 | 3.76 | 297 | 0.36 | 0.44 |
| 470 | MUC 29 | 1 | 11°00.02’ | 77°56.60’ | 145 | <2 | 7.61 | 139 | 0.19 | 0.42 |
| 16 | BIGO T | 1 | 10°59.80’ | 78°05.91’ | 259 | <2 | 13.54 | 171 | 0.12 | 0.41 |
| 535 | BIGO T3 | 1 | 11°00.00’ | 78°09.12’ | 305 | <2 | 15.18 | 140 | | |
| 566 | BIGO T4 | 1 | 11°00.00’ | 78°09.13’ | 309 | <2 | 11.48 | | | |
| 464 | BIGO 1 | 1 | 11°00.00’ | 78°09.92’ | 315 | <2 | 15.45 | 134 | | |
| 586 | BIGO T5 | 1 | 11°00.00’ | 78°09.40’ | 316 | <2 | 13.79 | 128 | | |
| 449 | MUC 19 | 1 | 11°00.01’ | 78°09.97’ | 319 | <2 | 10.65 | 88 | 0.08 | 0.42 |
| 481 | MUC 33 | 1 | 11°00.00’ | 78°14.19’ | 376 | <2 | 10.86 | 58 | 0.09 | 0.38 |
| 526 | BIGO 3 | 1 | 11°00.02’ | 78°15.27’ | 397 | <2 | 14.75 | 95 | | |
| 519 | MUC 43 | 1 | 11°00.01’ | 78°16.29’ | 410 | <2 | 8.50 | 43 | 0.07 | 0.36 |
| 455 | MUC 21 | 1 | 11°00.00’ | 78°19.23’ | 466 | <2 | 4.50 | 25 | 0.14 | 0.42 |
| 516 | MUC 40 | 1 | 11°00.00’ | 78°20.00’ | 512 | <2 | 6.07 | 3 | | 0.42 |
| 487 | MUC 39 | 1 | 11°00.02’ | 78°23.17’ | 579 | 4 | 6.48 | 26 | 0.12 | 0.37 |
| 474 | BIGO 2 | 1 | 11°00.01’ | 78°25.55’ | 695 | 12 | 6.53 | 38 | | |
| 459 | MUC 25 | 1 | 11°00.03’ | 78°25.60’ | 697 | 12 | 6.72 | 53 | 0.32 | 0.48 |
| 25 | BIGO | 2 | 10°59.47’ | 78°26.10’ | 716 | 7 | 8.08 | 39 | | |
| 445 | MUC 15 | 1 | 11°00.00’ | 78°30.02’ | 928 | 39 | 5.15 | 20 | 0.26 | 0.87 |
| 13 | BIGO | 2 | 10°59.82’ | 78°31.05’ | 978 | 40 | 4.09 | 14 | | |
| 549 | MUC 53 | 1 | 10°59.81’ | 78°31.27’ | 1005 | 40 | 4.00 | 30 | 0.20 | 0.56 |
| | | | | | | | | | | |
| 438 | CTD-RO 16 | 1 | 11°00.69’ | 78°35.03’ | 1261 | | | | | |
| 463 | CTD-RO 22 | 1 | 11°00.01’ | 78°44.86’ | 2031 | | | | | |

*From Scholz et al. 2011.

argon atmosphere. The sediments were transferred to 50 mL centrifuge tubes pre-flushed with argon, and pore water was separated using a refrigerated centrifuge for 20 min at 4.500 revolutions per minute (rpm). Supernatant pore fluids were filtered under argon through 0.2 $\mu$m CA syringe filters. Centrifuge residuals were stored frozen for total sediment digestion and the extraction of highly reactive iron phases after the cruise. Pore water from the sediments retrieved at Sta. 543 and 516 was extracted using rhizons (Seeberg-Elverfeldt et al. 2005) instead of the glovebag method. Prior to deployment, the rhizons were preconditioned in an oxygen-free water bath. To ensure that the samples had not been in contact with air, the first 0.5 mL of extracted pore water were discarded. Pore waters from the other parallel core were extracted using a pore-water press (Teflon squeezers equipped with 0.2 $\mu$m CA filters), which was operated with argon at pressure gradually increasing to 2.5 bar. Additional samples for the determination of water content and porosity, as well as for total organic carbon (TOC) analyses, were taken from each depth interval, filled into pre-weighed plastic vials, and stored refrigerated for subsequent processing in the home laboratory. Squeeze cakes were also kept refrigerated until onshore preparation for x-ray fluorescence (XRF) analyses. Only the results from the glove bag extractions are presented in this study, if not otherwise indicated.

In situ benthic flux measurements were conducted using the Biogeochemical Observatories BIGO and BIGO-T (Sommer et al. 2009). BIGO contained two circular flux chambers (internal diameter 28.8 cm, area 651.4 $cm^2$). BIGO-T is similar to BIGO but contained only one benthic chamber of the same size as those deployed in BIGO. An online video-controlled launching system allowed smooth placement of the observatories at selected sites on the sea floor. Two hours after the observatories were placed on the sea floor, the chamber(s) were slowly driven into the sediment (~ 30 cm $h^{-1}$). During this initial time period, the water inside the flux chamber was periodically replaced with ambient bottom water. After the chamber was fully driven into the sediment, the chamber water was again replaced with ambient bottom water to flush out solutes that might have been released from the sediment during chamber insertion. The water volume enclosed by the benthic chamber was in the range of 8.8 L to 18.5 L. To determine $Fe^{2+}$ and $TPO_4$ fluxes, four sequential water samples were removed from the chamber with glass syringes (volume: ~ 47 mL). The glass syringes were connected to the chamber using 1 m long Vygon tubes with a dead volume of 6.9 mL. Prior to deployment, these tubes were filled

with distilled water. In case of the BIGO-T, the chamber was completely flushed with ambient sea water after half of the total deployment time, and a series of four water samples was taken before and after flushing, henceforth referred to as first incubation and second incubation, respectively. The flux measurements were conducted for different time periods in the range from 17.8 h to 23 h as defined from the time interval between the first and the last syringe water sampling. After recovery of the observatories, short cores (inner diameter: 10 cm) were retrieved from the incubated sediments and processed in the glove bag as described above for MUCs.

### *2.2.3 Chemical analyses*

#### 2.2.3.1 Onboard analytics

All shipboard analyses were performed shortly after pore-water extraction or recovery of benthic landers. Ammonium ($NH_4^+$), total dissolved sulfide ($TH_2S$), and total dissolved phosphate ($TPO_4$) analyses — in pore-water and incubated bottom-water samples — as well as dissolved ferrous iron ($Fe^{2+}$) analyses (in pore-water samples only) were realized onboard with a Hitachi U-2001 spectrophotometer, applying standard techniques (Grasshoff et al. 1999). Where necessary, subsamples of pore water were diluted with oxygen-free artificial sea water prior to analysis. Ascorbic acid was added, still within the glove bag, to subsamples of pore and bottom waters for onboard $Fe^{2+}$ analyses. Total alkalinity (TA) was determined by titration following the method of Ivanenkov and Lyakhin (1978). For selected cores, sulfate ($SO_4^{2-}$) was measured onboard by Ion Chromatography (716 IC-Compact, Metrohm). Sample aliquots for additional $SO_4^{2-}$ analyses in the home laboratories were stored in plastic vials. Further information about the above-described analytical methods is available on the GEOMAR web site (www.geomar.de). For Fe analyses in the incubated bottom-water samples retrieved by benthic landers, aliquots were stored in acid-washed plastic vials and acidified with supra-pure $HNO_3$. All sample aliquots were kept refrigerated until performance of analysis. Fe determinations were performed in the home laboratory by inductively coupled plasma mass spectrometry (ICP-MS Agilent 7500 series). Precision, determined by replicate analyses of calibration standards was ≤ 2%. We assume that all dissolved Fe released from the pore water is present as $Fe^{2+}$. Data on conductivity, temperature, depth (CTD) as well as oxygen bottom-water levels were taken from casts of a Sea-Bird

Electronics, Inc., CTD-system equipped with a water sampling rosette (RO), which were conducted nearby at each station investigated. During the CTD casts CTD-RO 16 and 22, water samples from Niskin bottles were spectrophotometrically analyzed for dissolved phosphate.

2.2.3.2 Solid phase analyses

Porosity was calculated from the weight loss of wet sediment during freeze-drying, assuming a dry solid density of 2 g $cm^{-3}$ based on data published by Böning et al. (2004). Freeze-dried sediments were ground, pre-treated with HCl to drive out carbonate carbon, and analyzed for TOC by flash combustion using a Carlo Erba Elemental Analyzer. Analytical precision for replicate samples was found to be 1%**.** The water content of centrifuge residuals was determined separately in order to recalculate the highly reactive Fe content for dry sediments. Reactive Fe (term used in this article, which mainly combines Fe oxyhydroxides, Fe monosulfides (FeS) and Fe carbonates [Kostka and Luther 1994]) was extracted by adding 20 mL of cold 0.5 mol $L^{-1}$ HCl to 0.5 g of wet sediment in 50 mL centrifuge tubes and shaking the samples for 1 h. The extracts were centrifuged, pipetted off, and filtered through 0.2 $\mu$m CA syringe filters. For total Fe determinations, 0.1 mL samples were added to 5 mL of a reducing Ferrozine solution (1 g $L^{-1}$ Ferrozine in 50 mmol $L^{-1}$ 4-(2-hydroxyethyl)-1-piperazineethanesulfonic acid (HEPES) buffer, pH 7, plus hydroxylammonium chloride (10 g $L^{-1}$)). After 20 min, Fe was measured at 562 nm using a Hitachi U-2001 spectrophotometer. Long-term precision of the in-house standard OMZ-1 was < 5% relative standard deviation.

Total concentrations of phosphorus and aluminum were analyzed by XRF spectrometry using a Philips PW 1480 spectrophotometer (equipped with a rhodium x-ray tube) on samples prepared as lithiumtetraborate fused glass beads (ratio sample:flux 1:6). Loss on ignition was not determined for the samples, and P and Al contents were calculated from unnormalized oxides ($P_2O_5$, $Al_2O_3$). Average values of replicate analyses of different rock reference samples agreed well with the recommended values, and precision was better than 2% and 5% for $P_2O_5$ and $Al_2O_3$, respectively. Excess phosphorus ($P_{excess}$) was calculated as $P_{sample}$-($P{:}Al_{andesite}$ x $Al_{sample}$) to remove the detrital P fraction according to Böning et al. (2004). The P:Al ratio for andesite was derived from Le Maitre (1976).

*2.2.4 Flux calculations*

Diffusive fluxes of $Fe^{2+}$ and $TPO_4$ across the sediment-water interface (SWI) were calculated through application of Fick's first law of diffusion (Boudreau 1997):

$$J = - \Phi_0 D_s (dC/dz) \quad (2.1)$$

where $\Phi_0$ is the porosity at the SWI (0-1 cm), $D_s$ is the effective diffusion coefficient in the sediment at the SWI, and dC/dz is the pore-water gradient estimated from the concentration difference between the uppermost sediment interval (0-1 cm) and the bottom water. Bottom-water concentrations of $TPO_4$ were typically taken from measurements of Niskin bottle samples (463 CTD-RO 22, position shown in Table 2.1). In some cases, bottom-water concentrations of MUC samples seem to be artificially elevated because of sediment dispersal during sampling. However, the resulting difference in flux calculations is negligible. For each sampling site, molecular diffusion coefficients for ferrous iron ($Fe^{2+}$) and phosphate ($HPO_4^-$) in sea water corrected for in situ temperature (CTD measurements) were taken from Boudreau (1997) and further adjusted to in situ salinities and pressures by the Stokes Einstein relationship (Li and Gregory 1974). The effective diffusion coefficient in the sediment was calculated from the adjusted molecular diffusion coefficient and tortuosity (derived by the empirical equation of Boudreau (1997).

Solute concentrations obtained from the benthic chamber incubations were corrected for dilution with Milli-Q water originating from the water-filled Vygon tubing (V = 6.9 mL) connecting the individual syringes and the chamber. Benthic chamber fluxes were calculated from the slope determined by linear regression of the concentration versus the incubation time. During the deployments of BIGO 5 chamber 1 and 13 BIGO chamber 1 and chamber 2, the first data points were deviating from the subsequent ones. This might be due to a variety of reasons, such as contamination during sub-sampling onboard and laboratory handling, mixing of pore water into the enclosed water body when the benthic chamber was driven into the sediment, or failure of the water sampling system. In these cases, the first sample was excluded from the regression to calculate the respective fluxes. At the deeper, more oxygenated stations below ~ 700 m water depth, it was not possible to measure a reliable flux of $Fe^{2+}$ during the course of the benthic chamber incubations.

## 2.3 Results

*2.3.1 Pore water*

Pore-water profiles of $Fe^{2+}$ and $TPO_4$ (from multicorer deployments) are shown in Fig. 2.3. Typically, distinct concentration maxima of $Fe^{2+}$ were located close to the SWI in sediments overlain by the oxygen-depleted water body (< 2 $\mu$mol $L^{-1}$, Fig. 2.3). With increasing sediment depth, concentrations showed a strong decrease, and $Fe^{2+}$ generally was no more detectable within 7 cm to 14 cm below the sediment surface. Highest concentrations of $Fe^{2+}$ were measured in pore waters from the uppermost shelf station (543: 79.8 $\mu$mol $L^{-1}$, 1.5 cm depth) imposing a steep concentration gradient to the SWI. At stations underlying oxic bottom waters, the concentration peak shifted deeper into the sediment, and gradients between the uppermost sediment interval and the bottom water were very small or non-existing. Similar to $Fe^{2+}$, highest $TPO_4$ concentrations typically occurred close to the sediment surface. Peaks generally shifted to greater sediment depth with increasing water depth. Except for the two shallowest stations, the concentrations decreased with increasing sediment depth below the maximum.

Profiles of some major pore-water constituents are exemplarily shown in Fig. 2.4 for three stations from the shallow shelf (Sta. 543), the OMZ core (Sta. 481), and below the OMZ (Sta. 549) to present trends across the transect and to provide the basis to relate $TPO_4$ and $Fe^{2+}$ to the overall geochemistry of the setting (*see* General aspects of pore-water geochemistry). $NH_4^+$ and TA concentrations generally increased with sediment depth, reaching maximum values of 1.3 mmol $L^{-1}$ and 13.7 meq $L^{-1}$, respectively, at shelf Sta. 543. Both $NH_4^+$ and TA markedly decreased with increasing water depth. $SO_4^{2-}$ decreased only slightly with depth and at the shelf station, from 29.5 mmol $L^{-1}$ to 23.5 mmol $L^{-1}$ within 28 cm sediment depth, whereas no gradients were observed at the deeper stations. $TH_2S$ was present only below 18 cm on the shelf, increasing to 760 $\mu$mol $L^{-1}$ in the 26-30 cm interval; and it was undetectable over the sampled sediment length in the two other cores.

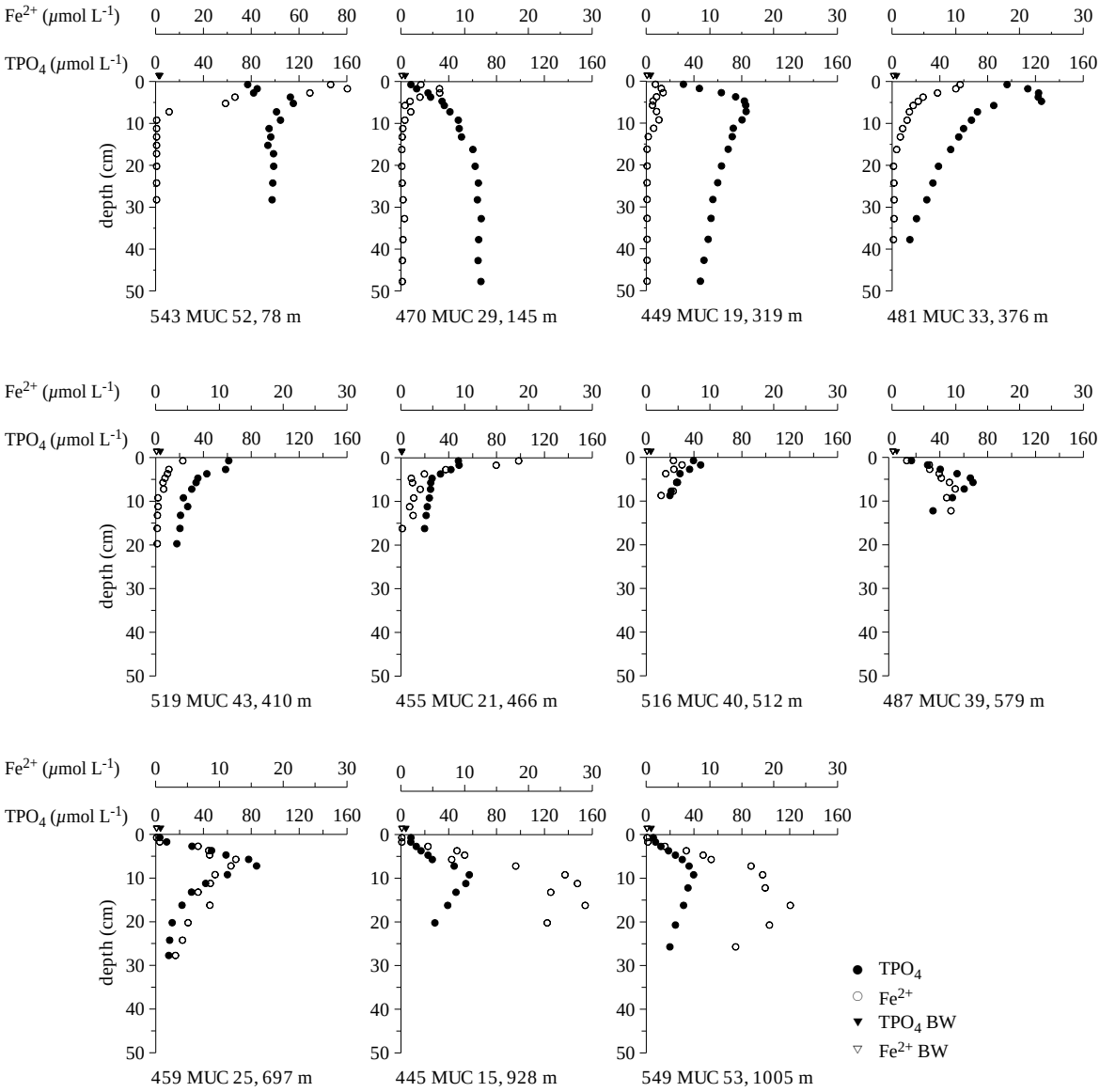


**Fig. 2.3:** Dissolved iron ($Fe^{2+}$, open circles) and phosphate ($TPO_4$, closed circles) pore-water profiles across the transect at 11°S. Sediments were retrieved using a multiple corer. Note: pore water at Sta. 543 and 516 was obtained by rhizon sampling. Triangles (open and closed for $Fe^{2+}$ and $TPO_4$, respectively) indicate bottom-water concentrations, taken from CTD measurements for $TPO_4$.

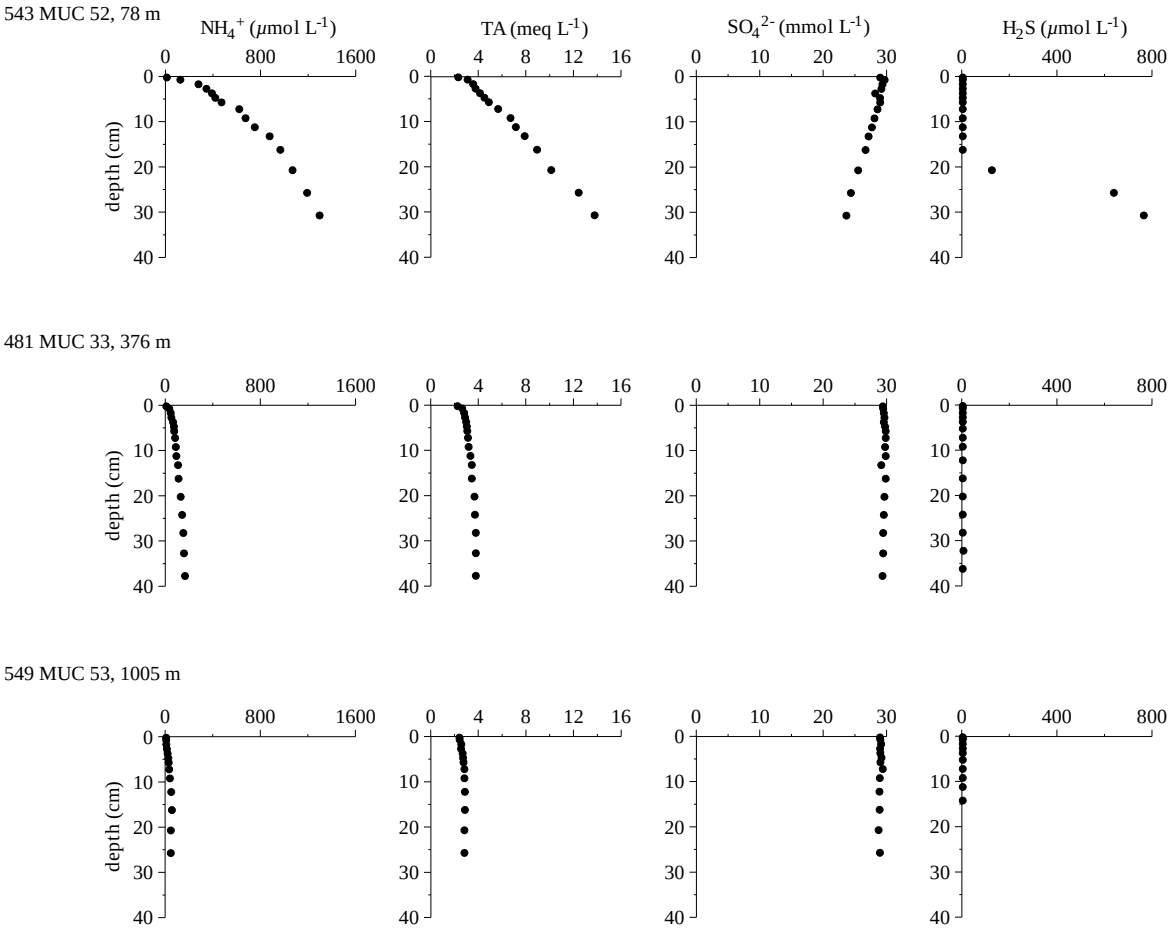


**Fig. 2.4:** Pore-water profiles of major pore-water constituents ($NH_4^+$, TA, $SO_4^{2-}$, and $TH_2S$) shown exemplarily for stations from the shallow shelf (Sta. 543), the OMZ core (Sta. 481), and below the OMZ (Sta. 549). The uppermost data point from each profile (depth of zero) represents the bottom-water concentration.

*2.3.2 Benthic fluxes*

The diffusive fluxes, as well as the chamber fluxes, of $Fe^{2+}$ and $TPO_4$ are presented in Table 2.2 and illustrated in Figs. 2.5A and 2.6A, respectively, with positive fluxes being defined as from the sediment into the water column. The original data from the benthic chamber incubations can be provided from the authors on demand.

Total fluxes of dissolved $Fe^{2+}$ and $TPO_4$ measured in benthic chambers were, in most cases, higher than the diffusive fluxes derived from pore-water gradients (Table 2.2). For sites located within the OMZ, ratios between fluxes measured by the chamber and diffusive fluxes average to 2.1 and 1.3 for $Fe^{2+}$ and $TPO_4$, respectively. Limitations by depth resolution during pore-water sampling, leading to possible underestimation of the gradient's steepness, could have caused part of the discrepancy between the two methods. Furthermore, a significant fraction of the flux may have originated from the degradation of fresh organic matter (indicated by a thin fluffy layer covering numerous of the M77 cores) at the sediment-water interface that was not recorded in the pore-water profiles (Slomp et al. 1998). Contribution of biological pore-water irrigation to benthic chamber fluxes was probably negligible in the OMZ, due to its low significance in anoxic sediments, but may have been more important at the more-oxygenated stations. Consistently, diffusive phosphate fluxes displayed stronger deviations from chamber fluxes at deeper stations below the OMZ (range of ratios between chamber and diffusive fluxes: 3.3 to 8.6). On the shelf, benthic fluxes may have also been influenced by bioirrigation. Despite the strong oxygen deficiency, numerous small polychaetes were observed in sediment cores retrieved by the benthic chambers. This observation is in agreement with Levin et al. (2002) and Gutiérrez et al. (2008), who reported that bioturbating organisms rapidly invade the Peruvian shelf and upper slope during oxygenation events, and may persist for several months after the recurrence of anoxic conditions.

Although these uncertainties are inherent to the pore-water-derived fluxes, these data reveal a spatial pattern across the transect similar to the benthic chamber fluxes. Hence the diffusive flux calculations provide reasonable approximations to total fluxes and can be used for a comparative study in the investigated area.

**Table 2.2**: Chamber flux measurements and diffusive (pore water-derived) fluxes of dissolved $Fe^{2+}$ and $TPO_4$. Fluxes are given in mmol $m^{-2}$ $yr^{-1}$. Averages are given for chamber fluxes and for diffusive fluxes from lander deployments with more than one sediment core recovered, where ± corresponds to the minimum and maximum fluxes; dashes indicate that at the station reliable chamber flux calculations were not possible because $Fe^{2+}$ concentration changes with time did not exceed the analytical error. At the MUC stations chamber fluxes are not available because chambers were not deployed. Also included are flux ratios (chamber:diffusive) of $Fe^{2+}$ and $TPO_4$, molar Fe:P pore-water concentration ratios (calculated for the $Fe^{2+}$ peak position), and organic carbon oxidation rates ($C_{ox}$). $C_{ox}$ was estimated by calculating $HCO_3^-$ fluxes from TA gradients where bottom-water $O_2$ concentration was < 2 $\mu$mol $L^{-1}$, in order to provide for each diffusive $TPO_4$ flux an organic carbon oxidation rate (*see* text for further explanation).

| Station | Device | Cruise leg | Depth (m) | $Fe^{2+}$ flux chamber | $Fe^{2+}$ flux diffusive | ratio $Fe^{2+}$ flux chamber:diffusive | $TPO_4$ flux chamber | $TPO_4$ flux diffusive | ratio $TPO_4$ flux chamber:diffusive | Fe:$TPO_4$ pore water | $C_{ox}$ |
|---|---|---|---|---|---|---|---|---|---|---|---|
| 543 | MUC 52 | 1 | 78 | | 179.3 | | | 193.7 | | 0.95 | 3274* |
| 568 | BIGO 5 | 1 | 85 | 316.1 ± 33.6 | 88.3 ± 0.9 | 3.6 | 169.9 ± 15.9 | 75.8 ± 10.2 | 2.2 | | 2822 ± 399 |
| 470 | MUC 29 | 1 | 145 | | 6.6 | | | 12.3 | | 0.27 | 1220 |
| 16 | BIGO T | 1 | 259 | — | 18.9 | — | 211.4 ± 4.3 | 148.3 | 1.4 | | 3852 |
| 535 | BIGO T3 | 1 | 305 | 3.8 | 6.8 | 0.56 | 209.2 ± 14.2 | 151.1 | 1.4 | | 888 |
| 566 | BIGO T4 | 1 | 309 | 31.3 | 13.0 | 4 | 64.9 ± 12.8 | 83.4 | 0.78 | | 1244 |
| 464 | BIGO 1 | 1 | 315 | 14.9 | 9.8 ± 3.4 | 1.5 | 292.2 ± 1.4 | 144.4 ± 28.1 | 2 | | 2634 ± 729 |
| 586 | BIGO T5 | 1 | 316 | — | 8.4 | - | 83.5 ± 3.2 | 116.9 | 0.71 | | 638 |
| 449 | MUC 19 | 1 | 319 | | 3.3 | | | 73.1 | | 0.04 | 814 |
| 481 | MUC 33 | 1 | 376 | | 23.0 | | | 210.9 | | 0.11 | 1374 |
| 526 | BIGO 3 | 1 | 397 | 30 ± 6.1 | 30.7 | 0.98 | 179.2 ± 13.6 | 227.6 | 0.79 | | 1442 |
| 519 | MUC 43 | 1 | 410 | | 8.5 | | | 123.1 | | 0.07 | 518 |
| 455 | MUC 21 | 1 | 466 | | 31.9 | | | 79.9 | | 0.39 | 216 |
| 516 | MUC 40 | 1 | 512 | | 7.8 | | | 69.7 | | 0.12 | 425* |
| 487 | MUC 39 | 1 | 579 | | 4.3 | | | 25.4 | | 0.16 | |
| 474 | BIGO 2 | 1 | 695 | — | 0.4± 0.4 | — | 20.5 ± 6.1 | 2.9 ± 1.2 | 7.1 | | |
| 459 | MUC 25 | 1 | 697 | | 0.0 | | | -1.0 | | 0.16 | |
| 25 | BIGO | 2 | 716 | — | 0.0 | — | 18.2 | 5.5 | 3.3 | | |
| 445 | MUC 15 | 1 | 928 | | 0.0 | | | 6.3 | | 0.51 | |
| 13 | BIGO | 2 | 978 | — | 0.0 | — | 64.6 ± 1.8 | 7.5 | 8.6 | | |
| 549 | MUC 53 | 1 | 1005 | | 0.0 | | | 2.3 | | 0.74 | |

*Obtained by pore-water squeezing.

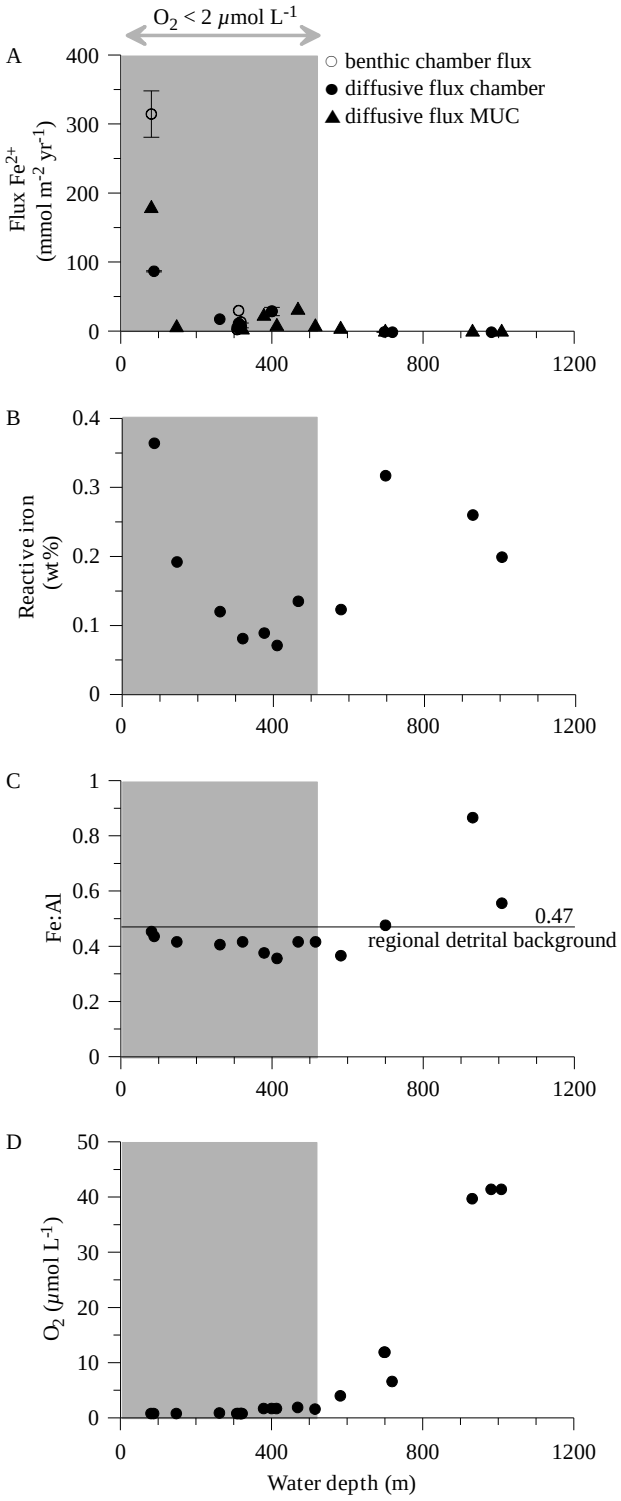


**Fig. 2.5:** Benthic $Fe^{2+}$ fluxes and various parameters along the 11°S transect. (A) Fluxes of dissolved iron ($Fe^{2+}$; mmol $m^{-2}$ $yr^{-1}$). Error bars correspond to minimum and maximum values of double measurements in lander deployments. (B) Reactive Fe contents (wt%) in surface sediments (0-1 cm). (C) Fe:Al ratios in surface sediments (0-1 cm; data from Scholz et al. 2011). Normalized Fe concentrations were used to eliminate the effect of varying dilution with detrital material. The black horizontal line depicts the Fe:Al ratio of the detrital background of 0.47 (andesite in the Andean Arc; Scholz et al. 2011). (D) Concentrations of dissolved $O_2$ in bottom waters. The gray array in each panel represents the OMZ where $O_2$ concentrations were < 2 $\mu$mol $L^{-1}$.

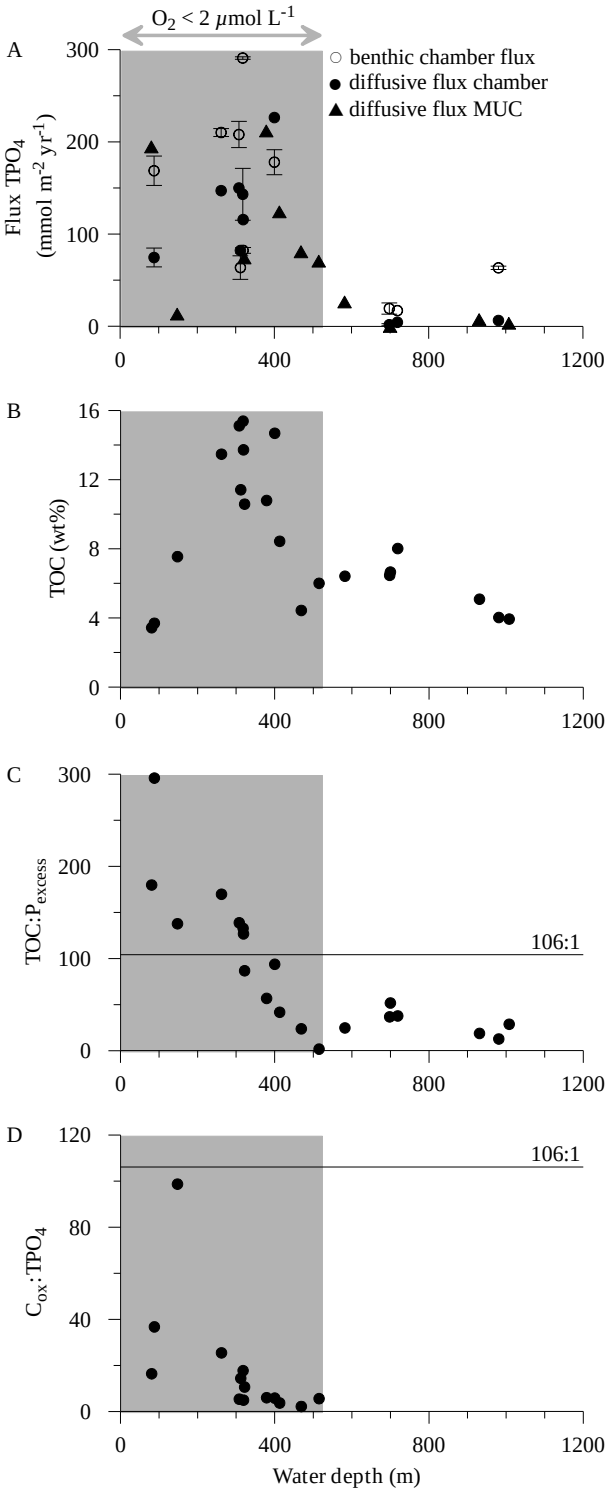


**Fig. 2.6:** Benthic $TPO_4$ fluxes and various parameters along the 11°S transect. (A) Fluxes of dissolved phosphate ($TPO_4$; mmol $m^{-2}$ $yr^{-1}$). Error bars correspond to minimum and maximum values of double measurements in lander deployments. (B) TOC contents (wt%) in surface sediments (0-1 cm). (C) $TOC:P_{excess}$ ratios in surface sediments (0-1 cm). The black horizontal line depicts the TOC:P Redfield ratio of 106:1. (D) $C_{ox}$:$TPO_4$ flux ratios. The black horizontal line depicts the C:P Redfield ratio of 106:1. The gray array in each panel represents the OMZ where $O_2$ concentrations were < 2 $\mu$mol $L^{-1}$).

*2.3.3 Solid phase data*

Sediment geochemical data for reactive Fe, Fe:Al, TOC, and TOC:$P_{excess}$ are provided in Table 2.1, Fig. 2.5B,C (reactive Fe, Fe:Al) and Fig. 2.6B,C (TOC, TOC:$P_{excess}$). Concentrations of reactive Fe were distinctively elevated at the shallow shelf stations, which are subjected to periodic oxygenation events (Gutiérrez et al. 2008), and below 600 m water depth, where $O_2$ levels increased (Fig. 2.5D). Concurrently with these increasing $O_2$ levels, Fe:Al ratios were above average detrital background concentrations of 0.47 (Andean andesite; Scholz et al. 2011). In contrast, at all shallower stations Fe:Al ratios were at and below the average (Fig. 2.5C). Measured TOC values were overall high, with a minimum concentration of 3.5 wt% on the shallow shelf and a maximum concentration of 15.5 wt% in the core of the OMZ (Fig. 2.6B). TOC:$P_{excess}$ ratios were elevated above Redfield ratio (106:1) at water depths ≤ 316 m; below 400 m values were typically below 50 (Fig. 2.6C).

## 2.4 Discussion

*2.4.1 General aspects of pore-water geochemistry*

Peru margin sediments are characterized by significant organic matter degradation rates, which is demonstrated by the concurrent buildup of $NH_4^+$ and TA with sediment depth at all stations (Fig. 2.4). Pore-water gradients of $NH_4^+$ and TA reflect a decrease in organic matter degradation with increasing water depth, which is generally consistent with the organic carbon oxidation rates of 8.2 mmol $m^{-2}$ $d^{-1}$ to 2.1 mmol $m^{-2}$ $d^{-1}$ derived from pore-water modeling that was conducted on selected stations from the same cruise (Bohlen et al. 2011). At the shelf (Sta. 543, Fig. 2.4), decreasing pore-water $SO_4^{2-}$ concentrations and the presence of $TH_2S$ below 20 cm sediment depth indicate intense sulfate reduction. In fact, pore-water modeling indicates that sulfate reduction at the shelf and upper slope contributes 80% to the entire organic carbon degradation (Bohlen et al. 2011). At the deeper stations (Sta. 481 and 549 in Fig. 2.4), no $TH_2S$ was detected, which can be explained by complete precipitation of $TH_2S$ as Fe sulfides or $Fe^{2+}$ availability exceeding sulfide release from sulfate reduction. Under nearly anoxic conditions down to ~ 500 m water depth, reduction of Fe oxyhydroxides in the uppermost sediment horizon supports diffusion of $Fe^{2+}$ into the bottom water (Table 2.2 and Fig. 2.3). In this area near-surface $TPO_4$ and $Fe^{2+}$ enrichments point towards P release during the reductive dissolution of Fe

oxyhydroxides. However, only the pore-water profiles from sites at water depths > 400 m mostly have coincident concentration maxima indicative for the direct coupling of P and Fe cycles. Whereas, at shallower stations, maxima of both species are at slightly different vertical positions, suggesting other P sources and Fe precipitation (*see* Controls on benthic phosphate release). At the more-oxygenated stations below ~ 500 m water depth, the Fe diagenetic front is located deeper in the sediment. Here, pore-water profiles of $Fe^{2+}$ indicate the precipitation of upward-diffusing $Fe^{2+}$ into Fe oxyhydroxides within the thin oxic surface layer (Fig. 2.3). The concurrent decline of $TPO_4$ indicates that this $TPO_4$ is adsorbed or coprecipitated. Below the $TPO_4$ maxima, concentrations decrease until the base of the cores. Similar pore-water profiles of $TPO_4$ have previously been observed in the Peruvian (Froelich et al. 1988) as well as the Pakistan margin OMZ (Woulds et al. 2009) and have been attributed to carbonate fluorapatite precipitation.

### *2.4.2 Controls on benthic iron release*

Dissolved $Fe^{2+}$ fluxes across the sediment-water interface are controlled primarily by the bottom-water oxygen concentrations and the availability of reactive Fe (Pakhomova et al. 2007; Severmann et al. 2010). Under almost anoxic conditions (< 5 $\mu$mol $O_2$ $L^{-1}$; Table 1.1; Fig. 2.5D), elevated $Fe^{2+}$ fluxes were observed down to ~ 600 m water depth. Below this depth, $Fe^{2+}$ fluxes were negligible due to rising oxygen levels in the bottom water.

The highest $Fe^{2+}$ fluxes measured on the shallow shelf at Sta. 543 and Sta. 568 (Table 2.2; Fig. 2.5A) coincide with the highest concentrations of reactive Fe (Fig. 2.5B); indicating high deposition rates of Fe oxyhydroxides. However, due to anoxic conditions right at the sediment surface, these become rapidly altered to Fe sulfides. Fe:Al ratios were close to the detrital background (Fig. 2.5C), which indicates that the reactive Fe is primarily supplied with Al and reflects a high input of detrital Fe oxyhydroxides from the continent. However, it is further plausible that part of the available Fe pool was deposited on the shelf during periods of bottom-water oxygenation, similar to those that were recorded during a long-term time series at a 94 m deep site off Callao (Gutiérrez et al. 2008; M. Graco unpubl.). This time series revealed that, just prior to our research cruise, the shelf was oxygenated concurrent with a strong deepening of the oxycline (Fig. 2.7), reflecting the occurrence of a warming event along the Peruvian coast in association with Kelvin waves and the weakening of the coastal upwelling. During September 2008, the

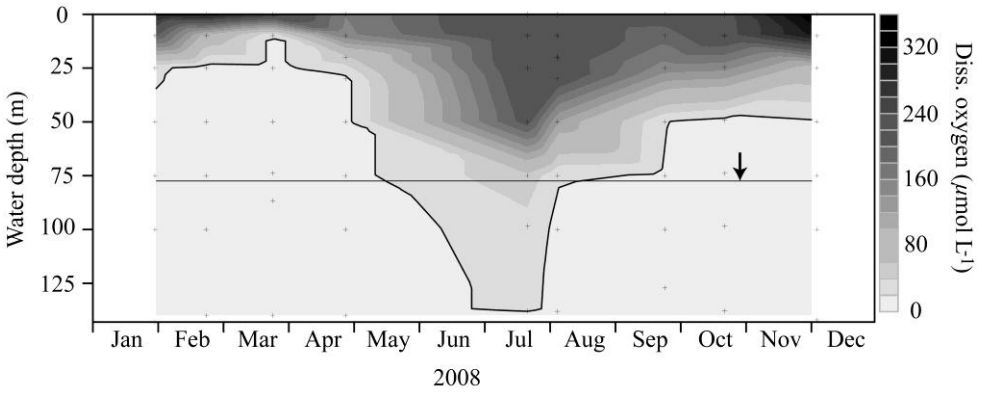


**Fig. 2.7:** Time-series of dissolved (diss.) oxygen ($\mu$mol $L^{-1}$) in the year 2008 off Callao (12°S). The gray horizontal line denotes the water depth of the shallowest station during the R/V *Meteor* cruise M77/1-2. The arrow denotes the start of this cruise. The black isoline corresponds to an oxygen concentration of 20 $\mu$mol $L^{-1}$.

oceanographic conditions normalized and upwelling intensified. During such periods of shelf oxygenation, $Fe^{2+}$ supplied from the deeper, permanent part of the OMZ, may be reoxidized at the interface between anoxic and hypoxic water masses and be deposited on the sea floor. This mechanism has been suggested by Scholz et al. (2011), who showed that deposition and mobilization of trace metals on the Peruvian shelf is strongly affected by ENSO-related high amplitude oscillations of bottom-water oxygen concentrations (cf. Regional setting). During El Niño periods, surface sediments may also receive higher amounts of Fe oxyhydroxides from the continent because of heavy rainfall enhancing surface erosion and sediment discharge (Wells 1990). Dissolution of these Fe oxyhydroxides from either source induces increased $Fe^{2+}$ fluxes when bottom-water conditions turn again anoxic, as was the case in September 2008, about 1 month prior to the begin of our research cruise at the end of October.

Intense sulfate reduction in the shelf sediments leads to the formation of Fe sulfides, which would be ultimately buried under permanently anoxic conditions. Under oxic bottom-water conditions, Fe sulfides may be recycled to the sediment surface by bioturbation, and reoxidized to Fe oxyhydroxides (Jørgensen and Nelson 2004). As mentioned in the results section, there is a high potential for bioturbation at the shelf. However, the extent to which bioturbation affects the cycling of different Fe phases under oscillating oxic and anoxic bottom-water conditions and contributes to enhance overall $Fe^{2+}$ fluxes on the shelf is not clear yet.

Within the core OMZ, $Fe^{2+}$ fluxes were distinctly lower than at the 80 m stations, even

though nearly anoxic bottom-water conditions (Table 2.1; Fig. 2.5A) provided suitable conditions for reductive Fe dissolution and release of $Fe^{2+}$ across the benthic boundary. As oxygenation events can be assumed to occur more rarely down to these water depths, low bottom-water oxygen conditions in this region are supposed to be a persistent feature. Under such conditions, the reactive Fe pool will become progressively depleted over time. This is in agreement with the low reactive Fe concentrations as well as Fe:Al ratios significantly below the detrital background (Fig. 2.5B,C). Apparently, there is a strong imbalance between the reductive losses and the replenishment by detrital inputs from the continent in this region of the Peruvian margin.

Below about 700 m, increasing bottom-water oxygen concentrations (Table 2.1; Fig. 2.5D) cause the deepening of the redox front. Here, $Fe^{2+}$ will be recycled within the sediment through reoxidation and reprecipitation in the surface layer (Fig. 2.3). Consequently, at these stations there was no flux of $Fe^{2+}$ into the bottom water (Table 2.2; Fig. 2.5A). Both Fe:Al ratios and reactive Fe contents showed their maximum at ~ 900 m water depth (Fig. 2.5B,C) and showed decreasing values below. This strongly suggests that a large part of the Fe enrichment at the sediment surface derives from oxidative removal of $Fe^{2+}$ that has been relocated from the core of the OMZ into the more-oxygenated deeper water layers. This is consistent with previous studies within the Arabian and Mexican OMZs observing Fe enrichments linked to mechanisms of oxidative scavenging and OMZ relocation in sediments located below the OMZ (Van der Weijden et al. 1999; Nameroff et al. 2002).

### *2.4.3 Controls on benthic phosphate release*

The distribution of $TPO_4$ fluxes along the transect (Fig. 2.6A) differs from that of $Fe^{2+}$ (Fig. 2.5A), indicating different control mechanisms. While the release of $Fe^{2+}$ from the sea bed is largely determined by the availability of reactive iron that is reduced at the sediment surface, there are several sedimentary P sources that may contribute to the $TPO_4$ flux, comprising organic matter, iron bound P, and fish debris (Schenau and De Lange 2001).

With regard to P release driven by the reductive dissolution of Fe oxyhydroxides, the transect can be subdivided into distinct zones. At the sites shallower than 400 m water depth, non-coincident peaks of $Fe^{2+}$ and $TPO_4$ indicate that $TPO_4$ liberation is at least

partially decoupled from the reductive dissolution of Fe oxyhydroxides. In contrast, pore-water profiles of $TPO_4$ and $Fe^{2+}$ from below 400 m water depth display similar trends, suggesting concurrent P release from the reductive dissolution of Fe oxyhydroxides. At all sites, the molar Fe:P ratios in the pore water at the peak position of $Fe^{2+}$ ranged from 0.04 to 0.95 (Table 2.2), which is similar to Fe:P ratios measured in coastal sediments under anoxic conditions (Gunnars and Blomqvist 1997; Rozan et al. 2002; Lehtoranta and Heiskanen 2003). Such low Fe:P ratios indicate that, in addition to P release during reductive Fe dissolution, there was a further P source. If P release would be driven by the reductive Fe dissolution alone, one would expect Fe:P ratios in the range of 2 to 20 (Slomp et al. 1996; Gunnars and Blomqvist 1997; Anschutz et al. 1998). Another explanation for these low Fe:P ratios and the decoupling of pore-water $TPO_4$ and $Fe^{2+}$ is the rapid formation of Fe sulfides (Rozan et al. 2002). For sites shallower than 400 m, sulfate reduction represents the major pathway of organic matter degradation (Bohlen et al. 2011), so that free dissolved $Fe^{2+}$ can only exist in a narrow zone (< 10 cm) below the sediment surface.

At water depths between 250 m and 600 m ($O_2$ < 5 $\mu$mol $L^{-1}$), reactive Fe oxyhydroxides were almost absent (Fig. 2.5B); hence, Fe-bound P can obviously not serve as an important P source. At these sites, P release might be driven by organic matter degradation and dissolution of fish scales (*see* below). Only at the shallow shelf (Sta. 543), where the Fe:P ratio was close to unity, and at stations deeper than 600 m, Fe-bound P might be of some importance to the P cycle. On the shallow shelf, Fe oxyhydroxides are mainly supplied by the discharge of detrital sediments and reoxidation of dissolved $Fe^{2+}$ when the shelf is oxygenated. Below 600 m water depth, Fe oxyhydroxides accumulate in the sediments, mainly due to the precipitation of dissolved $Fe^{2+}$ at the lower oxycline (Scholz et al. 2011). However, at these stations both Fe and P are recycled within the sediment resulting in low to zero fluxes.

In general, the deposition and degradation of organic matter in surface sediments underlying the OMZ is enhanced by enormous rates of surface-water productivity (Suess 1981). Consequently, organically bound P can be assumed as a major source contributing to the benthic $TPO_4$ flux. This is corroborated by the general agreement between $TPO_4$ fluxes (Fig. 2.6A) and the TOC content in surface sediments along the entire transect except the shallow shelf (Fig. 2.6B). Despite the lower TOC contents on the shelf, high

organic carbon degradation rates of up to 8.2 mmol $m^{-2}$ $d^{-1}$ were calculated (Bohlen et al. 2011). Transient bottom-water oxygen levels are assumed to enhance organic matter degradation in sediments, leading to comparatively low TOC contents (Aller 1994). Another explanation is that at this site the solid phase composition is likely altered due to higher detrital sediment input. Below 600 m water depth, $TPO_4$ fluxes decreased distinctively despite still relatively high levels of TOC contents. This is due to increasing bottom-water $O_2$ levels and decreasing carbon degradation rates (Bohlen et al. 2011). Typically, high TOC:P ratios are observed in oxygen-deficient environments, indicating the preferential release of P over C (Ingall et al. 1993). The TOC:$P_{excess}$ ratio shown in Fig. 2.6C is corrected for the detrital P fraction (Böning et al. 2004) and represents a measure for the total reactive P. Down to 300 m water depth, the TOC:$P_{excess}$ ratios in surface sediments were distinctively elevated above the Redfield ratio, which is in agreement with TOC:$P_{excess}$ ratios measured previously in the same area (Böning et al. 2004). At sites below 300 m water depth, the strong decrease of TOC:$P_{excess}$ ratios may indicate the formation of authigenic P bearing minerals and the accumulation of fish debris. Particularly, between 300 m and 400 m water depth, where high $TPO_4$ fluxes correspond to low TOC:$P_{excess}$ ratios in the sediment, it is likely that P regeneration from organic matter is masked by the formation of authigenic minerals. Phosphorus accumulation in form of phosphorites is well known for the Peruvian OMZ (Glenn and Arthur 1988), and we also found numerous macroscopic phosphorite concretions in sediment cores retrieved from water depths between 300 m and 600 m.

In order to provide a first-order estimate on how the measured $TPO_4$ fluxes relate to available P-sources in the sediment, we exemplarily calculated "theoretical" $TPO_4$ fluxes for the sites at 85 m and 309 m water depth that would result from organic matter degradation in surface sediments (assuming Redfield ratio) and Fe-bound P. $TPO_4$ fluxes related to the reduction of Fe oxyhydroxides ($TPO_4$-Fe) were calculated from benthic $Fe^{2+}$ fluxes (Table 2.2) and the molar Fe:P ratio of Fe oxyhydroxides, which is typically about 10 (Slomp et al. 1996). P release from the breakdown of organic matter ($TPO_4$-$C_{ox}$) was derived by approximating organic carbon degradation ($C_{ox}$, Table 2.2) in surface sediments underneath a nearly anoxic water body ($O_2$ < 2 $\mu$mol $L^{-1}$) using TA pore-water gradients. $C_{ox}$ can be calculated from TA gradients, because $HCO_3^-$ rather than $CO_2$ is produced in anoxic diagenetic pathways (Froelich et al. 1979). Under near neutral

conditions, $HCO_3^-$ contributes more than 90% to TA, so that the TA gradient can be reasonably well applied to calculate a diffusive $HCO_3^-$ flux, and, hence, use it as a proxy for $C_{ox}$. In addition, the values presented in Table 2.2 are in good agreement with modeled values of $C_{ox}$ (Bohlen et al. 2011). The combined average flux of $TPO_4$-$C_{ox}$ and $TPO_4$-Fe at the shelf (78-85 m, $n = 2$) was 53.5 mmol $m^{-2}$ $yr^{-1}$ and in the core of the OMZ (305-319 m, $n = 5$) was 13.0 mmol $m^{-2}$ $yr^{-1}$. We are aware that the P release calculated from the $Fe^{2+}$ flux represents a minimum estimate because it does not account for $Fe^{2+}$ that is precipitated as FeS. These fluxes are a factor of 3 and 12 lower than the measured fluxes, which is in agreement with low molar $C_{ox}$:$TPO_4$ ratios of benthic fluxes (Fig. 2.6D, calculated from $C_{ox}$ and $TPO_4$, Table 2.2). These results highlight the preferential release of P over C with respect to the average composition of marine organic matter from OMZ sediments. At the 85 m station, some of the mismatch between theoretical and measured $TPO_4$ fluxes could be leveled out, if the Fe:P ratio of Fe oxyhydroxides was distinctively lower. However, at 309 m, and at similar sites with low $Fe^{2+}$ but high $TPO_4$ fluxes, any change in the Fe:P ratio would not help to further resolve the mismatch.

Apart from the non-Redfield degradation of organic matter there are a few other processes that may explain the high $TPO_4$ fluxes. Fish scales are exceptionally abundant in sediments of the Peruvian OMZ (Suess 1981), hence their dissolution may represent an important source of pore-water $TPO_4$ (Suess 1981; Schenau and De Lange 2001). In addition, storage and release of P by microorganisms and protozoans under oscillating oxic and anoxic conditions has been supposed to contribute to the benthic $TPO_4$ flux (Sannigrahi and Ingall 2005). Sannigrahi and Ingall (2005) provided evidence for the accumulation of polyphosphates in oxic sediments, whereas in anoxic sediments polyphosphates were absent. This has been interpreted as release of P under anoxic conditions when these organisms degrade their intracellular polyphosphate storage that was built up under oxic conditions, to gain energy. Recently, transient uptake and release of P under oscillating redox conditions has been reported for the giant sulfide-oxidizing bacteria *Thiomargarita namibiensis* and members of the genus *Beggiatoa* (Schulz and Schulz 2005; Brock and Schulz-Vogt 2011; Goldhammer et al. 2010). Widespread occurrence of filamentous sulfur bacteria on the Peruvian shelf and upper slope was observed in sediment samples and in sea-floor images acquired during the same cruise

(T. Mosch unpubl.). In fact, sulfur bacteria of the genera *Beggiatoa* and *Thioploca* are very common in OMZ sediments of the Peruvian and Chilean continental shelf as well as in other OMZs worldwide (Gallardo 1977; Levin et al. 2002; Gutiérrez et al. 2008). Within the context of episodic oxygenation events that occur at the Peruvian shelf and upper slope (Gutiérrez et al. 2008), we suggest that *Beggiatoa* can probably enhance $TPO_4$ fluxes via the above-described P metabolism. Sulfur bacteria have been further suggested to be involved in the formation of apatite, which contributes to mitigate P relase from the sea bed (Schulz and Schulz 2005). During $^{33}P$ radiotracer experiments, Goldhammer et al. (2010) observed the greatest conversion rates of phosphate to apatite mediated by sulfur bacteria under anoxic conditions. Apatite formation is indicated by decreasing phosphate pore-water concentrations with sediment depth at all sites except for the shelf. Despite constant P concentrations with increasing sediment depth, apatite formation can be also assumed for the shelf since in the absence of precipitation P would accumulate in the pore water due to organic matter degradation and the associated P release. However, it can not be resolved if, and to what extent, release of P from microbes contributes to apatite formation.

In conclusion, the OMZ represents an important $Fe^{2+}$ and $TPO_4$ source to the bottom water. The core of the OMZ (~ 250-500 m), with rather stable bottom-water $O_2$ levels close to anoxia, is characterized with persistent but comparatively low $Fe^{2+}$ and high $TPO_4$ fluxes. This is in strong contrast to the shelf region, which is subjected to oscillating bottom-water $O_2$ conditions triggering a complex biogeochemical reaction network of Fe, P, and S turnover, resulting in transient high $Fe^{2+}$ and $TPO_4$ release under anoxia. This renders the shelf as a sensitive region that provides limiting nutrients to the surface water, allowing extensive phytoplankton blooms to develop in the Peruvian upwelling system.

### *2.4.4 Global significance of benthic phosphorus and iron fluxes from OMZs*

To evaluate the importance of $TPO_4$ and $Fe^{2+}$ fluxes in the Peruvian OMZ from a more general perspective, we compiled a comparative data set from other coastal upwelling and OMZ regions (Fig. 2.8). Overall, $TPO_4$ fluxes measured in this study generally exceed those reported from other OMZs throughout the world. The global benthic $TPO_4$ flux from oxic shelf and slope sediments (> 20 $\mu$mol $L^{-1}$ $O_2$) has recently been estimated as

$75 \times 10^{10}$ mol $yr^{-1}$ for an area of $90 \times 10^{6}$ $km^2$ (Wallmann 2010), corresponding to an average $TPO_4$ flux of 8 mmol $m^{-2}$ $yr^{-1}$. The average $TPO_4$ flux from the Peruvian OMZ (< 2 $\mu$mol $L^{-1}$ $O_2$) exceeds the average global flux from oxic shelf and slope environments by a factor of 17, which highlights the significance of anoxic sediments underlying the Peruvian and other OMZs as major P source to the ocean.

Measurements of benthic Fe fluxes from continental shelf and slope sediments are only available from a very limited number of field studies. However, comparison with existing data reveals that fluxes presented in this study are among the highest recorded so far (Fig. 2.8). The highest total fluxes, associated with the highest variability, are observed on the shallow shelves, which typically experience the most intense environmental perturbations on various time scales. Including all stations of this study (Table 2.2), the resulting average flux in the Peruvian OMZ (< 2 $\mu$mol $O_2$ $L^{-1}$) is 44 mmol $m^{-2}$ $yr^{-1}$, which is comparable to the average of 49 mmol $m^{-2}$ $yr^{-1}$ (white bars in Fig. 2.8) calculated for the California borderland basins (San Pedro and Santa Monica). Similar to the Peruvian shelf and upper slope, these basins are periodically ventilated (Berelson 1991), resulting in variable bottom-water oxygen concentrations, and, hence, variable Fe fluxes (Severmann et al. 2010). The above average includes two high outlier fluxes (207 mmol $m^{-2}$ $yr^{-1}$, San Pedro basin; 150 mmol $m^{-2}$ $yr^{-1}$, Santa Monica basin; Severmann et al. 2010), measured when the basins were highly oxygen-deficient (< 5 $\mu$mol $O_2$ $L^{-1}$). Fluxes measured when these sites were slightly more oxygenated (< 10 $\mu$mol $O_2$ $L^{-1}$, 5 mmol $m^{-2}$ $yr^{-1}$) fall within the range of values measured in the Peruvian OMZ core at water depths > 85 m. Obviously, similar mechanisms of reoxidation during oxygenation periods and subsequent remobilization (resulting in highly elevated fluxes) during anoxic periods (*see* Controls on benthic iron release) are active in these settings.

Exclusion of the highest Fe fluxes measured at the Peruvian shelf stations (543, 568) and the outliers of the California borderland basins results in considerably lower average fluxes (gray bars in Fig. 2.8), which are comparable to those measured at river-dominated shelf sites (high reactive Fe input) from the Oregon and California margin (Severmann et al. 2010) or to those measured in the OMZ off Pakistan. Regardless of which data set is chosen, it is obvious that OMZs are major sources of dissolved Fe compared to normal marine environments. Based on an empirical relationship between Fe fluxes and organic carbon oxidation rates for settings > 20 $\mu$mol $L^{-1}$ $O_2$, Elrod et al. (2004) estimated a

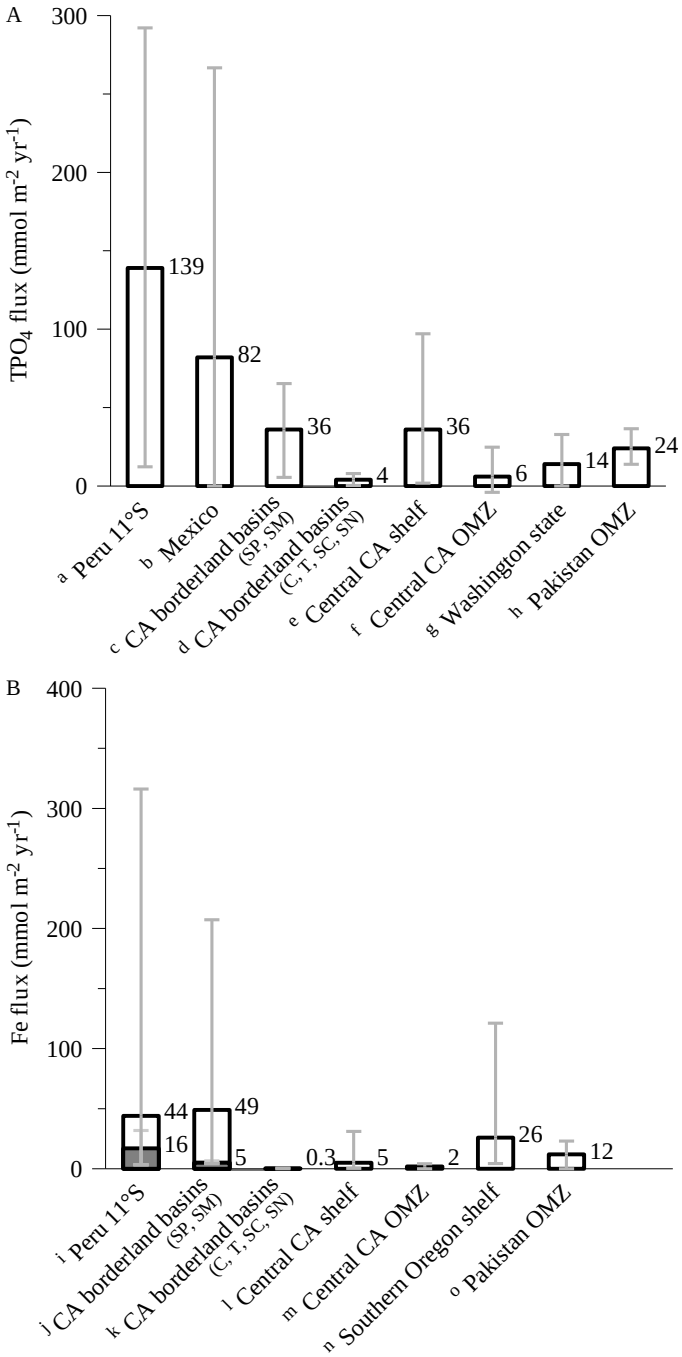


**Fig. 2.8:** Comparison of (A) phosphate ($TPO_4$) and (B) iron ($Fe^{2+}$) flux data from 11°S (total average of benthic chamber and diffusive fluxes for the OMZ ($O_2$ < 2 $\mu$mol $L^{-1}$, ~ 80-510 m water depth) to data from other oxygen-deficient environments. Fluxes are given in mmol $m^{-2}$ $yr^{-1}$. Values comprise single data points or total averages of all fluxes for any specific region. Fluxes shown by gray bars were calculated excluding high outlier Fe fluxes (*see* text for further explanation). (A) $TPO_4$ fluxes: [a]Peru 11°S; this study (water depth: 80-510 m, $O_2$: < 2 $\mu$mol $L^{-1}$), [b]Mexico; Hartnett and Devol 2003 (water depth: 100-1020 m, $O_2$: 0-6 $\mu$mol $L^{-1}$), [c]California borderland basins (SP = San Pedro basin, SM = Santa Monica basin); Berelson et al. 1987; Jahnke 1990; McManus et al. 1997; Hammond et al. 2004 (water depth: 900-910 m, $O_2$: 4-10 $\mu$mol $L^{-1}$), [d]California borderland basins (C = Catalina basin, T = Tanner basin, SC = San Clemente basin, SN = San Nicholas basin); Berelson et al. 1987; Bender et al. 1989; Ingall and Jahnke 1997; McManus et al. 1997; Hammond et al. 2004 (water depth: 1300-2070 m, $O_2$: 17-65 $\mu$mol $L^{-1}$),

**Fig. 2.8, continued:** [e]Central California shelf; McManus et al. 1997; Berelson et al. 2003; Hammond et al. 2004 (water depth: 95-200 m, $O_2$: 64-185 $\mu$mol $L^{-1}$), [f]Central California OMZ; Reimers et al. 1992; McManus et al. 1997 (water depth: 530-1370 m, $O_2$: 16-65 $\mu$mol $L^{-1}$), [g]Washington State; Devol and Christensen 1993 (water depth: 40-630 m, $O_2$: 25-240 $\mu$mol $L^{-1}$), [h]Pakistan OMZ; Woulds et al. 2009 (water depth: 140-940 m, $O_2$: 1-3 $\mu$mol $L^{-1}$, post-monsoon). (B) Fe fluxes: [i]Peru 11°S; this study (water depth: 80-510 m, $O_2$: < 2 $\mu$mol $L^{-1}$), [j]California borderland basins (SP = San Pedro basin, SM = Santa Monica basin); McManus et al. 1997; Elrod et al. 2004; Severmann et al. 2010 (water depth: 880-910 m, $O_2$: 4-10 $\mu$mol $L^{-1}$), [k]California borderland basins (C = Catalina basin, T = Tanner basin, SC = San Clemente basin, SN = San Nicholas basin); McManus et al. 1997; Elrod et al. 2004 (water depth: 1300-2070 m, $O_2$: 17–65 $\mu$mol $L^{-1}$ ), [l]Central California shelf; McManus et al. 1997; Elrod et al. 2004; Severmann et al. 2010 (water depth: 95-200 m, $O_2$: 64-185 $\mu$mol $L^{-1}$), [m]Central California OMZ; McManus et al. 1997, Elrod et al. 2004 (water depth: 530-1370 m, $O_2$: 16-65 $\mu$mol $L^{-1}$), [n]Southern Oregon shelf; Severmann et al. 2010 (water depth: 90-190 m, $O_2$: 60-142 $\mu$mol $L^{-1}$), [o]Pakistan OMZ; Law et al. 2009 (water depth: 140-940 m, $O_2$: 1- 3 $\mu$mol $L^{-1}$, post-monsoon).

dissolved Fe input of 8.9 x $10^{10}$ mol $yr^{-1}$ for the global shelf area (3 x $10^7$ $km^2$). This corresponds to an average Fe flux of 3 mmol $m^{-2}$ $yr^{-1}$, which is obviously much lower than the average benthic Fe fluxes from sediments underlying oxygen-deficient waters and, hence, must be regarded as a minimum estimate.

An important pathway of Fe input to the surface ocean is atmospheric dust deposition. The following "back-of-the-envelope" calculation may illustrate how hotspots of benthic Fe mobilization compare to areas of high Fe input by dust deposition. One of the largest areas of atmospheric dust deposition is the tropical North Atlantic. Based on a composite map of dust delivery to the global oceans (Jickells et al. 2005) we calculated that the area of the North Atlantic hotspot (between 0-30°N) annually receives about 9.6 x $10^{10}$ kg dust, which translates into dissolved Fe fluxes of 3.4 x $10^7$ kg $yr^{-1}$ to 3.4 x $10^8$ kg $yr^{-1}$ that may become biologically available (assuming an Fe content of 3.5% in soil dust and an aerosol Fe solubility of 1% to 10% [Jickells and Spokes 2001]). Projecting the average Fe flux of 16 mmol $m^{-2}$ $yr^{-1}$ to 44 mmol $m^{-2}$ $yr^{-1}$ (Fig. 2.8) to a total area of the Peruvian OMZ ($O_2$ < 0.5 mL $L^{-1}$ or 22 $\mu$mol $L^{-1}$) of 77,000 $km^2$ (Helly and Levin 2004) adds up to a total benthic flux of 6.9 x $10^7$ kg $yr^{-1}$ to 1.9 x $10^8$ kg $yr^{-1}$ and indicates that the source strengths of these completely different input mechanism are comparable in magnitude. However, at this time it is not clear, if, and on which time scales, benthic Fe release may be considered as a potentially important source to the surface ocean. At least this could be significant in coastal upwelling systems with low input of atmospheric dust, such as the Peruvian margin.

This study underlines the role of sediments underlying OMZs as important $Fe^{2+}$ and $TPO_4$ sources to the bottom water, which provide important feedbacks that may affect surface-

water primary-productivity (Wallmann 2003), and, hence, accelerate the worldwide expansion of OMZs. Therefore, the investigation of benthic-pelagic coupling in oxygen-deficient waters along continental margins will require explicit consideration in the future.

## Acknowledgments

We thank the captain and crew of the R/V *Meteor* for their effort and help during cruise M77/1-2, and A. Bleyer, B. Domeyer, M. Dibbern, R. Ebbinghaus, S. Kriwanek, D. Rau, and R. Surberg for help with biogeochemical analyses onboard and in the home laboratory. Furthermore, many thanks are due to B. Bannert, A. Petersen, and M. Türk for their technical assistance during benthic lander deployments; to P. Appel for management of XRF measurements; and, as well, to E. Piñero for her help with data treatment. We appreciate the editorial handling by Dr. Ronnie Glud and the constructive comments of three anonymous reviewers, which very much helped to improve the manuscript. This is a contribution of the Sonderforschungsbereich 754 "Climate – Biogeochemistry Interactions in the Tropical Ocean", which is supported by the Deutsche Forschungsgemeinschaft.

## References

Aller, R. C. 1994. Bioturbation and remineralization of sedimentary organic matter: Effects of redox oscillation. Chem. Geol. **144:** 331–345.

Anschutz, P., S. Zhong, and B. Sundby. 1998. Burial efficiency of phosphorus and the geochemistry of iron in continental margin sediments. Limnol. Oceanogr. **43:** 53-64.

Bakun, A. 1985. Comparative studies and the recruitment problem: Searching for generalizations. CalCOFI Rep. **26:** 30-40.

Bender, M., R. Jahnke, R. Weiss, W. Martin, D. T. Heggie, J. Orchardo, and T. Sowers. 1989. Organic carbon oxidation and benthic nitrogen and silica dynamics in San Clemente Basin, a continental borderland site. Geochim. Cosmochim. Acta **53:** 685-697.

Berelson, W. M., D. E. Hammond, and K. S. Johnson. 1987. Benthic fluxes and the cycling of biogenic silica and carbon in two southern California borderland basins. Geochim. Cosmochim. Acta **51:** 1354-1363.

Berelson, W. M. 1991. The flushing of two deep-sea basins, southern California borderland. Limnol. Oceanogr. **36:** 1150-1166.

Berelson, W., J. McManus, K. Coale, K. Johnson, D. Burdige, T. Kilgore, D. Colodner, F. Chavez, D. Kudela, and J. Boucher. 2003. A time series of benthic flux measurements from Monterey Bay, CA. Cont. Shelf Res. **23:** 457-481.

Bohlen, L., A. W. Dale, S. Sommer, T. Mosch, C. Hensen, A. Noffke, F. Scholz, and K. Wallmann. 2011. Benthic nitrogen cycling traversing the Peruvian oxygen minimum zone. Geochim. Cosmochim. Acta **75:** 6094-6111.

Böning, P., H.-J. Brumsack, M. E. Böttcher, B. Schnetger, C. Kriete, J. Kallmeyer, and S. L. Borchers. 2004. Geochemistry of Peruvian near-surface sediments. Geochim. Cosmochim. Acta **68:** 4429-4451.

Boudreau, B. P. 1997. Diagenetic models and their implementation. Springer.

Brock, J., and H. N. Schulz-Vogt. 2011. Sulfide induces phosphate release from polyphosphate in cultures of a marine *Beggiatoa* strain. ISME J. **5:** 497-506.

Devol, A. H., and J. P. Christensen. 1993. Benthic fluxes and nitrogen cycling in sediments of the continental margin of the eastern North Pacific. J. Mar. Res. **51:** 345-372.

Elrod, V. A., W. M. Berelson, K. H. Coale, and K. S. Johnson. 2004. The flux of iron from continental shelf sediments: A missing source for global budgets. Geophys. Res. Lett. **31:** L12307, doi: 10.1029/2004GL020216

Froelich, P. N., G. P. Klinkhammer, M. L. Bender, N. A. Luedtke, G. R. Heath, D. Cullen, and P. Dauphin. 1979. Early oxidation of organic matter in pelagic sediments of the eastern equatorial Atlantic: Suboxic diagenesis. Geochim. Cosmochim. Acta **43:** 1075-1090.

Froelich, P. N., M. A. Arthur, W. C. Burnett, M. Deakin, V. Hensley, R. Jahnke. L. Kaul, K.-H. Kim, R. Roe, A. Soutar, and C. Vathakanon. 1988. Early diagenesis of organic matter in Peru continental margin sediments: Phosphorite precipitation. Mar. Geol. **80:** 309-343.

Fuenzalida, R., W. Schneider, J. Garcés-Vargas, L. Bravo, and C. Lange. 2009. Vertical and horizontal extension of the oxygen minimum zone in the eastern South Pacific Ocean. Deep-Sea Res. II **56:** 992-1003.

Gallardo, V. A. 1977. Large benthic microbial communities in sulfide biota under Peru-Chile subsurface countercurrent. Nature **268:** 331-332.

Glenn, C. R., and M. A. Arthur. 1988. Petrology and major element geochemistry of Peru margin phosphorites and associated diagenetic minerals: Authigenesis in modern organic-rich sediments. Mar. Geol. **80:** 231-267.

Goldhammer, T., V. Brüchert, T. G. Ferdelman, and M. Zabel. 2010. Microbial sequestration of phosphorus in anoxic upwelling sediments. Nat. Geosc. **3:** 557-561.

Grasshoff, K., M. Erhardt, and K. Kremling. 1999. Methods of seawater analysis. 3rd ed., Wiley-VCH.

Gunnars, A., and S. Blomqvist. 1997. Phosphate exchange across the sediment-water interface when shifting from anoxic to oxic conditions—an experimental comparison of freshwater and brackish-marine systems. Biogeochemistry **37:** 203-226.

Gutiérrez, D., E. Enríquez, S. Purca, L. Quipúzcoa, R. Marquina, G. Flores, and M. Graco. 2008. Oygenation episodes on the continental shelf of central Peru: Remote forcing and benthic ecosystem response. Prog. Oceanogr. **79:** 177-189.

Hammond, D. E., K. M. Cummins, J. McManus, W. M. Berelson, G. Smith, and F. Spagnoli. 2004. Methods for measuring benthic nutrient flux on the California margin: Comparing shipboard core incubations to in situ lander results. Limnol Oceanogr.: Methods **2:** 146-159.

Hartnett, H. E., and A. H. Devol. 2003. Role of a strong oxygen-deficient zone in the preservation and degradation of organic matter: A carbon budget for the continental margins of northwest Mexico and Washington State. Geochim. Cosmochim. Acta **67:** 247-264.

Helly, J. J., and L. A. Levin. 2004. Global distribution of naturally occurring marine hypoxia on continental margins. Deep-Sea Res. I **51:** 1159-1168.

Hutchins, D. A., G. R. DiTullio, Y. Zhang, and K. W. Bruland. 1998. An iron limitation mosaic in the California upwelling regime. Limnol. Oceanogr. **43:** 1037-1045.

Ingall, E. D., R. M. Bustin, and P. Van Cappellen. 1993. Influence of water column anoxia on the burial and preservation of carbon and phosphorus in marine shales. Geochim. Cosmochim. Acta **57:** 303-316.

Ingall, E., and R. Jahnke. 1997. Influence of water column anoxia on the elemental fractionation of carbon and phosphorus during sediment diagenesis. Mar. Geol. **139:** 219-229.

Ivanenkov, V. N., and Y. I. Lyakhin. 1978. Determination of total alkalinity in seawater, p. 110-114. *In* O. K. Bordovsky and V. N. Invanenkov [eds.], Methods of hydrochemical investigations in the Ocean. Nauka Publ. House.

Jahnke, R. A. 1990. Early diagenesis and recycling of biogenic debris at the seafloor, Santa Monica Basin, California. J. Mar. Res. **48:** 413-436.

Jensen, H. S., P. B. Mortensen, F. Ø. Andersen, E. Rasmussen, and A. Jensen. 1995. Phosphorus cycling in a coastal marine sediment, Aarhus Bay, Denmark. Limnol. Oceanogr. **40:** 908-917.

Jickells, T. D., and L. J. Spokes. 2001. Atmospheric iron inputs to the oceans, p. 85-121. *In* D. R. Turner and K. A. Hunter [eds.], The biogeochemistry of iron in seawater. Wiley.

Jickells, T. D., Z. S. An, K. K. Andersen, A. R. Baker, G. Bergametti, N. Brooks, J. J. Cao, P. W. Boyd, R. A. Duce, K. A. Hunter, K. Kawahata, N. Kubilay, J. laRoche, P. S. Liss, N. Mahowald, J. M. Prospero, A. J. Ridgwell, I. Tegen, and R. Torres. 2005. Global iron connections between desert dust, ocean biogeochemistry, and climate. Science **308:** 67-71.

Johnson, K. S., F. P. Chavez, and G. E. Friedrich. 1999. Continental shelf sediment as a primary source of iron for coastal phytoplankton. Nature **398:** 697-700.

Jørgensen, B. B., and D. C. Nelson. 2004. Sulfide oxidation in marine sediments: Geochemistry meets microbiology. GSA Spec. Pap. **379:** 63-81.

Kostka, J. E., and G. W. Luther III. 1994. Partitioning and speciation of solid phase iron in saltmarsh sediments. Geochim. Cosmochim. Acta **58:** 1701-1710.

Krissek, L. A., K. F. Scheidegger, and L. D. Kulm. 1980. Surface sediments of the Peru-Chile continental margin and the Nazca Plate. Geol. Soc. Am. Bull. **91**: 321-331.

Law, G. T. W., T. M. Shimmield, G. B. Shimmield, G. L. Cowie, E. R. Breuer, and S. M. Harvey. 2009. Manganese, iron and sulphur cycling on the Pakistan margin. Deep-Sea Res. II **56:** 305-323.

Lehtoranta, J., and A.-S. Heiskanen. 2003. Dissolved iron:phosphate ratio as an indicator of phosphate release to oxic water of the inner and outer coastal Baltic Sea. Hydrobiologia **492:** 69-84.

Le Maitre, R. W. 1976. The chemical variability of some common igneous rocks. Petrol.**17:** 589-637.

Levin, L., D. Gutiérrez, A. Rathburn, C. Neira, J. Sellanes, P. Muñoz, V. Gallardo, and M. Salamanca. 2002. Benthic processes on the Peru margin: A transect across the oxygen minimum zone during the 1997-98 El Niño. Prog. Oceanogr. **53:** 1-27.

Li, Y.-H., and S. Gregory. 1974. Diffusion of ions in sea water and in deep-sea sediment. Geochim. Cosmochim Acta **38:** 703-714.

Matear, R. J., and A. C. Hirst. 2003. Long term changes in dissolved oxygen concentrations in the ocean caused by protracted global warming. Glob. Biogeochem. Cycles **17**: 1125, doi: 10.1029/2002GB001997

McManus, J., W. M. Berelson, K. H. Coale, K. S. Johnson, and T. E. Kilgore. 1997. Phosphorus regeneration in continental margin sediments. Geochim. Cosmochim. Acta **61:** 2891-2907.

Moore, J. K., and O. Braucher. 2008. Sedimentary and mineral dust sources of dissolved iron to the world ocean. Biogeosciences **5:** 631-656.

Nameroff, T. J., L. S. Balistrieri, and J. W. Murray. 2002. Suboxic trace metal geochemistry in the eastern tropical North Pacific. Geochim. Cosmochim. Acta **66:** 1139-1158.

Pakhomova, S. V., P. O. J. Hall, M. Y. Kononets, A. G. Rozanov, A. Tengberg, and A. V. Vershinin. 2007. Fluxes of iron and manganese across the sediment-water interface under various redox conditions. Mar. Chem. **107:** 319-331.

Pennington, J. T., K. L. Mahoney, V. S. Kuwahara, D. D. Kolber, R. Calienes, and F. P. Chavez. 2006. Primary production in the eastern tropical Pacific: A review. Prog. Oceanogr. **69:** 285-317.

Reimers, C. E., and E. Suess. 1983. Spatial and temporal patterns of organic matter accumulation on the Peru continental margin, p. 311-337. *In* J. Thiede and E. Suess [eds.], Coastal upwelling: Its sediment record. Part B: Sedimentary records of ancient coastal upwelling. Plenum Press.

Reimers, C. E., R. A. Jahnke, and D. C. McCorkle. 1992. Carbon fluxes and burial rates over the continental slope and rise off central California with implications for the global carbon cycle. Glob. Biogeochem. Cycl. **6:** 199-224.

Rozan, T. F., M. Taillefert, R. E. Trouwborst, B. T. Glazer, S. Ma, J. Herszage, L. M. Valdes, K. S. Price, and G. W. Luther III. 2002. Iron-sulfur-phosphorus cycling in the sediments of a shallow coastal bay: Implications for sediment nutrient release and benthic macroalgal blooms. Limnol. Oceanogr. **47:** 1346-1354.

Sannigrahi, P., and E. Ingall. 2005. Polyphosphates as a source of enhanced P fluxes in marine sediments overlain by anoxic water: Evidence from $^{31}$P NMR. Geochem. Trans. **6:** 52-59.

Schenau, S. J., and G. J. De Lange. 2001. Phosphorus regeneration vs. burial in sediments of the Arabian Sea. Mar. Chem. **75:** 201-217.

Scholz, F., C. Hensen, A. Noffke, A. Rohde, V. Liebetrau, and K. Wallmann. 2011. Early diagenesis of redox-sensitive trace metals in the Peruvian upwelling area-response to ENSO-related oxygen fluctuations in the water column. Geochim. Cosmochim. Acta **75:** 7257-7276.

Schulz, H. N., and H. D. Schulz. 2005. Large sulfur bacteria and the formation of phosphorite. Science **21:** 416-418.

Seeberg-Elverfeldt, J., M. Schlüter, T. Feseker, and M. Kölling. 2005. Rhizon sampling of porewaters near the sediment-water interface of aquatic systems. Limnol. Oceanogr.: Methods **3:** 361-371.

Severmann, S., J. McManus, W. M. Berelson, and D. E. Hammond. 2010. The continental shelf benthic iron flux and its isotope composition. Geochim. Cosmochim. Acta **74:** 3984-4004.

Slomp, C. P., S. J. Van der Gaast, and W. Van Raaphorst. 1996. Phosphorus binding by poorly crystalline iron oxides in North Sea sediments. Mar. Chem. **52:** 55-73.

Slomp, C. P., J. F. P. Malschaert, and W. Van Raaphorst. 1998. The role of adsorption in sediment-water exchange of phosphate in North Sea continental margin sediments. Limnol. Oceanogr. **43:** 832-846.

Sommer, S., P. Linke, O. Pfannkuche, T. Schleicher, J. Schneider v. Deimling, A. Reitz, M. Haeckel, S. Flögel, and C. Hensen. 2009. Seabed methane emissions and the habitat of frenulate tube worms on the Captain Arutyunov mud volcano (Gulf of Cadiz). Mar. Ecol. Prog. Ser. **382:** 69-86.

Stramma, L., G. C. Johnson, J. Sprintall, and V. Mohrholz. 2008. Expanding oxygen-minimum zones in the tropical oceans. Science **320:** 655-658.

Strub, P. T., J. M. Mesías, V. Montecino, R. Rutlland, and S. Salinas. 1998. Coastal ocean circulation of western South America, p. 273-313. *In* A. R. Robinson and K. H. Brink [eds.], The sea, vol.11. Wiley.

Suess, E. 1981. Phosphate regeneration from sediments of the Peru continental margin by dissolution of fish debris. Geochim. Cosmochim. Acta **45:** 577-588.

Suess, E., L. D. Kulm, and J. S. Killingley. 1987. Coastal upwelling and a history of organic rich mudstone deposition off Peru, p. 181-197. *In* J. Brooks and A. J. Fleet [eds.], Marine petroleum source rocks. Geological Society Spec. Publ. **26**.

Sundby, B., L. G. Anderson, P. O. J. Hall, A. Iverfeldt, M. M. Rutgers van der Loeff, and S. F. G. Westerlund. 1986. The effect of oxygen on release and uptake of cobalt, manganese, iron and phosphate at the sediment-water interface. Geochim. Cosmochim Acta **50:** 1281-1288.

Sundby, B., C. Gobeil, N. Silverberg, and A. Mucci. 1992. The phosphorus cycle in coastal marine sediments. Limnol. Oceanogr. **37:** 1129-1145.

Van der Weijden, C. H., G. J. Reichart, and H. J. Visser. 1999. Enhanced preservation of organic matter in sediments deposited within the oxygen minimum zone in the northeastern Arabian Sea. Deep-Sea Res. I **46:** 807-830.

Wallmann, K. 2003. Feedbacks between oceanic redox states and marine productivity: A model perspective focused on benthic phosphorus cycling. Glob. Biogeochem. Cycles **17**: 1084, doi: 10.1029/2002GB001968

Wallmann, K. 2010. Phosphorus imbalance in the global ocean? Glob. Biogeochem. Cycles **24:** GB4030, doi: 10.1029/2009GB003643

Wells, L. E. 1990. Holocene history of the El Niño phenomenon as recorded in flood sediments of northern coastal Peru. Geology **18:** 1134-1137.

Woulds, C., M. C. Schwartz, T. Brand, G. L. Cowie, G. Law, and S. R. Mowbray. 2009. Porewater nutrient concentrations and benthic nutrient fluxes across the Pakistan margin OMZ. Deep-Sea Res. II **56:** 333-346.

Wyrtki, K. 1962. The oxygen minima in relation to ocean circulation. Deep Sea Research **9:** 11-23.

# 3 A missing source of phosphate in the sediment budget of the Peruvian oxygen minimum zone

Noffke, A.*[a], Hensen, C.,[a] Dale, A.W.,[a] Sommer, S.,[a] Mosch, T.,[a] Bohlen, L.,[a] Wallmann, K.[a]

[a] GEOMAR Helmholtz-Zentrum für Ozeanforschung Kiel, Wischhofstraße 1-3, 24148 Kiel, Germany
*author for correspondence: anoffke@geomar.de

Close to submission to Geochimica et Cosmochimica Acta

## Abstract

Due to the diminished phosphorus (P) retention capacity of sediments underneath oxygen minimum zones (OMZs), these represent regional hotspots for benthic mobilization and release of P to the water column. In this study a combined approach, including solid phase P speciation measurements, sediment burial fluxes, and in situ flux measurements, was used to investigate the source of the strong P release that characterizes sediments underneath the Peruvian OMZ. Sediment samples were obtained from six sites along a latitudinal transect at 11°S at water depths between 80 m and 1000 m and bottom-water $O_2$ concentrations ranging from < 2 µmol $L^{-1}$ to ca. 40 µmol $L^{-1}$. P speciation measurements revealed that authigenic calcium phosphate (authigenic Ca-P) was the major fraction along the transect, where it accounted for 35% to 47% of the depth-averaged total extracted P on the shelf and upper slope, but for > 70% below 300 m water depth. Below 259 m water depth, P from fish remains (fish-P) dominated the authigenic Ca-P pool (60-69%). Organic P was present in considerable amounts only at the shelf and upper slope (18-37%), whereas detrital P and iron-bound P (Fe-P) were typically of minor importance at all sites. High carbon to phosphorus (C:P) ratios of surface organic matter (0-1 cm) of up to 516 indicated that organic P was severely depleted in organic matter relative to the Redfield ratio. If this material reflects the stochiometry of the organic

matter raining to the sea floor, then mass balance calculations based on the benthic fluxes suggest that organic P accounts for only a small fraction of the total particulate P input to the sediment inside the OMZ. This result was corroborated using a diagenetic model, applied to data from the core of the OMZ at 319 m water depth. The model further showed that organic P could account for a maximum of 13% of the total dissolved phosphate ($TPO_4$) released to the pore water, if the organic material raining to the sea floor has a Redfield composition. In this case, the measured C:P ratios require that the organic P would have to be very rapidly mineralized in the upper 0.5 cm of sediment. A more likely, yet unconfirmed, scenario is that preferential mineralization of organic P may be already occurring in the water column. According to the solid phase speciation data, authigenic Ca-P, with a high contribution of fish debris, is the likely candidate for the missing source of P required to close the benthic P budget, although further data are needed to verify this assertion. Burial of P was very low throughout the entire OMZ, and more than 80% of the total P was recycled back into the bottom water and so has the potential to stimulate surface-water productivity.

## 3.1 Introduction

Time-series data of dissolved oxygen ($O_2$) in the ocean over the last 50 years indicate that the major oxygen minimum zones (OMZs) in the tropical Atlantic and Pacific are expanding (Stramma et al. 2008). Oxygen deficiency strongly affects the function of sediments to act as sites for release and removal of phosphorus (P). Enhanced benthic P release may stimulate primary production leading to positive feedbacks between export production and $O_2$ consumption (Slomp and Van Cappellen 2007; Wallmann 2010). It is presently unclear, whether this is a contributing factor to the growing extent of OMZs.

Under oxic bottom waters, total dissolved phosphate ($TPO_4$) in sediments is efficiently scavenged by iron oxyhydroxides (Sundby et al. 1992; Slomp et al. 1998), limiting the rate of $TPO_4$ release to the overlying water. Under hypoxic or anoxic bottom waters, this efficiency is diminished and enhanced $TPO_4$ mobilization across the sediment-water interface is driven by the reductive dissolution of iron oxyhydroxides. Preferential release of organic phosphorus during organic matter degradation (Ingall et al. 1993; Van Cappellen and Ingall 1997; Jilbert et al. 2011; Steenbergh et al. 2011) further contributes to high $TPO_4$ mobilization from anoxic sediments. An additional source of $TPO_4$ that can

ultimately be mobilized back into the water column is the dissolution of biogenic apatite from fish debris (herein referred to as fish-P), as has been shown for the Peruvian and Arabian Sea OMZs (Suess 1981; Froelich et al. 1988, Schenau and De Lange 2000).

Elevated dissolved $TPO_4$ concentrations can induce the precipitation of calcium phosphate minerals, mainly in the form of carbonate fluorapatite, which is considered to be an important sink for reactive P in the ocean (Benitez-Nelson 2000; Paytan and McLaughlin 2007; Slomp and Van Cappellen 2007). An additional important sink is the burial of P in association with particulate organic matter (Föllmi 1996; Benitez-Nelson 2000). Burial of P bound to iron oxyhydroxides is considered negligible in $O_2$-deficient environments (Mort et al. 2010; Tsandev et al. 2012). Removal of P as fish debris in upwelling systems appears to be of minor significance, and is dependent on several factors such as water depth, sediment accumulation rate, and bottom-water $O_2$ concentration (Schenau and De Lange 2000). Off Callao (Peru), the burial of phosphatic fish debris was estimated to be only 10% of the surface-water fish-P production (Suess et al. 1981, Froelich et al. 1982). For sediments underlying the Arabian Sea OMZ the maximum burial efficiency was in the range of 10% to 22% (Schenau and De Lange 2000). However, despite these rather low burial efficiencies, fish debris represents a high proportion of the total P in sediments of these highly productive systems (Schenau and De Lange 2000; Diaz-Ochoa et al. 2009).

Beside these P sources and sinks, microbes but also protozoans have been shown to interact with the benthic P cycle in a unique way by the transient removal and release of P during oscillating bottom-water oxygen availability (Sannigrahi and Ingall 2005; Schulz and Schulz 2005).

Noffke et al. (2012) provided a comprehensive study on $TPO_4$ and ferrous iron ($Fe^{2+}$) release along a latitudinal depth transect across the Peruvian OMZ at 11°S. High in situ $TPO_4$ release rates in the range of 0.2 mmol $m^{-2}$ $d^{-1}$ to 0.8 mmol $m^{-2}$ $d^{-1}$ were measured in sediments underlying bottom waters depleted in dissolved $O_2$ down to < 2 µmol $L^{-1}$. This high $TPO_4$ release could not be explained by organic matter degradation following Redfield stoichiometry, pointing towards preferential P release relative to organic carbon ($C_{org}$). Dissolution of fish debris as well as reductive iron dissolution especially for the shelf were hypothesized as further sources of P. The aim of this study is to further investigate the drivers of the strongly elevated benthic $TPO_4$ release rates that were

measured across the Peruvian OMZ (Noffke et al. 2012). We focus on solid phase P speciation, in combination with a mass balance approach and a diagenetic P model analysis. The mass balance further resolves the magnitude of P burial efficiencies in Peruvian OMZ sediments and helps to identify the potential of these sediments for providing a positive feedback on surface-water primary production.

## 3.2 Regional setting

The Peruvian coastal upwelling region represents one of the most productive marine ecosystems in the world (Chavez et al. 2011). High primary productivity of up to 3.6 g C $m^{-2}$ $d^{-1}$ (Pennington et al. 2006) is sustained by coastal upwelling of cold, oxygen-poor but nutrient-rich water to the well-mixed surface layer, driven by offshore Ekman transport. Upwelled waters are predominantly Equatorial Subsurface Water, ESSW, transported poleward along the Peruvian coast with the Peru Chile Undercurrent, PCU (Strub et al. 1998). The ESSW is located between 75 m and ca. 500 m water depth and associated with a minimum in dissolved $O_2$ of 4.5 µmol $L^{-1}$ (Silva et al. 2009).

At 11°S to 15°S organic carbon rich muds ($C_{org}$ > 5 wt%) accumulate between 50 m and 500 m water depth, where reduced velocities of the bottom water in the PCU favor high bulk sedimentation rates and associated enhanced preservation and burial (Suess et al. 1987).

This fine-grained, diatomaceous mud lens extends from outer shelf to upper slope at 10.5°S to 13.6°S (Krissek et al. 1980). At greater water depths, increasing bottom current velocities result in lower sedimentation rates (Reimers and Suess 1983), winnowing and the accumulation of phosphorite crusts and nodules (Reimers and Suess 1983; Glenn and Arthur 1988).

## 3.3 Materials and Methods

*3.3.1 Sediment sampling and processing*

Sediment samples were taken during R/V *Meteor* cruise M77/1-2 in October-December 2008 along a latitudinal depth-transect at 11°S (Fig. 3.1; Table 3.1). Pore-water solutes and benthic fluxes at the same stations have been presented by Noffke et al. (2012). Water-column $O_2$ concentrations nearby to each station were derived from a CTD system (Sea-Bird Electronics) equipped with an $O_2$ sensor (Table 3.1). Sediment cores were

retrieved using a video-guided multiple corer (MUC) and two benthic landers (Biogeochemical Observatories — BIGO and BIGO-T; Sommer et al. 2009). Upon retrieval of the MUC or the lander, sediment liners (inner diameter: 10 cm) or subsamples from the benthic chambers were immediately transferred into a cold room which was kept at 4°C. Cores were vertically sectioned into 1-5 cm intervals with the highest resolution at the sediment surface. A sediment sample from each depth interval was taken, and stored refrigerated in pre-weighed plastic vials for the determination of total $C_{org}$. A second subsample was kept frozen at -20°C under an argon atmosphere in air-tight glass jars for sequential extractions of P phases. The surplus squeeze cakes were refrigerated until x-ray fluorescence (XRF) analyses onshore.

Pore water extraction techniques are described in detail by Noffke et al. (2012).

### *3.3.2 Chemical analyses*

Total concentrations of particulate P ($P_{tot}$) were analyzed by XRF using a Philips PW 1480 spectrophotometer equipped with a rhodium x-ray tube. Samples were prepared as lithium tetraborate fused glass beads (ratio sample:flux 1:6). Loss on ignition was not determined for the samples and P contents were calculated from unnormalized oxides ($P_2O_5$). Average values of replicate analyses of different rock reference samples agreed well with the recommended values and precision was better than 2%. Some of the beads prepared from MUC 19 as well as MUC 25 were affected by graphite schlieren, caused by high contents of $C_{org}$. These affected beads were dissolved in 140 ml of supra-pure $HNO_3$ (8% v/v) using an overhead shaker. Solutions were further diluted for analysis by inductively coupled plasma-optimal emission spectrometry (ICP-OES, Spectro Ciros CCD SOP). Duplicate flux-fusion preparations of the USGS reference standards SCO-1 and MAG-1 were generally well within the recommended ranges, with precisions better than 5% and 10%, respectively.

Sediment P was separated into four fractions using the SEDEX sequential extraction procedure (Ruttenberg 1992) as modified by Anderson and Delaney (2000). These include (1) P associated with iron oxyhydroxides, henceforth referred to as Fe-P, (2) authigenic calcium phosphate (Ca-P, which includes carbonate fluorapatite, $CaCO_3$-bound P, and biogenic apatite), (3) organic P, and (4) detrital P that is associated with detrital fluorapatite, certain clays and any residual phase not dissolvable in weak acid.

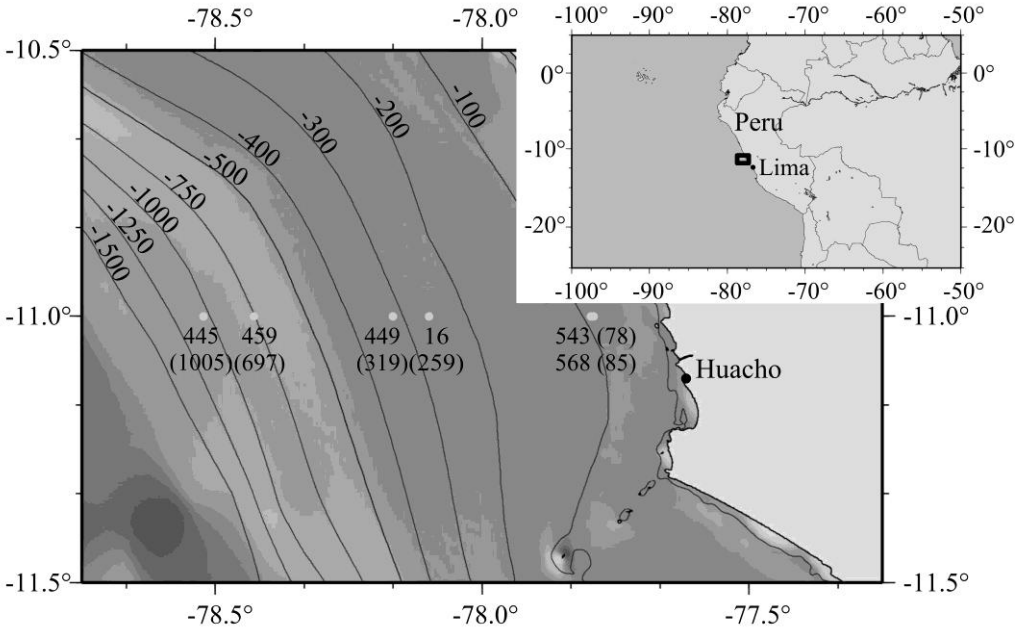


**Fig. 3.1:** Sampling sites along the latitudinal depth transect at 11°S across the Peruvian continental margin (bathymetry based on the Earth Topography Five Minute Grid (ETOPO5)). Station numbers are indicated. The respective water depths are given in brackets.

**Table 3.1:** Location of sites where sediments were sampled with the multiple corer (MUC) or lander (BIGO, BIGO-T) along with water depth and bottom-water oxygen concentration (BW $O_2$). Also shown are CTD positions deployed close to the sampling sites.

| Cruise leg | Station | Device | Date (2008) | Depth (m) | Latitude (S) | Longitude (W) | BW $O_2$ (µM) |
|---|---|---|---|---|---|---|---|
| M77-1 | 543 | MUC 52 | 12.11. | 78 | 10°59.99’ | 77°47.40’ | <2 |
| M77-1 | 568 | BIGO 5 | 15.11. | 85 | 11°00.02’ | 77°47.72’ | <2 |
| M77-2 | 16 | BIGO-T | 29.11. | 259 | 10°59.80’ | 78°05.91’ | <2 |
| M77-1 | 449 | MUC 19 | 03.11. | 319 | 11°00.01’ | 78°09.97’ | <2 |
| M77-1 | 459 | MUC 25 | 04.11. | 697 | 11°00.03’ | 78°25.60’ | 12 |
| M77-1 | 549 | MUC 53 | 13.11. | 1005 | 10°59.81’ | 78°31.27’ | 40 |
| M77-1 | 436 | CTD-RO 15 | 02.11. | 86 | 11°00.03’ | 77°47.48’ | — |
| M77-1 | 575 | CTD-RO 41 | 15.11. | 304 | 10°59.77’ | 78°09.19’ | — |
| M77-1 | 443 | CTD-RO 19 | 03.11. | 695 | 11°00.00’ | 78°25.55’ | — |
| M77-1 | 501 | CTD-RO 32 | 08.11. | 988 | 11°00.00’ | 78°31.00’ | — |

Biogenic Ca-P was considered to be predominantly derived from fish debris, and is henceforth referred to as fish-P (Schenau and De Lange 2000). Detrital P is considered to be non-reactive in marine environments (Ruttenberg 1992; 1993). These fractions were determined by sequentially treating 0.1 g of freeze-dried and ground sediment with (1) a solution of 0.22 M sodium citrate, 0.033 M sodium dithionite, and 1.0 M sodium bicarbonate (pH 7.6), (2) 1 M sodium acetate (pH 4), (3) 1 N HCl, and (4) 1 N HCl after

ignition at 550°C. Rinsing with 1 M $MgCl_2$ (pH 8) and MilliQ followed steps 1 and 2 to reverse secondary adsorption of $TPO_4$. A reagent blank was included for each of the extraction steps. Solutions of the different treatments were pooled and, except for Fe-P (step 1), analyzed for $TPO_4$ with the phosphomolybdate blue method after Grasshoff et al. (1999) using a Hitachi U-2800A spectrophotometer at 880 nm. Solutions from step 1 were treated with 1% v/v $FeCl_3$ (Lucotte and D'Anglejan 1985) and afterwards analyzed for $TPO_4$ after Watanabe and Olsen (1962), but reading absorbances at 730 nm. To eliminate the matrix effect of extraction solutions, samples from steps 2 to 4 were typically diluted in the ratio of 1:20 for authigenic P and 1:5 for detrital P and organic P. Additional dilutions were made to ensure that concentrations of samples were within the linear absorption range of the spectrophotometer. Standards were prepared to match the chemical matrix of the pooled solutions from the individual extraction steps, and diluted to the same degree as the samples.

For sediment samples, the average total recovery of the sequential extraction with respect to $P_{tot}$ measured by XRF was 90%. Long term runs of the in-house standard OMZ-1, which was prepared as a mixture of sediment samples from a moderately C-enriched ($C_{org}$: 8 wt%) core from the 11°S transect, resulted in a precision of 22% for Fe-bound P, 3% for authigenic P, 14% for detrital P, and 5% for organic P.

To assess the contribution of fish-P to $P_{tot}$, all surface samples and selected down-core samples from the 85 m, 319 m, and 697 m sites were treated with $NH_4Cl$ according to Schenau and De Lange (2000). This method was slightly modified by using a smaller amount of sediment (0.1 g), as we expected to find elevated concentrations of fish-P in the sediments underlying this highly productive upwelling system (Suess et al. 1981).

The $C_{org}$ content was determined to help constrain the P mass balance (see below). Sediment samples were freeze-dried and ground and treated with HCl (0.25 N) to drive out inorganic carbonates. $C_{org}$ was then measured on a Carlo Erba Elemental Analyzer with an analytical precision for replicate samples of 1%.

### *3.3.3 Sedimentary $C_{org}$ and $P_{tot}$ mass balance*

A mass balance for the upper 10 cm of sediment was developed to resolve the spatial trends in P recycling and burial across the transect and to assess the importance of different P phases on the high benthic $TPO_4$ fluxes measured in the OMZ (Noffke et al. 2012).

Assuming steady state conditions, the sum of the burial flux of $C_{org}$ and the $C_{org}$ degradation rate is equal to the rain rate of $C_{org}$. Similarly, the sum of the burial flux of $P_{tot}$ and the benthic release of $TPO_4$ equals the rain rate of $P_{tot}$:

$$RR_{Corg} = F_{Corg} + R_{Corg} \quad (3.1a)$$

$$RR_{Ptot} = F_{Ptot} + F_{TPO4} \quad (3.1b)$$

where $RR_i$ (mmol $m^{-2}$ $d^{-1}$) denotes the rain rate of $i$ = $C_{org}$ or $P_{tot}$, $F_i$ (mmol $m^{-2}$ $d^{-1}$) is the burial flux at 10 cm depth in the sediment, $R_{Corg}$ (mmol $m^{-2}$ $d^{-1}$) is the depth-integrated $C_{org}$ degradation rate down to 10 cm and $F_{TPO4}$ (mmol $m^{-2}$ $d^{-1}$) is the benthic $TPO_4$ flux. $R_{Corg}$ was derived by diagenetic modeling following Bohlen et al. (2011) and $F_{TPO4}$ was measured using benthic landers (Noffke et al. 2012). Burial fluxes were calculated from the concentrations of $C_{org}$ ($C_{Corg}(10)$, mmol $g^{-1}$) and $P_{tot}$ ($C_{Ptot}(10)$, mmol $g^{-1}$) at 10 cm where their concentrations approached asymptotic levels and the sediment accumulation rate ($F_{sed}$, g $m^{-2}$ $d^{-1}$ ):

$$F_{Corg} = F_{sed} * C_{Corg}(10) \quad (3.2a)$$

$$F_{Ptot} = F_{sed} * C_{Ptot}(10) \quad (3.2b)$$

The concentration at 10 cm depth was taken as the average concentration in the 8-10 cm and 10-12 cm intervals. Due to scatter in the $C_{org}$ and $P_{tot}$ data at all sites, the $F_i$ and hence $RR_i$ estimates bear uncertainties, with an error based on this scatter of 15% to 25%.
$F_{sed}$ was calculated as:

$$F_{sed} = ds \times (1-\varphi) \times w \times \zeta \quad (3.3)$$

where ds (g $cm^{-3}$) is the density of dry solids, φ (dimensionless) is the porosity of compacted sediment, w (cm $yr^{-1}$) is the burial velocity of compacted sediment, and ζ is a factor that converts $F_{sed}$ from g $cm^{-2}$ $yr^{-1}$ to g $m^{-2}$ $d^{-1}$. Ds, φ, and w were taken from Bohlen et al. (2011).

The burial efficiencies ($BE_i$, %) of $i = C_{org}$ and $P_{tot}$ were subsequently estimated as:

$$BE_{Corg}(\%) = \frac{F_{Corg}}{RR_{Corg}} \times 100 \quad (3.4a)$$

$$BE_{Ptot}(\%) = \frac{F_{Ptot}}{RR_{Ptot}} \times 100 \quad (3.4b)$$

## 3.4 Results

*3.4.1 Oxygen availability through the OMZ*

At the time of sampling the OMZ ($O_2$ < 2 µmol $L^{-1}$) extended from ca. 50 m to 500 m water depth (Fig. 3.2). Below 500 m, bottom-water $O_2$, measured 5-8 m above the sea floor, started to increase and reached ca. 40 µmol $L^{-1}$ at 1000 m. Although the $O_2$ was < 2 µmol $L^{-1}$ on the shelf (78 m and 85 m water depth) at the time of the investigation, these sites experience periodic oxygenation events (Gutiérrez et al. 2008; Noffke et al. 2012). With increasing water depth, such oxygenation events can be assumed to occur more rarely, and we henceforth refer to the depth range from 250 m down to 500 m water depth as the core of the OMZ.

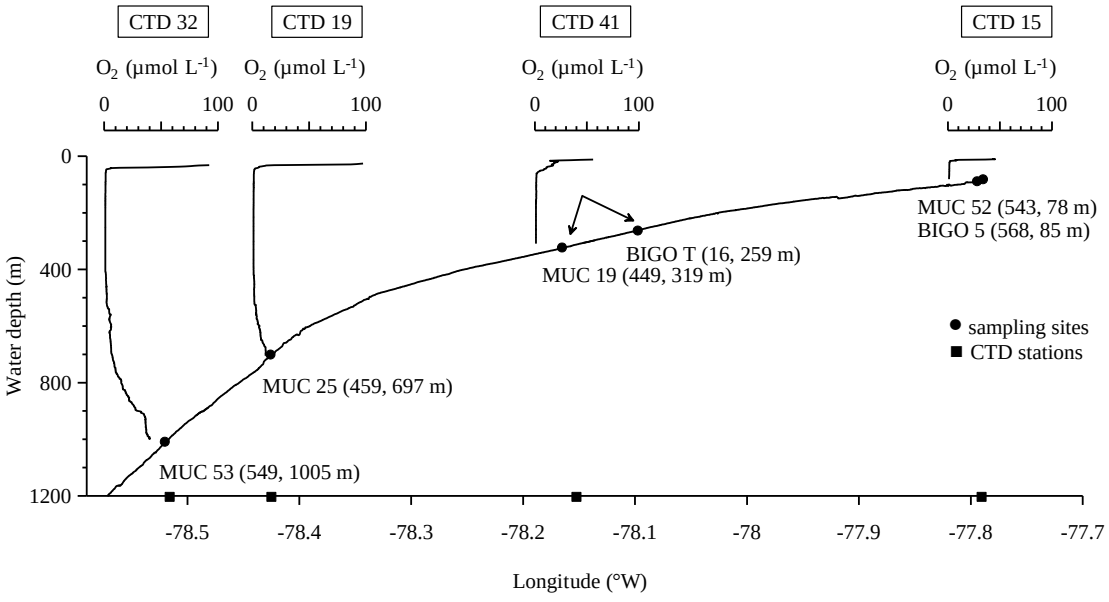


**Fig. 3.2:** Bathymetry at 11°S (Mosch et al. 2012) and dissolved oxygen profiles from CTD deployments taken closest to each of the benthic sampling sites (Table 3.1). Locations of sampling sites are indicated on the bathymetry, whereas locations of the CTD deployments are indicated on the x-axis. Site numbers and respective water depths are given in brackets.

*3.4.2 Particulate phosphorus speciation*

Vertical concentration-depth profiles of the different P phases for each site are displayed in Fig. 3.3. Fig. 3.4 shows the depth-averaged P concentrations along the transect and their relative proportions of the total extracted P.

Fe-P was enriched at the sediment surface at all sampling sites (8.6-34.2 µmol P $g^{-1}$, Fig. 3.3). Within the OMZ (78-319 m), Fe-P abruptly decreased to rather constant concentrations just below the surface-enriched layer. Below the OMZ (697-1005 m), there was a more gradual decline throughout the uppermost ca. 10 cm, until constant concentrations were reached. Along the transect, the relative proportion of depth-averaged Fe-P to total extracted P was 20% and 22% on the shelf, but distinctively declined towards the core of the OMZ, to 5% at the deepest site (Fig. 3.4). Absolute Fe-P concentrations averaged over the entire core were, however, similar throughout the entire depth transect. Authigenic Ca-P was the most abundant fraction at all sites. On the shelf and the upper slope it constituted 35% to 47% (depth-averaged) of the total extracted P, but rapidly increased to > 70% below 300 m water depth (Fig. 3.4). Depth-averaged authigenic Ca-P concentrations on the shelf and upper slope ranged from 10.1 µmol $g^{-1}$ to 32.7 µmol $g^{-1}$, whereas at the deeper sites authigenic Ca-P levels were ca. 100 µmol $g^{-1}$ (Figs. 3.3, 3.4). The observed increase of total P with sediment depth (Fig. 3.3) was primarily due to the presence of this authigenic Ca-P phase. Despite the rather low authigenic Ca-P inventories on the shelf sites (78 m and 85 m), subsurface peaks were observed in sediment depths between 1-8 cm and 1-5 cm, respectively (Fig. 3.3). Fish-P dominated the authigenic Ca-P pool at water depths > 259 m, with depth-averaged fractions of 60% to 69% of authigenic Ca-P (Fig. 3.4). Depth-averaged concentrations of fish-P were in the range of 62.2 µmol $g^{-1}$ to 68.8 µmol $g^{-1}$. On the shelf, fish-P was almost negligible with absolute depth-averaged concentrations of 0.6 µmol $g^{-1}$ and 3.3 µmol $g^{-1}$ (Figs. 3.3, 3.4). At the 259 m site, fish-P slightly increased to 9.4 µmol $g^{-1}$. Organic P constituted the second largest fraction at all locations, except for the deepest stations at 697 m and 1005 m. Here, it was comparable to Fe-P (Fig. 3.4). At 78 m, 85 m, 259 m, and 319 m, the depth-averaged proportion of organic P was 18% to 37% of the total extracted P, and was either dominant or comparable to authigenic Ca-P within the upper 3-6 cm of sediment. The highest depth-averaged organic P concentrations of 21.9 µmol $g^{-1}$ and 24 µmol $g^{-1}$ were measured at 259 m and 319 m, respectively (Fig. 3.4).

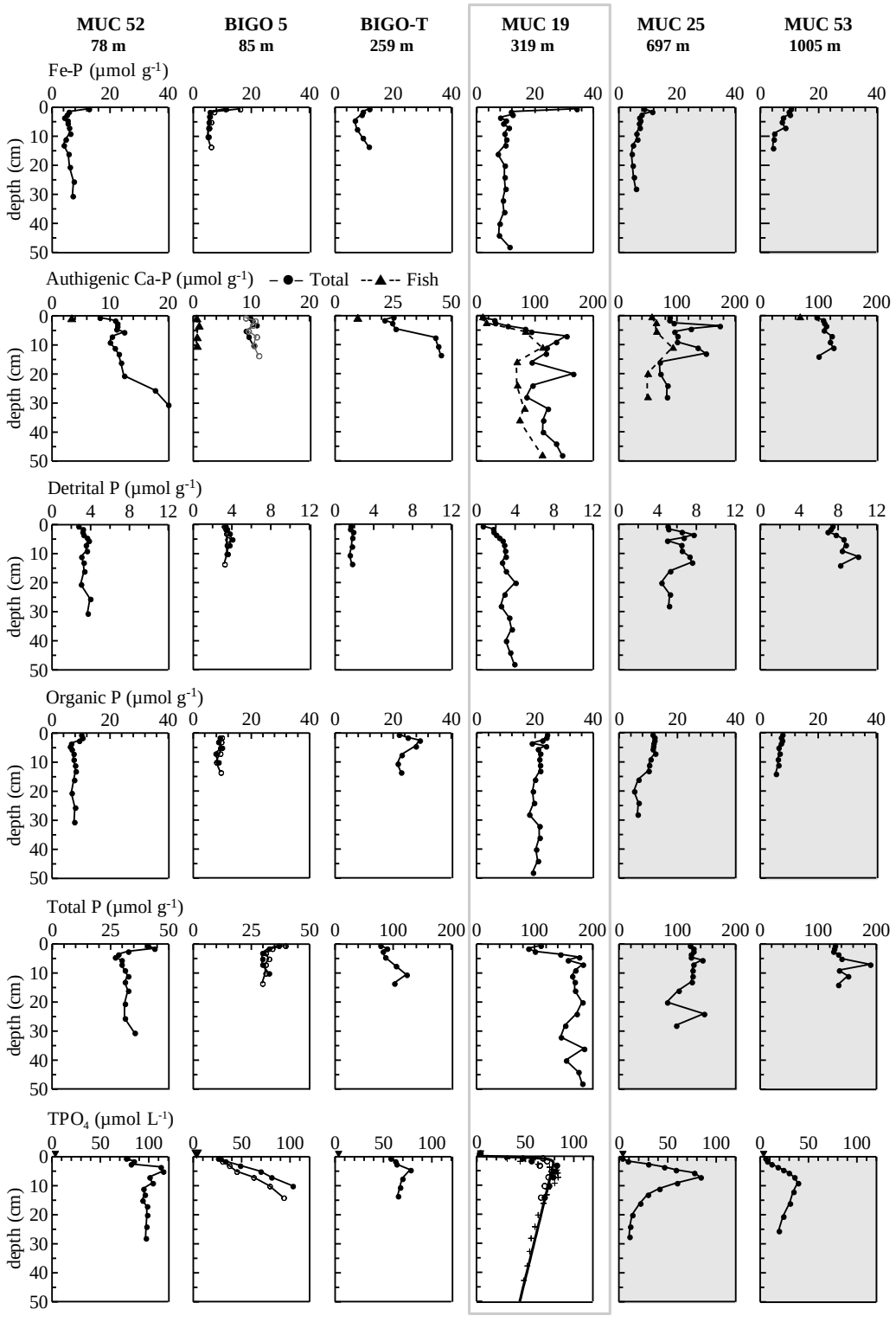


**Fig. 3.3:** Solid phase sediment profiles of different phosphorus (P) species and total P measured by XRF, for all sampling sites at 11°S. Also included are pore-water profiles of dissolved phosphate ($TPO_4$). Except for the 85 m site the pore-water profiles were taken from Noffke et al. (2012). Triangles indicate bottom-water concentrations, which were taken from CTD measurements. Sampling sites characterized with elevated bottom-water $O_2$ levels are shaded in light gray. For the 319 m site reactive transport modeling was conducted (indicated by the gray rectangle, see section 3.5.2 for details). The model fit (solid line) to the $TPO_4$ profiles is based on all available $TPO_4$ data from this sampling site including MUC 19 and BIGO 1.

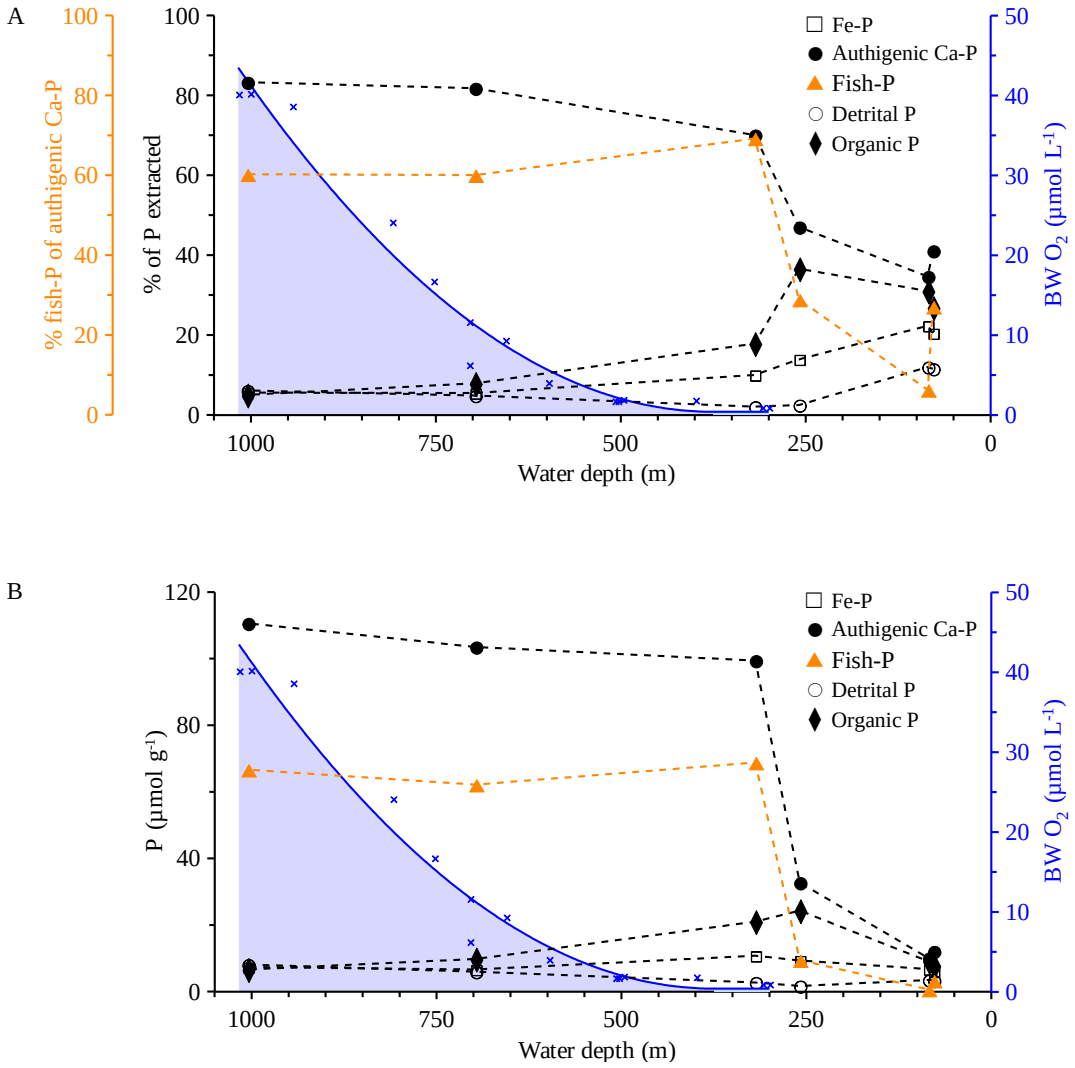


**Fig. 3.4:** Changes of the relative contribution of the different P species to total extracted P (A) and their concentrations (B) along the transect at 11°S. Percentages as well as total concentrations are whole core averages. Fish-P (orange triangles) is given as percentages relative to authigenic Ca-P. Bottom-water $O_2$ concentrations between 300 m and ~ 1000 m water depth are indicated. For clarity the area below the polynomial fit is filled. For sites, where fish-P was only measured at the sediment-surface (see Fig. 3.3), this value was assumed to represent the depth-averaged value. At the 259 m site, this may be an underestimate, since a distinct rise of fish-P with depth was observed at 319 m and 697 m water depth (Fig. 3.3).

At all sites, detrital P constituted only a minor fraction (2-12%) of the total extracted P (Fig. 3.4). Depth-averaged detrital P levels varied between 1.7 µmol $g^{-1}$ and 8.1 µmol $g^{-1}$ (Fig. 3.4).

## 3.5 Discussion

*3.5.1 A missing source of phosphorus*

Benthic P cycling in OMZs is generally poorly understood and mass balance calculations considering input, burial as well as release are largely missing in the literature. Previous studies have typically focused on in situ flux measurements (Ingall and Jahnke 1994; McManus et al. 1997; Hartnett and Devol 2003; Woulds et al. 2009; Noffke et al. 2012) or solid phase P distributions (Jahnke et al. 1983; Ingall et al. 1993; Schenau et al. 2000), the latter often in the context of present day apatite formation. To our best knowledge, there are so far only two studies that use solid phase P data in combination with $TPO_4$ release rates to resolve P regeneration versus burial in OMZs. Ingall and Jahnke (1994) provided in situ $TPO_4$ fluxes and P burial rates for one site from the Santa Monica Basin, two sites from the California margin and one anoxic shelf site at Peru. Schenau and De Lange (2001) investigated P regeneration versus burial in the Arabian Sea OMZ using a set of diffusive P fluxes. For one site at the lower boundary of this OMZ, Kraal et al. (2012) reconstructed the sedimentary P budget using a diagenetic model. However, this site is characterized with $O_2$ levels of 14 µmol $L^{-1}$, and thus does not represent anoxic conditions. For the Peruvian upwelling system, a P budget was determined for a site at 186 m water depth at 11°15`S, which was solely based on the P burial flux as well as estimates of particle fluxes (Suess 1981). In this study, the sedimentary P mass balance in the Peruvian OMZ was calculated for six sites covering an anoxic to oxic gradient using in situ $TPO_4$ fluxes as well as P burial fluxes (Table 3.2). In the following, we will discuss this mass balance and explore the sources of P deposited on the sea floor.

It is generally assumed that particulate organic P ($P_{org}$) is the major P fraction deposited to sediments (Delaney 1998; Filippelli 2008). Under steady state conditions, benthic release of $TPO_4$ ($F_{TPO4}$) plus the burial flux of P ($F_{Ptot}$) should approximately balance the rain rate of $P_{org}$ ($RR_{Porg}$). Particle traps were not deployed at Peru at the time of sediment sampling to directly measure $RR_{Porg.}$ As an alternative, $RR_{Porg}$ at each site was estimated by dividing the organic carbon rain rate ($RR_{Corg}$) by its respective C:P ratio. Measurements of the C:P ratio of the phytoplankton community that were conducted during cruise M77-3 (Dec. 2008 - Jan. 2009) at 12°S, showed strong deviations from the Redfield stoichiometry, with values of up to 500 in water samples taken offshore (Franz et al. 2012). Depletion in organic P at all sites along the transect was also indicated in the

**Table 3.2:** Calculated parameters for the benthic P mass balance in the upper 10 cm. To explore the effect of P-enriched organic matter input on the P mass balance of the shelf (MUC 52*), an $r_{CP}$ value of 50 was used instead of 292 (see section 3.5.3).

| | Variable | Description | MUC 52 78 m | MUC 52* 78 m | BIGO 5 85 m | BIGO-T 259 m | MUC 19 319 m | MUC 25 697 m | MUC 53 1005 m | Unit |
|---|---|---|---|---|---|---|---|---|---|---|
| | | Input parameters | | | | | | | | |
| a. | Ds | Density of dry solids † | 2 | 2 | 2 | 2 | 2 | 2 | 2 | g $cm^{-3}$ |
| b. | Φ | Porosity of compacted sediment † | 0.80 | 0.80 | 0.80 | 0.89 | 0.85 | 0.71 | 0.67 | – |
| c. | $_w$ | Burial velocity of compacted sediment † | 0.30 | 0.30 | 0.30 | 0.06 | 0.05 | 0.08 | 0.05 | cm $yr^{-1}$ |
| d. | $F_{sed}$ | Sediment accumulation rate [a×(1-b)×c] | 1020 | 1020 | 1020 | 168 | 150 | 484 | 429 | g $m^{-2}$ $yr^{-1}$ |
| e. | $R_{Corg}$ | Depth-integrated $C_{org}$ decay rate (0-10 cm) ‡ | 7.13 | 7.13 | 7.23 | 5.28 | 3.84 | 1.68 | 2.08 | mmol $m^{-2}$ $d^{-1}$ |
| f. | $F_{TPO4}$ | Benthic $TPO_4$ flux †† | 0.47 | 0.47 | 0.47 | 0.58 | 0.80 | 0.06 | 0.18 | mmol $m^{-2}$ $d^{-1}$ |
| g. | $C_{Al}(0\text{-}1)$ | Concentration of Al at 0-1 cm | 2.4 | 2.4 | 2.5 | 1.2 | 0.9 | 1.5 | 1.7 | mmol $g^{-1}$ |
| h. | $C_{Corg}(10)$ | Concentration of $C_{org}$ at 10 cm | 2.3 | 2.3 | 2.6 | 10.0 | 14 .0 | 5.5 | 3.2 | mmol $g^{-1}$ |
| i. | $C_{Ptot}(10)$ | Concentration of $P_{tot}$ at 10 cm | 0.03 | 0.03 | 0.03 | 0.11 | 0.17 | 0.13 | 0.14 | mmol $g^{-1}$ |
| j. | $r_{CP}(0\text{-}1)$ | $C_{org}$:$P_{org}$ ratio at 0-1 cm | 292 | 50 | 315 | 516 | 466 | 495 | 440 | mol C (mol P)$^{-1}$ |
| k. | $F_{Al}(0\text{-}1)$ | Al depositional flux at 0-1 cm [d×g] | 6.71 | 6.71 | 6.99 | 0.55 | 0.37 | 1.99 | 2.00 | mmol $m^{-2}$ $d^{-1}$ |
| l. | $F_{Corg}$ | $C_{org}$ burial flux at 10 cm [d×h] | 6.43 | 6..43 | 7.27 | 4.60 | 5.74 | 7.29 | 3.76 | mmol $m^{-2}$ $d^{-1}$ |
| m. | $F_{Ptot}$ | $P_{tot}$ burial flux at 10 cm [d×i] | 0.08 | 0.08 | 0.08 | 0.05 | 0.07 | 0.17 | 0.16 | mmol $m^{-2}$ $d^{-1}$ |
| | | Derived fluxes and burial efficiencies | | | | | | | | |
| n. | $RR_{Corg}$ | $C_{org}$ rain rate [e+l] | 13.56 | 13.56 | 14.5 | 9.88 | 9.58 | 8.97 | 5.84 | mmol $m^{-2}$ $d^{-1}$ |
| o. | $RR_{Porg}$ | $P_{org}$ rain rate [n/j] | 0.046 | 0.271 | 0.046 | 0.019 | 0.021 | 0.018 | 0.013 | mmol $m^{-2}$ $d^{-1}$ |
| p. | $RR_{Ptot}$ | $P_{tot}$ rain rate [f+m] | 0.55 | 0.55 | 0.55 | 0.63 | 0.87 | 0.23 | 0.34 | mmol $m^{-2}$ $d^{-1}$ |
| q. | $RR_{Pterr}$ | P rain rate in terrigenous particles ††† | 0.134 | 0.134 | 0.140 | 0.011 | 0.007 | 0.040 | 0.040 | mmol $m^{-2}$ $d^{-1}$ |
| r. | $RR_{Pauth}$ | Rain rate of authigenic P phase [p-o-q] | 0.37 | 0.15 | 0.36 | 0.60 | 0.84 | 0.17 | 0.29 | mmol $m^{-2}$ $d^{-1}$ |
| s. | $BE_{Corg}$ | Burial efficiency of $C_{org}$ [l/n×100] | 47 | 47 | 50 | 47 | 60 | 81 | 64 | % |
| t. | $BE_{Ptot}$ | Burial efficiency of $P_{tot}$ [m/p×100] | 15 | 15 | 15 | 8 | 8 | 74 | 47 | % |

†From Bohlen et al. (2011).
‡Derived by diagenetic modeling following Bohlen et al. (2011).
††From Noffke et al. (2012); in situ flux measurements (BIGO and BIGO-T lander) that were conducted nearest to the above provided MUC stations were taken. For the 319 m site, the BIGO 1 deployment was used. BIGO 1 was also applied in the diagenetic P model that extends on the model of Bohlen et al. (2011).
†††Estimated by multiplying $C_{Al}(0\text{-}1)$ by $F_{sed}$ and a mean P:Al molar ratio of 0.02 for riverine suspended particles (Viers et al. 2002).

measured $C_{org}$:$P_{org}$ molar ratios ($r_{CP}$). Values of $r_{CP}$ in the surface 0-1 cm depth interval, $r_{CP}$(0-1), were highly elevated with values up to 516 at the 259 m site (line j, Table 3.2). On the shelf, the $r_{CP}$(0-1) values were lower but still elevated (292). Even though these high values are comparable to those offshore values reported by Franz et al. (2012), it is not clear, whether they are due to preferential P mineralization in the water column or in the uppermost surface sediment layer. Assuming for now, that these values are representative for the composition of the deposited organic matter on the shelf and upper slope, $RR_{Porg}$ would be equal to 0.046 at the shallowest station and equal to 0.013 mmol $m^{-2}$ $d^{-1}$ at the deepest (line o, Table 3.2). These values are 12 to 41 times lower than rain rate of total P (line p), hence immediately demonstrating that organic P is of minor importance (2-8%) to benthic P cycling, despite the highly productive regime in the OMZ.

Terrigenous P may constitute a high fraction of sinking particles in marine systems (Paytan et al. 2003; Faul et al. 2005). An estimate of the terrigenous P rain rate ($RR_{Pterr}$) was made by multiplying the Al concentration in the surface sediments (0-1 cm) by the sediment accumulation rate and a mean P:Al molar ratio of 0.02 for riverine suspended particles (Viers et al. 2009). However, even considering this contribution, $RR_{Ptot}$ was still 3- to 31-fold higher than $RR_{Porg} + RR_{Pterr}$ at all investigated sites, with the lowest discrepancy at the shelf (see section 3.5.3). Our estimate of the terrigenous P accounts for the contribution of P-bearing iron oxyhydroxides delivered from the continent. With regard to Fe-P, however, the potential additonal input arising from a vertical iron redox shuttle is not accounted for. This mechanism describes how particulate P is formed by adsorption or coprecipitation with authigenic iron oxyhydroxides at the water column redoxcline (e.g. Dellwig et al. 2010), which are subsequently deposited at the sea floor. The significance of this mechanism for the Peruvian OMZ is unknown. Although Fe-P was a minor fraction at all stations, we cannot exclude that authigenic P-bearing iron oxyhydroxides are involved in benthic P cycling, since the sampling resolution did not resolve the uppermost cm of the surface layer. $Fe^{2+}$ release from the permanently anoxic sediments within the core of the OMZ was relatively low (0.04 mmol $m^{-2}$ $d^{-1}$) (Noffke et al. 2012), implying that this shuttle may only be of some importance at the shelf station, where $Fe^{2+}$ fluxes were up to 0.87 mmol $m^{-2}$ $d^{-1}$ (Noffke et al. 2012). It can be expected to have no importance at the sites below the OMZ, with increasingly oxic conditions and no

$Fe^{2+}$ release from the sediment. Yet, enhanced deposition of P formed at the lower redoxcline, following lateral transport of $Fe^{2+}$ from the OMZ, might occur (Noffke et al. 2012; Scholz et al. 2011). However, our Fe-P data clearly do not argue for an increased importance of P deposition with iron oxyhydroxides at these sites.

Taken together, the previous considerations imply that a large additional P source is required to balance the burial flux of P and the benthic $TPO_4$ release along the transect. Detrital P and Fe-P was of minor significance at all stations, hence one may assume that the observed discrepancy can only be reasonably explained by an input of authigenic Ca-P. As shown by the solid phase profiles (Fig. 3.3), fish-P dominates the authigenic Ca-P fraction, except on the shelf. Based on analysis of pore-water $TPO_4$ profiles, fish remains, and acid soluble P, Suess et al. (1981) showed that fish dissolution of debris constitutes an important P source to the pore-water $TPO_4$ concentration in Peruvian margin sediments. Similarly, in the Arabian Sea OMZ, high $TPO_4$ fluxes across the sediment-water interface correlated well with the accumulation of fish-P in surface sediments (Schenau et al. 2001).

Nevertheless, all stations investigated off Peru showed enrichments of authigenic Ca-P in excess of fish-P even at the very surface. Besides the sedimentary transformation of dissolved $TPO_4$ into authigenic carbonate fluorapatite, deposition of authigenic apatite from the water column may be occurring here (Faul et al. 2005). P speciation measured in sediment traps along the California continental margin (Faul et al. 2005; Sekula-Wood et al. 2012) and in the Gulf of California, Mexico (Lyons et al. 2011), showed that authigenic Ca-P contributed 23% to 36% of the total P pool of settling particles. However, the sources constituting this authigenic Ca-P pool remained elusive. The process of authigenic apatite formation in the water column still has not been elucidated, but it has been proposed to occur in micro-environments within large particle aggregations (Faul et al. 2005). Additionally, polyphosphate granules that are stored by diatoms, and which are released during cell lysis or dissolution of tests, may serve as nuclei for apatite formation (Diaz et al. 2008). Carbonate fluorapatites at our study sites may, therefore, be partly related to a high sinking flux of diatoms, which dominate the phytoplankton community of the coastal upwelling on the shelf (Franz et al. 2012).

Lastly, phosphorite concretions that were retrieved in sediment cores from 400 m to 600 m water depth might further contribute excess P to the sediment. The most important

mineral of phosphorites is carbonate fluorapatite (e.g. McClellan 1980), and phosphorites will hence contribute to the pool of extracted authigenic Ca-P. Anticipating that such phosphorites are of allochthonous origin, i.e. originate from further upslope (Scholz et al. 2011), part of the authigenic Ca-P measured in excess to fish-P does not reflect in situ precipitation occurring either in the water column or the sediments. However, given the rather small discrepancy between fish-P and total authigenic Ca-P, the contribution of phosphorites from further upslope to the authigenic Ca-P pool can be considered to be rather insignificant in terms of burial. Furthermore, the possibility that such phosphorites might be involved in the benthic $TPO_4$ release can be excluded, since under near-neutral conditions carbonate fluorapatite has a very low solubility (Guidry and McKenzie 2003).

### *3.5.2 Preferential mineralization of organic phosphorus in the surface layers?*

The results from the mass balance above rely on the idea that the C:P ratio of the organic material sinking to the sea floor resembles the C:P ratios of the ambient phytoplankton community (Franz et al. 2012). The high $r_{CP}$(0-1) values measured in the surface layer also indicate strong P depletion. However, due to the centimeter vertical resolution of sediment sampling, it cannot be established, whether the organic material that reaches the sea floor does in fact have a Redfield composition, and then undergoes preferential mineralization of organic P relative to C in the uppermost 0.5 cm of sediment. In this section, we use a diagenetic reaction-transport model, previously developed for the Peruvian OMZ by Bohlen et al. (2011), to illustrate this idea more clearly and to quantify an upper limit for the potential role of $P_{org}$ to the total rate of $TPO_4$ released to the pore water.

The model considers transport of chemical species by advection due to sediment accumulation and compaction, molecular diffusion (for solutes), and sediment mixing by fauna (bioturbation). Bohlen et al. (2011) focused on nitrogen cycling using data from the same cores and benthic chambers as those presented here. We extended the model to include organic P dynamics as detailed below. The model is applied to data from the 319 m site inside the core of the OMZ, where anoxic conditions can be assumed to be quasi-permanent and bioturbation is negligible. This site is therefore least likely to experience fluctuations in bottom-water redox conditions in contrast to the shelf and lower chemocline (Scholz et al. 2011; Noffke et al. 2012).

In the model, the sum of biogeochemical reactions that contribute to the dissolved $TPO_4$ pool ($\Sigma R_{TPO4}$) was described using a dynamic fitting function of the following form:

$$\Sigma R_{TPO4} = k_{fit} \times (TPO_4 - TPO_{4\text{-}SIM}) \quad (3.5)$$

where $k_{fit}$ ($yr^{-1}$) is a kinetic constant, which ensures that the simulated $TPO_4$ concentrations ($TPO_{4\text{-}SIM}$ in the above equation) were maintained close to the observed values ($TPO_4$). This function is analogous to that used for ammonium by Bohlen et al. (2011) to determine organic matter degradation rates.

The curve that best described the measured $TPO_4$ concentrations is shown in Fig. 3.3. The diffusive flux of $TPO_4$ out of the sediment corresponding to this curve was equal to 268 mmol $m^{-2}$ $yr^{-1}$, which is in good agreement with the benthic chamber flux measured at the same site (292 mmol $m^{-2}$ $yr^{-1}$; Noffke et al. 2012).

The fitting function accounts for $TPO_4$ release by mineralization of $P_{org}$ ($R_{Porg}$) plus a number of other P sources and sinks lumped together as $\Sigma R_{PSS}$, which may include $TPO_4$ release from iron oxyhydroxides, fish-P and authigenic Ca-P minerals:

$$k_{fit} \times (TPO_4 - TPO_{4\text{-}SIM}) = R_{Porg} + \Sigma R_{PSS} \quad (3.6)$$

$\Sigma R_{PSS}$ thus represents the net uptake or release of $TPO_4$ required to fit the $TPO_4$ data once $TPO_4$ release from $P_{org}$ has been accounted for. The rate of P release from organic matter with depth in the sediment was quantified as:

$$R_{Porg} = R_{Corg} / r_{CP} \quad (3.7)$$

where $r_{CP}$ and $R_{Corg}$ are defined as previously. Similarly, the rain rate of $P_{org}$ to the sediment ($RR_{Porg}$) was determined as:

$$RR_{Porg} = RR_{Corg} / r_{CP}(flux) \quad (3.8)$$

where $r_{CP}(flux)$ is the (unknown) carbon-to-phosphorus ratio of organic matter deposited at the sediment-water interface and $RR_{Corg}$ is the model-derived rain rate (Bohlen et al. 2011).

Measured depth-dependent $r_{CP}$ values were imposed in the model (Eq. 3.7) as forcing functions. These are shown in Fig. 3.5 (left panels), and clearly illustrate that preferential mineralization of $P_{org}$ relative to $C_{org}$ has occurred by 0.5 cm sediment depth and continues down to 5 cm, at which point $r_{CP}$ reaches asymptotic values of ca. 600. However, as noted above, a value for $r_{CP}$ in the upper 0.5 cm is undefined due to the sampling resolution.

To test whether $P_{org}$ is undergoing depletion in the uppermost 0.5 cm of sediment, three different scenarios were tested, as indicated in Fig. 3.5. In Scenario 1, the model was run using a Redfield $r_{CP}$ value of 106 for the flux of organic matter to the sediment surface, $r_{CP}(flux) = 106$ (Fig. 3.5a). Below 0.5 cm, the imposed depth-dependent $r_{CP}$ follows the measured values. In Scenario 2, the material arriving at the sediment surface was again assumed to have Redfield composition, but now the model was modified to allow enhanced $P_{org}$ degradation in the upper 0.5 cm relative to the Redfield ratio (Fig. 3.5b). Finally, in Scenario 3, $r_{CP}(flux)$ was adjusted to values much higher than Redfield to reflect the measured data at 0.5 cm (Fig. 3.5c). Therefore, Scenario 1 assumes Redfield mineralization in the upper 0.5 cm, Scenario 2 assumes preferential organic P mineralization in the upper 0.5 cm, and Scenario 3 assumes very low rates of organic P mineralization relative to organic C. The $r_{CP}$ values from 0.5 cm down to the bottom of the modeled sediment core (50 cm) were the same in all three cases.

The results for Scenario 1 show that the assumption of a Redfield value for $r_{CP}(flux)$ and for organic matter mineralization in the upper 0.5 cm over-predicts the measured $P_{org}$ concentration by a factor of 4 to 5 (Fig. 3.5a). This is because a Redfield flux brings more $P_{org}$ into the sediment than can be mineralized using Redfield $r_{CP}$ values in the upper 0.5 cm. Consequently, the bulk of $P_{org}$ escapes mineralization in the surface layer and is buried below 0.5 cm where $P_{org}$ degradation slows down dramatically relative to organic C.The results for Scenario 2 show that the $P_{org}$ data can be simulated if the material arriving at the sea floor has Redfield composition, but only if there is enhanced mineralization of $P_{org}$ in the upper 0.5 cm. In this case, the C:P mineralization ratio of the material being degraded in the top 0.5 cm ($r_{CP}(0\text{-}0.5)$) is 56. The rate of $P_{org}$ mineralization in the surface layer in this scenario is high enough to remove the "excess" $P_{org}$ delivered to the sediment from the water column. Alternatively, Scenario 3 shows an equally good fit to the $P_{org}$ data using a $r_{CP}(flux)$ value of 450, which is similar to the

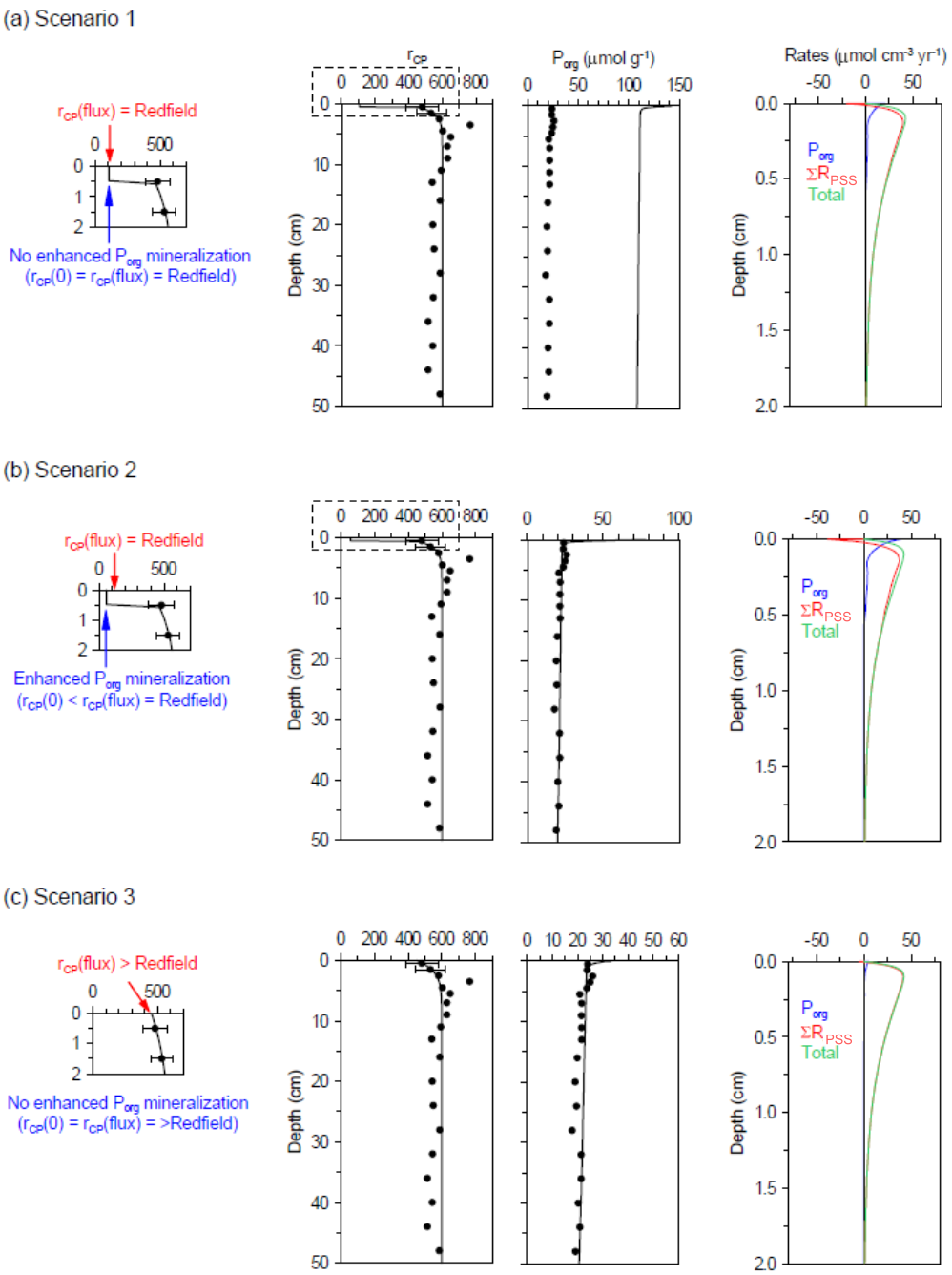


**Fig. 3.5:** Modeled rates of biogeochemical reactions contributing to the benthic $TPO_4$ pool. The contribution of $P_{org}$ to the benthic P turnover is investigated in three different scenarios. (a) In Scenario 1 organic matter flux to the sea floor has Redfield C:P stoichiometry and is degraded in Redfield proportions. (b) Scenario 2 also assumes Redfield organic matter flux, but allows enhanced $P_{org}$ release during organic matter degradation in the uppermost 0.5 cm of the sediment. (c) Scenario 3 assumes deposition of P- depleted organic matter with a C:P value of 450, and the mineralization ratio in the upper 0.5 cm is defined by the trend of the measured $r_{CP}$ values (see text). Release of $P_{org}$ during organic matter degradation is the only specified source of P; all other sources and sinks, such as release of P from Fe oxyhydroxides, fish debris and authigenic Ca-P minerals, are combined into a single rate $\sum R_{PSS}$ (see text).

suspended particulate organic matter off Peru (Franz et al. 2012). Based on these results, either Scenario 2 or 3 or a combination thereof can explain the measured data. Given the observed $r_{CP}$ of suspended organic matter by Franz et al. (2012), it could be argued that Scenario 3 provides a more reasonable explanation of the data compared to the other two cases.

If the organic material is already depleted in $P_{org}$ by the time it reaches the sediment-surface (i.e. Scenario 3), then this will have important implications for the benthic $TPO_4$ budget. Depth-integrated $TPO_4$ release rates predicted by the model indicate that mineralization of $P_{org}$ in Scenario 3 is almost negligible and contributes < 2% to the overall total release of $TPO_4$ in the sediment (Fig. 3.5c). However, even for Scenario 2, this fraction increases to only 13% (Fig. 3.5b). This represents an upper limit for the potential contribution of $P_{org}$ to benthic $TPO_4$ flux. Consequently, an additional P source with a maximum rate of ca. 40 µmol $cm^{-3}$ $yr^{-1}$ is required to cover the deficit ($\Sigma R_{PSS}$, right panels in Fig. 3.5).

As P release from iron oxyhydroxides is of minor importance in the core of the OMZ (Noffke et al. 2012), the source of $TPO_4$ likely originates from an authigenic Ca-P pool. This is consistent with the independent mass balance approach presented above.

In summary, the mass balance and the model approach provide corroborating ideas on the pathways of benthic P cycling off Peru. However, since the speciation of P raining to the sediment is not resolved by our measurements, future studies involving analysis of the suspended particulate matter and higher resolution sediment sampling are needed to unambiguously resolve the P fractions that contribute to the high measured $TPO_4$ fluxes.

### *3.5.3 Changes in phosphorus cycling through the OMZ*

Summarizing the mass balance approach, Fig. 3.6 illustrates variations in the degree of burial and release of P, as well as in the magnitude of the individual P fractions $P_{org}$, $P_{terr}$ and $P_{auth}$ occurring across the transect. Within the whole OMZ (ca. 50-500 m water depth), most of the deposited P is recycled back into the water column and burial is low (Table 3.2). Inside The core of the OMZ (250-500 m depth), $TPO_4$ release to the pore water is predominantly driven by authigenic P. This is in contrast to the 78 m shelf site, where terrestrial P, and to a minor extent organic P, contribute ca. 33% to the total P input. The mass balance does not identify the contribution of these three P phases to the

benthic $TPO_4$ flux. However, if the authigenic P source was completely dissolved, it would only amount to about 80% of the benthic $TPO_4$ release.

The mass balance uses the $r_{CP}$ values that were determined in the 0-1 cm sediment horizon for each of the sites investigated. However, in shallow shelf waters at 10°S, suspended particulate organic matter highly enriched in P, with $r_{CP}$ values as low as 50, has been observed (Franz et al. 2012). Assuming that similar organic matter is deposited at the sea floor at 11°S, the role of organically bound P in the P turnover of the shelf sites may have to be re-evaluated. Using a $r_{CP}$ value of 50 instead of 292 at 0.5 cm sediment depth, the organically bound P contribution would increase to 0.271 mmol $m^{-2}$ $d^{-1}$ (Table 3.2), contributing 54% to the $RR_{Ptot}$, and potentially up to 64% to the benthic $TPO_4$ flux (Fig. 3.6b). However, as the diagenetic P model has shown, this would require even stronger preferential P regeneration within the thin surface layer than for Scenario 2 described above. The deposition of P-enriched organic matter on the shelf would imply a decrease in the authigenic P input by a factor of 3 to 0.15 mmol $m^{-2}$ $d^{-1}$ (Fig. 3.6b). This would be consistent with the almost negligible fish-P levels and the generally low authigenic Ca-P inventory in the sediment here. Nonetheless, subsurface peaks of authigenic Ca-P, around 5 cm and 7 cm below the sediment surface, were observed on the shelf sites at water depths of 78 m and 85 m, respectively. A possible explanation for these subsurface enrichments is their in situ formation related to the activity of microbial mats. Members of the sulfide-oxidizing bacteria *Thiomargarita* spp. and *Beggiatoa* spp. have been reported to mediate the conversion of pore-water $TPO_4$ into apatite (Schulz and Schulz 2005; Goldhammer et al. 2010). During $^{33}$P-radiotracer experiments, Goldhammer et al. (2010) found the greatest conversion rates of $TPO_4$ to apatite mediated by sulfide-oxidizing bacteria under anoxic conditions. Indeed, extended microbial mat communities of the genus *Beggiatoa* spp. but also *Thioploca* spp. were observed at the sediment surface particularly at the shelf and upper slope of the investigated transect (Mosch et al. 2012).

The P retention capacity of the sediment increased at the deeper sites and 47% to 74% of the incoming P was buried (line t, Table 3.2). Enhanced P retention is likely related to the increased $O_2$ concentrations and resulting accumulation of iron oxyhydroxides at the sediment surface, which act as efficient scavengers for dissolved P (Sundby et al. 1992; Slomp et al. 1998). In our working area, reactive iron contents of the surface interval

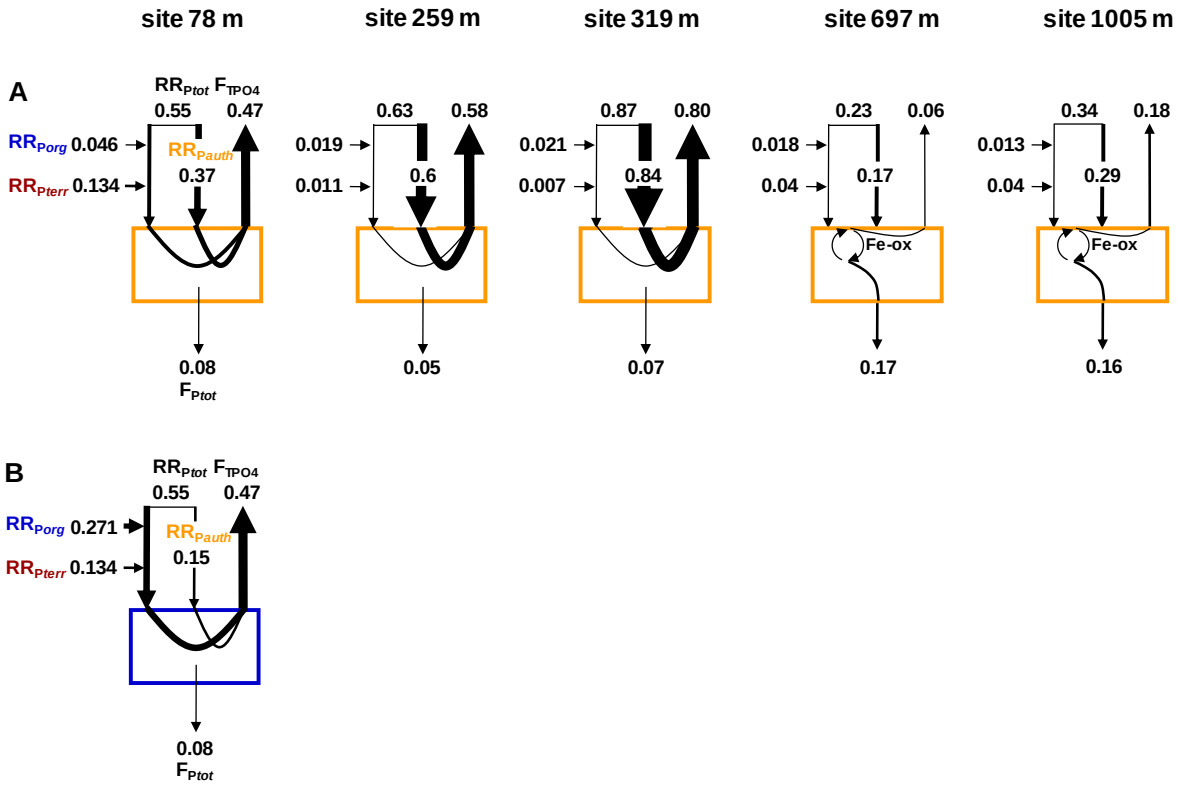


**Fig. 3.6:** Phosphorus mass balances along the latitudinal depth transect at 11°S. In panel A the mass balance is shown using the $r_{CP}$ values of the surface sediments (see Table 2); in panel B an alternative mass balance for the shelf based on a $r_{CP}$ value of 50 as derived from water column data (Franz et al. 2012) is shown. For details see text. The site at 78 m is exemplary shown for the two shelf sites investigated. All fluxes are given in mmol $m^{-2}$ $d^{-1}$. Thickness of the arrows indicates the magnitude of fluxes. The thickness of the arrows inside the boxes only represents probabilities as it is uncertain to what extent the different P sources contribute either to burial or release.

(0-1 cm) were found to be strongly elevated below 600 m water depth (Noffke et al. 2012). When mixed into deeper anoxic layers, iron oxyhydroxides further may play an important role as an intermediate during the formation of carbonate fluorapatite as has been shown for Arabian Sea OMZ sediments (Kraal et al. 2012). Subsequent $TPO_4$ release during reductive iron dissolution will elevate pore-water $TPO_4$ levels and induce the precipitation of carbonate fluorapatite. Evidence of biological mixing below 500 m water depth was observed during sea-floor imaging conducted along the 11°S transect (Mosch et al. 2012).

As for the sites inside the OMZ, the greatest fraction of buried P was related to the accumulation of fish debris. However, in order to explain the higher burial efficiencies at these deeper sites it has to be assumed that fish-P is less degradable here. This assertion is

based on the observation that the fish-P inventories between the sites at 697 m and 1005 m, and the site 319 m from the core of the OMZ are similar. If the degradability of the fish-P at either site would be the same, one should observe much higher release rates of $TPO_4$ at the two deeper sites or a higher burial efficiency at the 319 m site, which was not the case. Besides the strong contribution of fish debris, the input of authigenic apatite from the water column as well as down-slope transport of phosphorite may further contribute to the authigenic Ca-P inventory.

## 3.6 Conclusions

In this study, sources of the strongly elevated benthic $TPO_4$ fluxes that were measured in the Peruvian OMZ (Noffke et al. 2012) were investigated using solid phase speciation measurements in combination with a mass balance approach and a diagenetic P model analysis. Our investigations strongly suggest that the P release inside the Peruvian OMZ is driven by authigenic Ca-P rather than by the input of organic and terrigenous P. If P-enriched organic matter is deposited on the sea floor at the shelf, as water-column data on the shelf imply, then organic P has the potential to be important for the sedimentary P budget here.

The main source of the authigenic P is probably fish debris. However, authigenic calcium fluorapatites forming in the water column and down slope translocation of phosphorites might further contribute to the Ca-P inventory. The mass balance further allows to estimate burial efficiencies of P, and thus to better evaluate the high $TPO_4$ release rates that were measured by benthic landers with regard to their importance for surface-water productivity. Within the entire OMZ, a major proportion of the P input (> 80%) is recycled back to the water column, highlighting the prominent role of these sediments as sources of bioavailable P for phytoplankton.

## Acknowledgements

We thank the captain and crew of R/V *Meteor* for their support during cruise M77/1-2; A. Bleyer, B. Domeyer, M. Dibbern, R. Ebbinghaus, S. Kriwanek, and R. Surberg for help with geochemical analyses onboard and in the home laboratory; and, as well B. Bannert, A. Petersen, and M. Türk for ensuring system maintenance and benthic lander deployments. We further thank P. Appel and his team from the Institute of Geosciences,

University of Kiel, and D. Rau from GEOMAR for XRF analyses, and D. Garbe-Schönberg from the Institute of Geosciences, University of Kiel, for ICP-OES measurements. Special thanks are due to R. Ebbinghaus for spending extensive time in the lab during phosphorus extractions. This is a contribution of the Sonderforschungsbereich 754 "Climate-Biogeochemistry Interactions in the Tropical Ocean", which is supported by the Deutsche Forschungsgemeinschaft.

## References

Anderson, D. L., and M. Delaney 2004. Sequential extraction and analysis of phosphorus in marine sediments: Streamlining of the SEDEX procedure. Limnol. Oceanogr. **45:** 509-515.

Benitez-Nelson, C. R. 2000. The biogeochemical cycling of phosphorus in marine systems. Earth Sci. Rev. **51:** 109-135.

Bohlen, L., A. W. Dale, S. Sommer, T. Mosch, C. Hensen, A. Noffke, F. Scholz, and K. Wallmann 2011.Benthic nitrogen cycling traversing the Peruvian oxygen minimum zone. Geochim. Cosmochim. Acta **75:** 6094-6111.

Chavez, F. P., M. Messié, and J. T. Pennington 2011. Marine primary production in relation to climate variability and change. Ann. Rev. Mar. Sci. **3:** 227-260.

Delaney, M. L. 1998. Phosphorus accumulation in marine sediments and the oceanic phosphorus cycle. Glob. Biogeochem. Cycles **12:** 563-572.

Dellwig, O., T. Leipe, C. März, M. Glockzin, F. Pohllene, B. Schnetger, E. V. Yakushev, M. E. Böttcher, and H.-J. Brumsack 2010. A new particulate Mn-Fe-P shuttle at the redoxcline of anoxic basins. Geochim. Cosmochim. Acta **74:** 7100-7115.

Diaz, J., E. Ingall, C. R. Benitez-Nelson, D. Paterson, M. D. De Jonge, I. McNulty, and J. A. Brandes 2008. Marine polyphosphate: A key player in geologic phosphorus sequestration. Science **320:** 652-655.

Díaz-Ochoa, J. A., C. B. Lange, S. Pantoja, G. J. De Lange, D. Gutiérrez, P. Muñoz, and M. Salamanca. 2009. Fish scales in sediments from off Callao, central Peru. Deep Sea Res. II **56:** 1124-1135.

Faul, K. L., A. Paytan, and M. L. Delaney. 2005. Phosphorus distribution in sinking particulate oceanic matter. Mar. Chem. **97:** 307-333.

Filippelli, G. M. 2008. The global phosphorus cycle: Past, present, and future. Elements **4:** 89-95.

Föllmi, K. B. 1996. The phosphorus cycle, phosphogenesis and marine phosphate-rich deposits. Earth Sci. Rev. **40**: 55-124.

Franz, J., G. Krahmann, G. Lavik, P. Grasse, T. Dittmar, and U. Riebesell. 2012. Dynamics and stoichiometry of nutrients and phytoplankton in waters influenced by the oxygen minimum zone in the eastern tropical Pacific. Deep-Sea Res. I **62:** 20-31.

Froelich, P. N., M. L. Bender, N. A. Luedtke, G. R. Heath, and T. DeVries. 1982. The marine phosphorus cycle. Am. J. Sci. **282:** 474-511.

Froelich, P. N., M. A. Arthur, W. C. Burnett, M. Deakin, V. Hensley, R. Jahnke, L. Kaul, K.-H. Kim, R. Roe, A. Soutar and C. Vathakanon. 1988. Early diagenesis of organic matter in Peru continental margin sediments: Phosphorite precipitation. Mar. Geol. **80:** 309-343.

Glenn, C. R., and M. A. Arthur. 1988. Petrology and major element geochemistry of Peru margin phosphorites and associated diagenetic minerals: Authigenesis in modern organic-rich sediments. Mar. Geol. **80:** 231-267.

Goldhammer, T., V. Brüchert, T. G. Ferdelman, and M. Zabel. 2010. Microbial sequestration of phosphorus in anoxic upwelling sediments. Nat. Geosc. **3:** 557-561.

Grasshoff, K., M. Erhardt, and K. Kremling. 1999. Methods of Seawater Analysis. 3rd ed., Wiley VCH.

Guidry, M. W., and F. T. Mackenzie. 2003. Experimental study of igneous and sedimentary apatite dissolution: control of pH, distance from equilibrium and temperature on dissolution rates. Geochim. Cosmochim. Acta **67:** 2949-2963.

Gutiérrez, D., E. Enríquez, S. Purca, L. Quipúzcoa, R. Marquina, G. Flores, and M. Graco. 2008. Oxygenation episodes on the continental shelf of central Peru: Remote forcing and benthic ecosystem response. Prog. Oceanogr. **79**: 177-189.

Hartnett, H. E., and A. H. Devol. 2003. Role of a strong oxygen-deficient zone in the preservation and degradation of organic matter: A carbon budget for the continental margins of northwest Mexico and Washington State. Geochim. Cosmochim. Acta **67:** 247-264.

Ingall, E. D., R. M. Bustin, and P. Van Cappellen. 1993. Influence of water column anoxia on the burial and preservation of carbon and phosphorus in marine shales. Geochim. Cosmochim. Acta **57:** 303-316.

Ingall, E., and R. Jahnke 1994. Evidence for enhanced phosphorus regeneration from marine sediments overlain by oxygen depleted waters. Geochim. Cosmochim Acta **58:** 2571-2575.

Jahnke, R. A., S. R. Emerson, K. K. Roe, and W. C. Burnett. 1983. The present day formation of apatite in Mexican continental margin sediments. Geochim. Cosmochim. Acta **47:** 259-266.

Jilbert, T., C. P. Slomp, B. G. Gustafsson, and W. Boer. 2011. Beyond the Fe-P redox connection: Preferential regeneration of phosphorus from organic matter as a key control on Baltic Sea nutrient cycles. Biogeosciences **8:** 1699-1720.

Kraal, P., C. P. Slomp, D. C. Reed, G. J. Reichart, and S. W. Poulton. 2012. Sedimentary phosphorus and iron cycling in and below the oxygen minimum zone of the northern Arabian Sea. Biogeosciences **9:** 2603-2624.

Krissek, L. A., K. F. Scheidegger, and L. D. Kulm. 1980. Surface sediments of the Peru-Chile continental margin and the Nazca Plate. Geol. Soc. Am. Bull. **91:** 321-331.

Lucotte, M., and B. D'Anglejan. 1985. A comparison of several methods for the determination of iron hydroxides and associated orthophosphates in estuarine particulate matter. Chem. Geol. **48:** 257-264.

Lyons, G., C. R. Benitez-Nelson, and R. C. Thunell. 2011. Phosphorus composition of sinking particles in the Guaymas Basin, Gulf of California. Limnol Oceanogr. **56:** 1093-1105.

McClellan, G. H. 1980. Mineralogy of fluorapatites. J. Geol. Soc. **137:** 675-681.

McManus, J., W. M. Berelson., K. H. Coale, K. S. Johnson, and T. E. Kilgore. 1997. Phosphorus regeneration in continental margin sediments. Geochim. Cosmochim. Acta **61:** 2891-2907.

Mosch, T., S. Sommer, M. Dengler, A. Noffke, L. Bohlen, O. Pfannkuche, V. Liebetrau, and K. Wallmann. 2012. Factors influencing the distribution of epibenthic megafauna across the Peruvian oxygen minimum zone. Deep Sea Res. I **68:** 123-135.

Mort, H. P., C. P. Slomp., B. G. Gustafsson, and T. J. Andersen. 2010. Phosphorus recycling and burial in Baltic Sea sediments with contrasting redox conditions. Geochim. Cosmochim Acta **74:** 1350-1362.

Noffke, A., C. Hensen, S. Sommer, F. Scholz, L. Bohlen, T. Mosch, M. Graco, and K. Wallmann. 2012. Benthic iron and phosphorus fluxes across the Peruvian oxygen minim zone. Limnol. Oceanogr. **57:** 851-867.

Paytan, A., B. J. Cade-Menun, K. McLaughlin, and K. L. Faul. 2003. Selective phosphorus regeneration from sinking marine particles: evidence from $^{31}$P-NMR. Mar. Chem. **82:** 55-70.

Paytan, A., and K. McLaughlin. 2007. The oceanic phosphorus cycle. Cem. Rev. **107:** 563-576.

Pennington, J. T., K. L. Mahoney, V. S. Kuwahara, D. D. Kolber, R. Calienes, and F. P. Chavez. 2006. Primary production in the eastern tropical Pacific: A review. Prog. Oceanogr. **69:** 285-317.

Reimers, C. E., and E. Suess. 1983. Spatial and temporal patterns of organic matter accumulation on the Peru continental margin, p. 311-337. *In* J. Thiede, and E. Suess [eds.], Coastal Upwelling: Its Sediment Record. Part B: Sedimentary Records of Ancient Coastal Upwelling. Plenum Press.

Ruttenberg, K. C. 1992. Development of a sequential extraction method for different forms of phosphorus in marine sediments. Limnol. Oceanogr. **37:** 1460-1482.

Ruttenberg, K. C. 1993. Reassessment of the oceanic residence time of phosphorus. Chem. Geol. **107:** 405-409.

Sannigrahi, P., and E. Ingall. 2005. Polyphosphates as a source of enhanced P fluxes in marine sediments overlain by anoxic waters: Evidence from $^{31}$P NMR. Geochem. Trans. **6:** 52-59.

Schenau, S. J., and G. J. De Lange. 2000. A novel chemical method to quantify fish debris in marine sediments. Limnol. Oceanogr. **45:** 963-971.

Schenau, S. J., C. P. Slomp, and G. J. De Lange. 2000. Phosphogenesis and active phosphorite formation in sediments from the Arabian Sea oxygen minimum zone. Mar. Geol. **169:** 1-20.

Schenau, S. J., and G. J. De Lange. 2001. Phosphorus regeneration vs. burial in sediments of the Arabian Sea. Mar. Chem. **75:** 201-217.

Scholz, F., C. Hensen., A. Noffke, A. Rohde, V. Liebetrau, and K. Wallmann. 2011. Early diagenesis of redox-sensitive trace metals in the Peruvian upwelling area-response to ENSO-related oxygen fluctuations in the water column. Geochim. Cosmochim. Acta **75:** 7257-7276.

Schulz, H. N., and H. D. Schulz. 2005. Large sulfur bacteria and the formation of phosphorite. Science **21:** 416-418.

Sekula-Wood, E., C. R. Benitez-Nelson, M. A. Bennett, and R. Thunell. 2012. Magnitude and composition of sinking particulate phosphorus fluxes in Santa Barbara Basin, California. Glob. Biogeochem. Cycles **26:** GB2023, doi: 10.1029/2011GB004180

Silva, N., N. Rojas, and A. Fedele. 2009. Water masses in the Humboldt Current System: Properties, distribution and the nitrate deficit as a chemical water mass tracer for equatorial subsurface water off Chile. Deep-Sea Res. II **56:** 1004-1020.

Slomp, C.P., J. F. P. Malschaert, and W. Van Raaphorst. 1998. The role of adsorption in sediment-water exchange of phosphate in North Sea continental margin sediments. Limnol. Oceanogr. **43:** 832-846.

Slomp, C.P., and P. Van Cappellen. 2007. The global marine phosphorus cycle: sensitivity to oceanic circulation. Biogeosciences **4:** 155-171.

Sommer, S., P. Linke, O. Pfannkuche, T. Schleicher, J. Schneider v. Deimling, A. Reitz, M. Haeckel, S. Flögel, and C. Hensen. 2009. Seabed methane emissions and the habitat of frenulate tube worms on the Captain Arutyunov mud volcano (Gulf of Cadiz). Mar. Ecol. Prog. Ser. **382:** 69-86.

Steenbergh, A. K., P. L. E. Bodelier, H. L. Hoogveld, C. P. Slomp, and H. J. Laanbroek. 2011. Phosphatases relieve carbon limitation of microbial activity in Baltic Sea sediments along a redox-gradient. Limnol. Oceanogr. **56:** 2018-2026.

Stramma, L., G. C. Johnson, J. Sprintall, and V. Mohrholz. 2008. Expanding oxygen-minimum zones in the tropical oceans. Science **320:** 655-658.

Strub, P. T., J. M. Mesías, V. Montecino, R. Rutlland, and S. Salinas. 1998. Coastal ocean circulation of western South America, p. 273-313. *In* A. R. Robinson, and K. H. Brink [eds.], The Sea. Wiley.

Suess, E. 1981. Phosphate regeneration from sediments of the Peru continental margin by dissolution of fish debris. Geochim. Cosmochim. Acta **45:** 577-588.

Suess, E., L. D. Kulm, and J. S. Killingley. 1987. Coastal upwelling and a history of organic rich mudstone deposition off Peru, p. 181-197. *In* J. Brooks and A. J. Fleet [eds.], Marine Petroleum Source rocks. Geological Society Spec. Publ. **26**.

Sundby, B., C. Gobeil, N. Silverberg, and A. Mucci. 1992. The phosphorus cycle in coastal marine sediments. Limnol. Oceanogr. **37:** 1129-1145.

Tsandev, I., D. C. Reed, and C. P. Slomp. 2012. Phosphorus diagenesis in deep sea sediments: Sensitivity to water column conditions and global scale implications. Chem. Geol. **330:** 127-139.

Van Cappellen, P., and E. D. Ingall. 1997. Response to comment "Redox stabilization of the atmosphere and oceans and marine productivity" by Colman et al. 1997. Science **475:** 407-408.

Viers, J., B. Dupré, and J. Gaillardet. 2009. Chemical composition of suspended sediments in world rivers: New insights from a new database. Sci. Tot. Environ. **407:** 853-868.

Wallmann, K. 2010. Phosphorus imbalance in the global ocean? Glob. Biogeochem. Cycles **24:** GB4030, doi: 10.1029/2009GB003643

Watanabe, F. S., and S. R. Olsen. 1962. Colorimetric determination of phosphorus in water extracts of soil. Soil Sci. **93:** 183-188.

Woulds, C., M. C. Schwartz., T. Brand, G. L. Cowie, G. Law, and S. R. Mowbray. 2009. Porewater nutrient concentrations and benthic nutrient fluxes across the Pakistan margin OMZ. Deep-Sea Res. II **56:** 333-346.

# 4 Gotland Basin (Baltic Sea) sediments constitute an important internal nutrient source to the water column

A. Noffke[a*], S. Sommer,[a] V. Bertics,[a,b] A. W. Dale,[a] P. O. J. Hall,[c] O. Pfannkuche[a]

[a]Helmholtz-Zentrum für Ozeanforschung Kiel, Wischhofstraße 1-3, 24148 Kiel

[b]now at: Harvard University, Cambridge MA, USA

[c]University of Gothenburg, 41296 Göteborg, Sweden

*author of correspondence: anoffke@geomar.de

Close to submission to Limnology and Oceanography

## Abstract

Benthic fluxes of DIN ($NH_4^+$, $NO_3^-$, $NO_2^-$) and $TPO_4$ were investigated in situ at 7 sites across an oxic to anoxic depth gradient in the Eastern Gotland Basin (Baltic Sea) using benthic landers. In situ fluxes were complemented by CTD casts for water-column nutrient and oxygen ($O_2$) measurements. Based on bottom-water $O_2$ contents, the study area was divided into three different zones: the oxic zone at 60 m to < 80 m water depth, the hypoxic transition zone between 80 m and 120 m, and the deep anoxic and sulfidic basin > 120 m. The hypoxic transition zone was characterized by the occurrence of extended mats of vacuolated sulfur bacteria. High amounts of $NH_4^+$ were released from deep basin sediments and particularly from sediments in the hypoxic transition zone with rates of up to 0.6 mmol $m^{-2}$ $d^{-1}$ and 1 mmol $m^{-2}$ $d^{-1}$, respectively. In the transition zone, in addition to ammonification and benthic nitrogen fixation, dissimilatory nitrate reduction to ammonium (DNRA) was identified as a likely $NH_4^+$ source. $NO_3^-$ fluxes were directed into the sediment at all stations between 80 m and 124 m, and were zero below, due to the absence of $NO_3^-$ in the bottom water. $TPO_4$ release was also highest in the hypoxic transition zone with 0.2 mmol $m^{-2}$ $d^{-1}$. Further, high $TPO_4$ release of up to

0.15 mmol $m^{-2}$ $d^{-1}$ was measured in the deep basin. At the oxic sites, $TPO_4$ fluxes were directed into the sediment except at the 66 m site. At this site, the $TPO_4$ release could be fully explained by the Redfield degradation of organic matter, but was not sufficient in the hypoxic transition zone nor in the deep basin. In these environments, preferential phosphorous (P) release during organic matter degradation appeared to be the major contributor. In the hypoxic transition zone, microbial mats might further have interacted with benthic P turnover.

Up-scaling of the benthic fluxes to the Baltic Proper, excluding the Arkona basin and shallow sandy sites < 60 m water depth, resulted in a high internal $TPO_4$ and DIN load of 109 kt $yr^{-1}$ and 295 kt $yr^{-1}$, respectively. This is 7.8-fold higher than the total external P load of 14 kt $yr^{-1}$ and 2.1-fold higher than the external DIN load of 140 kt $yr^{-1}$ for the year 2006 (HELCOM 2009*b*). This study highlights the importance of the hypoxic transition zone for the internal nutrient loading, which only covered 51% of the total area, but released as much as 70% (76 kt $yr^{-1}$) of the total $TPO_4$ load. Likewise, 75% of the internal $NH_4^+$ load (200 kt $yr^{-1}$) was released from this particular environment. In contrast to $TPO_4$, the released DIN from the sediments apparently does not reach the euphotic zone, except at the shallower sites. This, in combination with P and N turnover in the water column results in the supply of low N:P ratio water from the anoxic water column to the euphotic zone. In summertime, this favors the development of $N_2$-fixing cyanobacterial blooms which significantly counteract the Baltic Proper from recovering from eutrophication. As distinct bottom-water $O_2$ fluctuations were reported from the hypoxic transition zone, we suspect that transient nutrient release takes place on different time scales that needs particular attention in Baltic Sea management plans.

## 4.1 Introduction

Hypoxia is a worldwide growing problem and occurred in the Baltic Sea since its formation at about 8000 yr BP (Conley et al. 2009). In association with anthropogenically induced eutrophication and inflows of North Sea water ventilating the deeper areas, the spatial extent and intensity of hypoxia is variable but increasing overall (Conley et al. 2009; HELCOM 2009*a*). Oxygen ($O_2$)-deficient conditions not only reduce habitats for higher organisms (Diaz and Rosenberg 2008; Karlson et al. 2002), but also strongly affect the redox-sensitive cycling of nitrogen (N), phosphorus (P) and iron (Fe), and

concentrations of these nutrients in the water column. In response to an expansion of the hypoxic bottom waters since the mid 20th century (Jonsson et al. 1990) intense efforts backed by the Helsinki Commission have been made to reduce anthropogenic nutrient inputs to the Baltic Sea. However, although a reduction of nutrient discharge has been achieved by the majority of the Baltic Sea states, there has presently been no significant mitigation of eutrophication (HELCOM 2009*b*).

In offshore regions, internal feedback processes have been identified to counteract the recovery from eutrophication (Vahtera et al. 2007). These authors described a succession of phytoplankton and cyanobacterial blooms, which is largely controlled by a shift in the water-column nitrogen to phosphorus (N:P) ratio. In spring, the water-column nitrate ($NO_3^-$) inventory is consumed by N-limited phytoplankton. Subsequently to this spring bloom, sedimentation and degradation of phytoplankton lead to $O_2$-deficient bottom waters and enhanced removal of dissolved inorganic nitrogen (DIN, here defined as sum of ammonium ($NH_4^+$), $NO_3^-$ and nitrite ($NO_2^-$)) by denitrification and anammox, releasing di-nitrogen gas ($N_2$). Elevated fluxes of phosphate ($TPO_4$) under low-$O_2$ bottom waters further lower the N:P ratio in the water column and allow extensive growth of P-limited diazotrophic cyanobacteria during summer. These organisms facilitate $N_2$-fixation, restoring the N:P ratio in the water column. This sequence of planktonic- and cyanobacterial blooms represents a vicious cycle, which is considered to prevent the recovery of the Baltic Sea from eutrophication.

Despite the strong significance of the benthos as major feedback mechanism changing the water-column N:P ratio, comprehensive benthic flux studies in these offshore regions of the Baltic Proper are scarce. Benthic N cycling in the Baltic Sea has been predominantly studied under the aspect of N loss, with denitrification and, more recently, anammox as major processes that both release $N_2$ into the environment. Therewith, either process removes reactive N and counteracts eutrophication. Most of these studies were conducted in coastal areas, particularly in the Gulf of Finland (Hietanen and Lukkari 2007; Hietanen and Kuparinen 2008; Jäntti et al. 2011), but studies in the Baltic Proper are scarce (Tuominen et al. 1998; Deutsch et al. 2010). Furthermore, most of the rate measurements were conducted during ex situ incubations. The release of $NH_4^+$ from sediments has not been studied systematically in the Baltic Sea. $NH_4^+$ is released when organic matter is decomposed (ammonification), and accumulates in the anoxic bottom water. Despite that

$NH_4^+$ flux measurements from the central Baltic Proper are largely missing, in several water-column investigations an enrichment of $NH_4^+$ in the deep basin water has been measured, whose source was assumed to be the underlying sediments (e.g. Nehring 1987; Voss et al. 1997). Another process that releases $NH_4^+$ into the ambient sea water is the dissimilatory nitrate reduction to ammonium (DNRA). DNRA is mediated by sulfide-oxidizing bacteria, such as *Thiomargarita* spp. or filamentous *Beggiatoa* spp. and *Thioploca* spp., which often form dense mats on organic–rich surface sediments in $O_2$-deficient environments (Gallardo 1977; Gutiérrez et al. 2008; Schmaljohann et al. 2001). Instead of using $O_2$ as an electron acceptor for sulfide oxidation, these organisms have the capacity to switch to a $NO_3^-$- or potentially $NO_2^-$-based (Zopfi et al. 2001) metabolism, and thereby release $NH_4^+$ into the environment (Jørgensen and Nelson 2004). This process retains DIN in the ecosystem, and thereby opposes denitrification and anammox. DNRA has been discussed as a potentially important process under low-$O_2$ conditions in sediments from the northern Baltic Proper and the coastal Gulf of Finland (Kuparinen and Tuominen 2001; Hietanen and Lukkari 2007). However, first DNRA rate measurements, during ex situ sediment incubations, were only recently determined for the Gulf of Finland (Jäntti et al. 2011) and two oxic sites ($O_2$ > 170 $\mu$mol $L^{-1}$) in the Baltic Proper (Jäntti et al. 2012).

Based on the analysis of water-column time series data, it has been shown that annual changes of $TPO_4$ in the Baltic Proper correlated with the sea-floor area covered with hypoxic bottom water, but not with the external P input, indicating that the sediments act as an internal source for P (Conley et al. 2002). Budget calculations for the years 1991 to 1999 revealed that the Baltic Sea sub-basins, except the Baltic Proper, retain more P than they received from external sources (Savchuck 2005). In the Baltic Proper, the high average P amount in the water column can not be covered by the external P load and P input from the other sub-basins compared to the net P export, implying that an internal P source is needed to account for the discrepancy in the budget. Such an internal P source has been related to P release from the anoxic sea bed (Savchuk 2005). However, as for N, still actual rate measurements are scarce. Few studies were conducted in the Gulf of Finland, mostly deriving $TPO_4$ fluxes from pore-water gradients or ex situ core incubations, except the study of Viktorsson et al. (2012) who were using benthic landers. Hille et al. (2005) and Matthiesen et al. (1998) provide diffusive flux estimates for the

eastern Gotland Basin. On a basin-wide scale, recent advances and understanding of P dynamics in relation to bottom-water $O_2$ concentrations have been made by Mort et al. (2010) and Jilbert et al. (2011) who provide diffusive $TPO_4$ fluxes, which for the deep basins were assumed to be driven by preferential P release during organic matter degradation (Jilbert et al. 2011). In hypoxic environments, elevated $TPO_4$ release has been further attributed to the reductive dissolution of iron oxides and iron hydroxides (hereafter referred to as Fe oxyhydroxides) (Mort et al. 2010; Jilbert et al. 2011). Just recently, first in situ $TPO_4$ fluxes have been measured in the eastern Gotland Basin (Viktorsson et al. 2013).

In the present study, the significance of the sea floor for internal nutrient loading was investigated along an oxic to anoxic depth gradient in the eastern Gotland Basin by measuring in situ fluxes of $TPO_4$ but also of N species using benthic landers. By presenting combined DIN and $TPO_4$ fluxes, this study further addressed the function of the sea bed affecting N:P ratios in the water column, which in turn govern primary production at the sea surface. Besides the deep, persistently anoxic basin, whose importance for nutrient release can be expected, our investigations identified a second zone characterized by high N and P fluxes at the transition between the deep anoxic basin and the oxic surface layer. This zone, in the following referred to as hypoxic transition zone, was located between the deep anoxic basin and the oxic surface layer. The hypoxic transition zone, which in previous studies has not been considered explicitly, is characterized by bottom-water $O_2$ levels that are fluctuating on various time scales from days to weeks (Sommer et al. unpubl. data) and the occurrence of extended microbial mats of sulfur bacteria. These bacteria are known to respond to variable $O_2$ regimes, thereby strongly affecting turnover of not only sulfur and N, but also of P, in form of transient storage and release of P under oxic and anoxic conditions (Dale et al. 2013). Hence, this hypoxic transition zone is to expect to exert significant variability in the benthic nutrient release, which needs to be considered in Baltic Sea management activities.

## 4.2 Methods

### *4.2.1 Regional setting*

The Baltic Sea is landlocked, with a topography that consists of a series of basins separated from each other by shallow sills and narrow channels. The eastern Gotland Basin (hereafter also referred to as Gotland Basin) is the largest basin, and the second deepest with a maximum water depth of 249 m. Restricted water exchange of the Baltic Sea with the North Sea and freshwater input from river run-off maintain a strong horizontal salinity gradient from the south to the north. Density differences of saline and fresher water masses result in a strong stratification of the central basins, with a stable halocline located at water depths of 60 m to 80 m (HELCOM 2009*b*). Ventilation of the deep basins occurs through major inflow events from the North Sea (Matthäus and Franck 1992; Stigebrandt 2003). Stagnation periods in between inflow events cause strong $O_2$ depletion due to remineralization of organic carbon that is exported from the sea surface. This often leads to fully anoxic conditions and the built-up of elevated sulfide concentrations in the deep water (Schincke and Matthäus 1998). The deeper part of the Gotland Basin has remained sulfidic since the end of 2005 (Nausch et al. 2006; Nausch et al. 2012). A recent, relatively large inflow event was recorded in winter 2011-2012, which ventilated the Bornholm Basin (Nausch et al. 2012). This inflow could be traced until the southern part of the Gotland Basin, but was not able to renew its deep water.

Holocene sediments in the Gotland Basin are typically organic rich, highly porous muds. At shallow depths < 60 m sandy sediments prevail, with patchy occurrence of hard grounds (www.helcom.fi/GIS/en_GB/HelcomGIS/). Since ca. 8000 yr BP laminae formation occurred basin-wide in the Baltic Proper at water depths between 73 m and 250 m during periods of hypoxic conditions (Zillén et al. 2008).

### *4.2.2 Sampling of the water column*

Data on conductivity, temperature, depth (CTD) were taken from casts of a Hydrobios CTD system equipped with a water sampling rosette (RO). These casts were conducted at water depths between 50 m and 223 m along an oxic to anoxic depth transect in the eastern Gotland Basin during the R/V *Alkor* cruise 355 in May-June 2010 (Table 4.1; Fig. 4.1). Immediately after retrieval, water samples from Niskin bottles were geochemically analyzed for $O_2$, $NO_3^-$, $NO_2^-$, $NH_4^+$, $TPO_4$, nitrogen:argon ($N_2$:Ar), and total sulfide

**Table 4.1:** Locations of the sites of benthic lander deployments during the R/V *Alkor* cruise 355, along with water depth as well as a characterization of the redox environment. Also shown are positions of CTD deployments where measurements of hydrographic data and nutrients of the water column were conducted, and locations where multiple cores (MUC) were taken for measurements of $N_2$-fixation rates.

| Station no. | Gear no. | Position (°N °E) | Water depth (m) | Environment | Date (2010) |
|---|---|---|---|---|---|
| 332 | BIGO-I-2 | 57°26.53' 20°43.54' | 65 | oxycline | 05 Jun |
| 313 | BIGO-I-1 | 57°26.49' 20°43.51' | 66 | oxycline | 01 Jun |
| 351 | BIGO-II-4 | 57°21.82' 20°35.87' | 80 | hypoxic transition | 14 Jun |
| 346 | BIGO-I-3 | 57°20.87' 20°35.23' | 96 | hypoxic transition | 10 Jun |
| 309 | BIGO-II-1 | 57°20.76' 20°35.22' | 97 | hypoxic transition | 31 May |
| 364 | BIGO-II-5 | 57°20.59' 20°34.34' | 110 | hypoxic transition | 17 Jun |
| 325 | BIGO-II-2 | 57°18,54' 20°33.04' | 124 | anoxic basin | 04 Jun |
| 354 | BIGO-I-4 | 57°20.99' 20°29.00' | 150 | anoxic basin | 15 Jun |
| 344 | BIGO-II-3 | 57°21.06' 20°27.97' | 173 | anoxic basin | 11 Jun |
| 338 | CTD/RO-8 | 57°29.99' 20°56.00' | 50 | oxycline | 06 Jun |
| 310 | CTD/RO-2 | 57°26.48' 20°43.50' | 65 | oxycline | 01 Jun |
| 315 | CTD/RO-3 | 57°21.44' 20°43.06' | 73 | oxycline | 01 Jun |
| 305 | CTD/RO-1 | 57°20.72' 20°35.34' | 94 | hypoxic transition | 31 May |
| 324 | CTD-RO-4 | 57°18.85' 20°33.08' | 124 | hypoxic transition | 03 Jun |
| 350 | CTD/RO-10 | 57°21.08' 20°28.98' | 152 | hypoxic transition | 11 Jun |
| 329 | CTD/RO-5 | 57°21.07' 20°27.98' | 172 | hypoxic transition | 04 Jun |
| 343 | CTD/RO-9 | 57°21.05' 20°27.95' | 173 | anoxic basin | 07 Jun |
| 333 | CTD/RO-6 | 57°22.00' 20°19.00' | 223 | anoxic basin | 05 Jun |
| 353 | CTD/RO-11 | 57°22.99' 20°18.98' | 223 | anoxic basin | 14 Jun |
| 355 | CTD/RO-12 | 57°23.00' 20°19.00' | 223 | anoxic basin | 15 Jun |
| 335 | CTD/RO-7 | 57°21.31' 20°08.62' | 235 | anoxic basin | 05 Jun |
| 365 | MUC 10 | 57°26.49' 20°43.51' | 65 | oxycline | 17 Jun |
| 370 | MUC 12 | 57°20.74' 20°35.35' | 94 | hypoxic transition | 18 Jun |
| 366 | MUC 11 | 57°20.52' 20°34.22' | 111 | hypoxic transition | 17 Jun |
| 371 | MUC 13 | 57°18.70' 20°33.00' | 123 | hypoxic transition | 18 Jun |
| 372 | MUC 14 | 57°20.80' 20°28.39' | 160 | anoxic basin | 18 Jun |

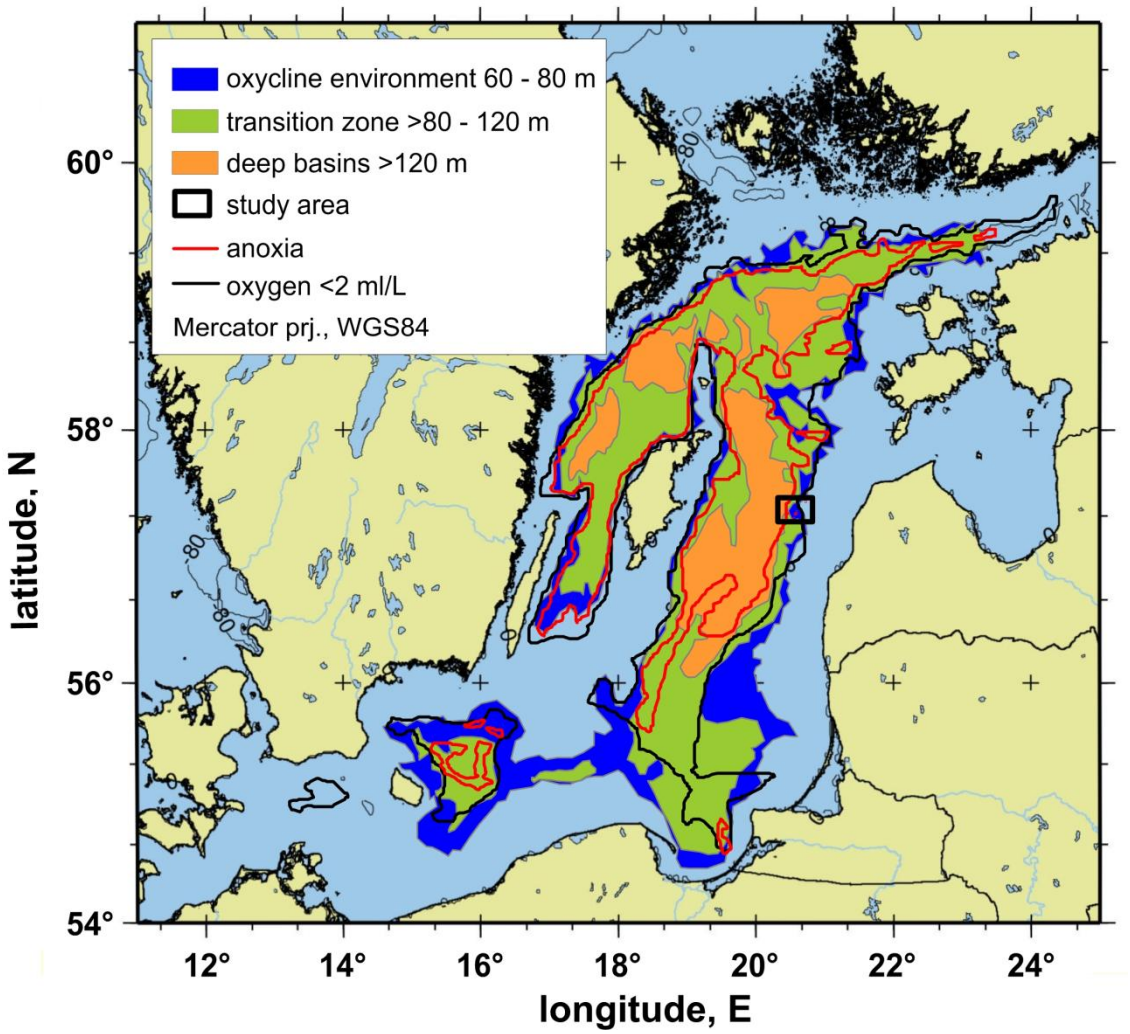


**Fig. 4.1:** Study location (black rectangle) in the eastern Gotland Basin. To extrapolate benthic DIN and $TPO_4$ release for the Baltic Proper, excluding regions < 60 m, in situ fluxes were related to three different depth zones as indicated, in order to account for different $O_2$ availabilities. For details *see* section "Baltic Proper internal loading of $TPO_4$, $NH_4^+$, and $NO_3$". Areas with $O_2$ levels of < 89 $\mu$mol $L^{-1}$ and anoxia for the year 2010 are indicated by black and red contours, respectively (Hansson et al. 2011).

(henceforth referred to as $HS^-$). For details of geochemical analyses *see* below. The water-column profiles of the different solutes shown in Fig. 4.2 (*see* Results section) represent compilations of all data available from the different CTD casts.

### *4.2.3 Sea-floor observation*

Sea-floor images were obtained using the towed camera system OFOS (Ocean Floor Observation System) equipped with a video- and a still camera (Nikon D70s), two Xenon lights (Oktopus) and a flashlight (Benthos). This system was towed ~ 1.5 m above the sea floor.

*4.2.4 In situ flux measurements*

In situ fluxes were measured using two Biogeochemical Observatories (BIGO), as described in detail by Sommer et al. (2009), at seven sites along the oxic to anoxic depth gradient (Table 4.1; Fig. 4.1). BIGO contained two circular flux chambers (internal diameter: 28.8 cm, area: 651.4 $cm^2$), herein referred to as chamber 1 (CH1) and chamber 2 (CH2). An online video-controlled launching system allowed smooth placement of the observatories at selected sites on the sea floor. Four hours after the observatories were placed on the sea floor, the chambers were slowly driven into the sediment (~ 30 cm $h^{-1}$). During this initial time period, the water inside the flux chamber was four times replaced with ambient bottom water. After the chamber was fully driven into the sediment, the chamber water was again replaced with ambient bottom water to flush out solutes that might have been released from the sediment during chamber insertion. The water volume enclosed by the benthic chamber ranged from 9.0 L to 11.9 L (average volume: 9.8 mL).

To determine $NO_3^-$, $NO_2^-$, $NH_4^+$, $TPO_4$, and $HS^-$ fluxes, 8 sequential water samples were removed periodically with glass syringes (volume of each syringe: ~ 47 mL). The syringes were connected to the chamber using 1 m long Vygon tubes with a dead volume of 6.9 mL. Prior to deployment, these tubes were filled with distilled water, and great care was taken to avoid enclosure of air bubbles. An additional syringe water sampler (8 sequential samples) was used to monitor the ambient bottom water. The sampling ports for ambient sea water were positioned about 30-40 cm above the sediment-water interface.

A different type of water sampler was used to take samples from inside each benthic chamber and the ambient bottom water for the analyses of $N_2$ and Ar. This water sampler allows taking a series of four water samples into pre-filled (distilled water), 75 cm long glass tubes (inner diameter: 0.5 cm, volume: 14.7 $cm^3$) using a peristaltic pump. The advantage of this water sampler compared to the syringe water sampler is firstly that the water samples are not diluted with distilled water and secondly that the sample can be transferred directly to a membrane inlet mass spectrometer for $N_2$ and Ar analyses, without risk of atmospheric contamination. The flux measurements were conducted for different time periods, ranging from 33 h to 62 h, as defined by the time interval between the first and the last syringe water sampling. Immediately after retrieval of the observatories, the water samples were stored (max. 4 h) in the onboard cold room (4°C) until geochemical analyses.

The $O_2$ concentration in each chamber and in the ambient bottom water was measured using optodes (Aanderaa Systems [Tengberg et al. 2006]). The precision of the sensors is better at lower concentrations ($\pm$ 0.5 $\mu$mol $L^{-1}$) than at higher concentrations of 300 $\mu$mol $L^{-1}$ to 500 $\mu$mol $L^{-1}$ ($\pm$ 1 $\mu$mol $L^{-1}$). The effect of salinity on the measured $O_2$ concentration was corrected internally by the optode using a setting of 1.12 psu. Pressure lowers the response of $O_2$ detection by about 4% per 100 bar pressure. Due to the low water depths, in which the landers were deployed, this effect was neglected. The fluxes of the different N species, $TPO_4$, and $HS^-$ were calculated from the linear increase or decrease of their concentrations with time. For the calculation of the total oxygen uptake (TOU) the linear part of the $O_2$ time series, well after the start of the chamber incubation, was used.

### *4.2.5 Geochemical measurements*

#### 4.2.5.1 N species

$NO_2^-$, $NH_4^+$, as well as $N_2$:Ar ratios were measured in the shipboard laboratory. $NO_3^-$ water samples were kept deep-frozen (-80°C) until analyses in the home laboratory. $NO_3^-$ was determined using ion chromatography, whereas $NO_2^-$ and $NH_4^+$ were measured using standard photometrical methods (Grasshoff et al. 1983). Detection limits for $NH_4^+$, $NO_3^-$, and $NO_2^-$ were 1 $\mu$mol $L^{-1}$, 1 $\mu$mol $L^{-1}$, and 0.1 $\mu$mol $L^{-1}$, respectively. $N_2$:Ar ratios were measured following the method of Kana et al. (1994). The water samples retrieved during CTD casts were carefully sub-sampled into slender glass bottles (Pyrex test tubes, volume: 25 mL) and immediately capped with a glass-stopper leaving no headspace. The samples were kept in a water bath at in situ temperature and were measured within about six hours after sampling. Dissolved $N_2$ and Ar concentrations were measured using a membrane inlet mass spectrometer (GAM 200, InProcessInstruments). Water samples were sucked through the membrane inlet using a peristaltic pump (Ismatec Reglo Digital) at a flow rate of 1.005 mL $min^{-1}$. The design of the glass membrane inlet followed that of G. Lavik (Max Planck Institute for Marine Microbiology, Bremen, Germany). Within the glass inlet, the water was flowing through a permeable silicone tube (length: 40 mm, inner diameter: 1.4 mm). Gas flow from the inlet to the mass spectrometer was supported with helium that was supplied through a fused silica capillary (inner diameter: 100 $\mu$m). A cryo trap (filled with ethanol at -35°C) inline between the inlet and the mass spectrometer

was used to reduce water vapor. Concentrations of $N_2$ and Ar were obtained from ion currents at a mass to charge ratio of 28 and 40, respectively. A secondary electron multiplier was used as a detector. Instrument response time was less than 4 min. Standards were produced by equilibrating pre-filtered (0.2 $\mu$m) sea-water samples of different salinities with air at the respective in situ temperature in a water bath. Different salinities were produced by appropriate dilution of bottom water from the respective working areas. The dissolved gas concentrations of the saturated air-equilibrated water standards were calculated using the solubility equations of Hamme and Emerson (2004). Calibrations were conducted before and after each measurement session.

4.2.5.2 $TPO_4$, $SO_4^{2-}$, $HS^-$, and $O_2$

$TPO_4$, $SO_4^{2-}$, and $HS^-$ were measured using standard spectrophotometrical methods according to Grasshoff et al. (1983). $O_2$ was determined using automated Winkler titration (Grasshoff et al. 1983). Detection limits were 1 $\mu$mol $L^{-1}$ for $TPO_4$ and $HS^-$, 10 $\mu$mol $L^{-1}$ for $SO_4^{2-}$, and 0.5 $\mu$mol $L^{-1}$ for $O_2$.

## 4.3 Results

### *4.3.1 Water column*

The $O_2$ profile showed a distinct oxycline at 60 m water depth, which was associated with the halocline (Fig. 4.2). Between 80 m and 120 m water depth there was a hypoxic transition zone with $O_2$ levels < 30 $\mu$mol $L^{-1}$. Below 120 m, the deep Gotland basin was anoxic and sulfidic.

The depth of the thermocline was in the range between 18 m and 28 m. At 48 m remaining winter water (Rheinheimer et al. 1989) resulted in a minimum temperature of 1.9°C. Below, the temperature increased again to a maximum of 7.3°C at 115 m water depth.

$NH_4^+$ accumulated in the deep basin, but was removed at the lower base of the hypoxic transition zone. $NO_3^-$ levels showed a distinct peak of 5.8 $\mu$mol $L^{-1}$ at 80 m, but $NO_3^-$ became depleted towards the surface and below ~ 120 m water depth. At the sea surface the saturation normalized $N_2$:Ar ratio was < 1, indicating $N_2$ fixation. Below 50 m, at the onset of the halocline, this ratio was strongly elevated indicating $N_2$ release from the water column and/or the sediment.

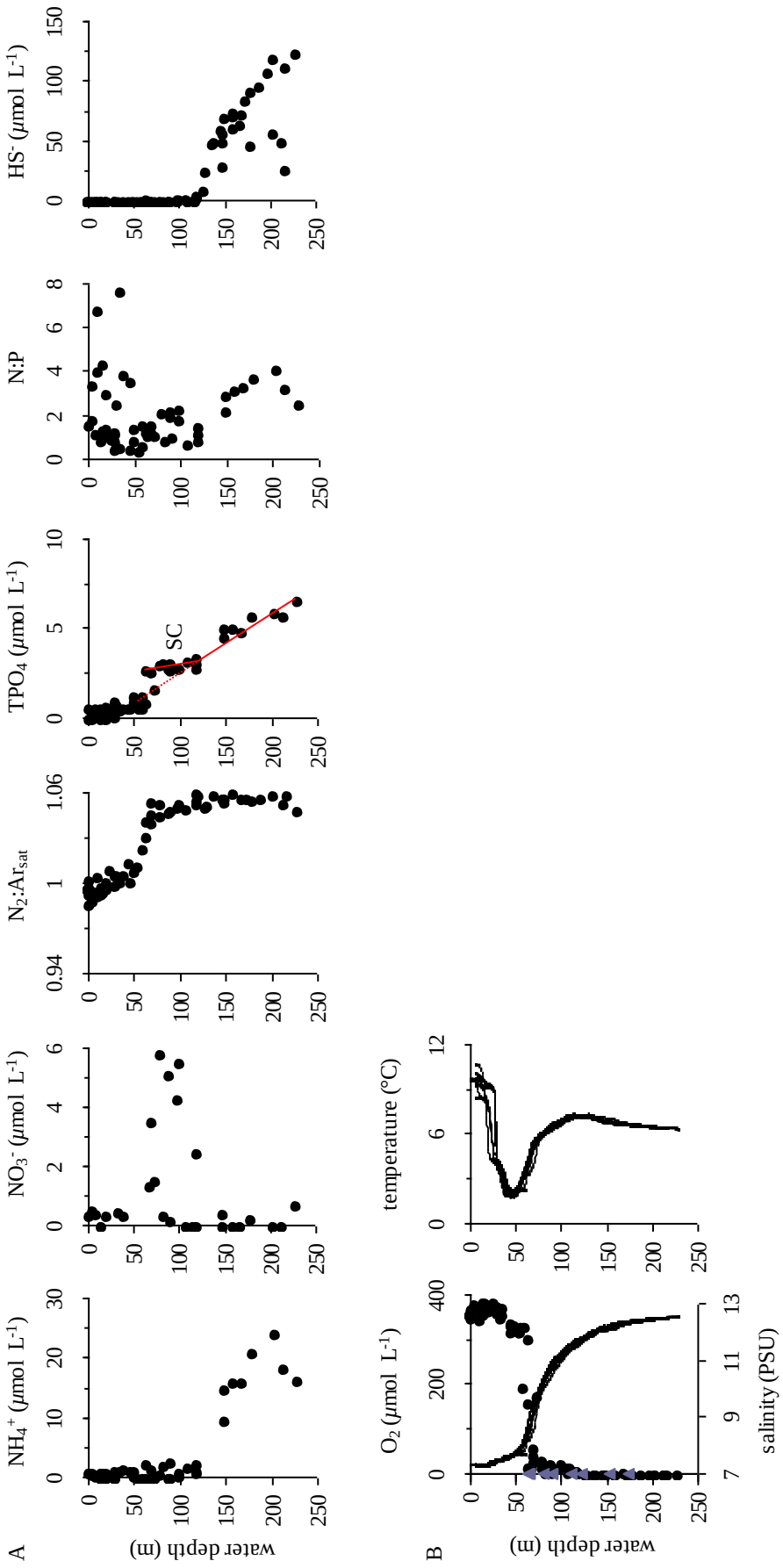


**Fig. 4.2:** Water-column concentration profiles of (A) $NH_4^+$, $NO_3^-$, $N_2$:$Ar_{sat}$, $TPO_4$, and $HS^-$, as well as (B) $O_2$, salinity, and temperature. Profiles represent a compilation of all available data from the CTD deployments indicated in Table 4.1. Rather than showing a steady decrease towards the surface (red dotted line), the TPO4 profile showed a change in the the slope at 120 m water depth (SC). *See* text for details. The gray triangles overlying the $O_2$ concentration profile show the water depth of the BIGO deployments indicated in Table 4.1.

The $TPO_4$ concentration was highest in the deep basin and declined towards the mixed surface layer indicating a source of $TPO_4$ in the deep anoxic basin. Rather than showing a steady decrease towards the surface (Fig. 4.2, red dotted line) the $TPO_4$ profile exhibited a change in the slope at 120 m water depth (Fig. 4.2, denoted as SC). In water depths between 60 m and 120 m, higher $TPO_4$ levels were measured than one would expect from the steady decrease denoted by the dotted line, indicating an additional P source in this zone.

N:P ratios (DIN:$TPO_4$) indicated an excess of $TPO_4$ as compared to Redfield stoichiometry. Highest N:P ratios were measured in the oxic surface layer, but were highly variable, and in the deep basin. $HS^-$ emanating from the anoxic deep basin was completely oxidized at the base of the hypoxic transition zone.

*4.3.2 Sea-floor observation*

Sea-floor images obtained during deployment of the towed camera system OFOS showed that between water depths of ~ 85 m to 120 m, coinciding with the hypoxic transition zone, the sediment surface was almost completely covered with sulfide-oxidizing microbial mats (Fig. 4.3b-e). Exposed sediment surfaces in this zone were very scarce. The onset of visible mats as faint grayish structures on the sediment surface was in ~ 75 m water depth (Fig. 4.3a). At 140 m water depth, bacterial mats were still apparent, but much less distinct than at 120 m (Fig. 4.3f). The extended occurrence of microbial mats at similar water depths in the Gotland Basin was further confirmed during two earlier cruises with R/V *Poseidon* (POS369 July-Aug. 2008) and R/V *Alkor* (AL346 Sept.-Oct. 2009) (O. Pfannkuche unpubl.).

*4.3.3 Bottom-water $O_2$ conditions and in situ fluxes of N species, $TPO_4$, and $HS^-$*

A total of 9 lander deployments were conducted at 7 different water depths from 65 m to 173 m (Table 4.1). The sites, where the different BIGOs were deployed, were classified according to the $O_2$ water-column profile displayed in Fig. 4.2. Two landers were deployed in the oxycline environment (BIGO-I-2, 65 m; BIGO-I-1, 66 m). Four lander deployments (BIGO-II-4, 80 m; BIGO-I-3, 96 m; BIGO-II-1, 97 m; BIGO-II-5, 110 m) were conducted within the hypoxic transition zone. During these deployments, microbial mats were recovered in the flux chambers. In the deep anoxic and sulfidic basin below

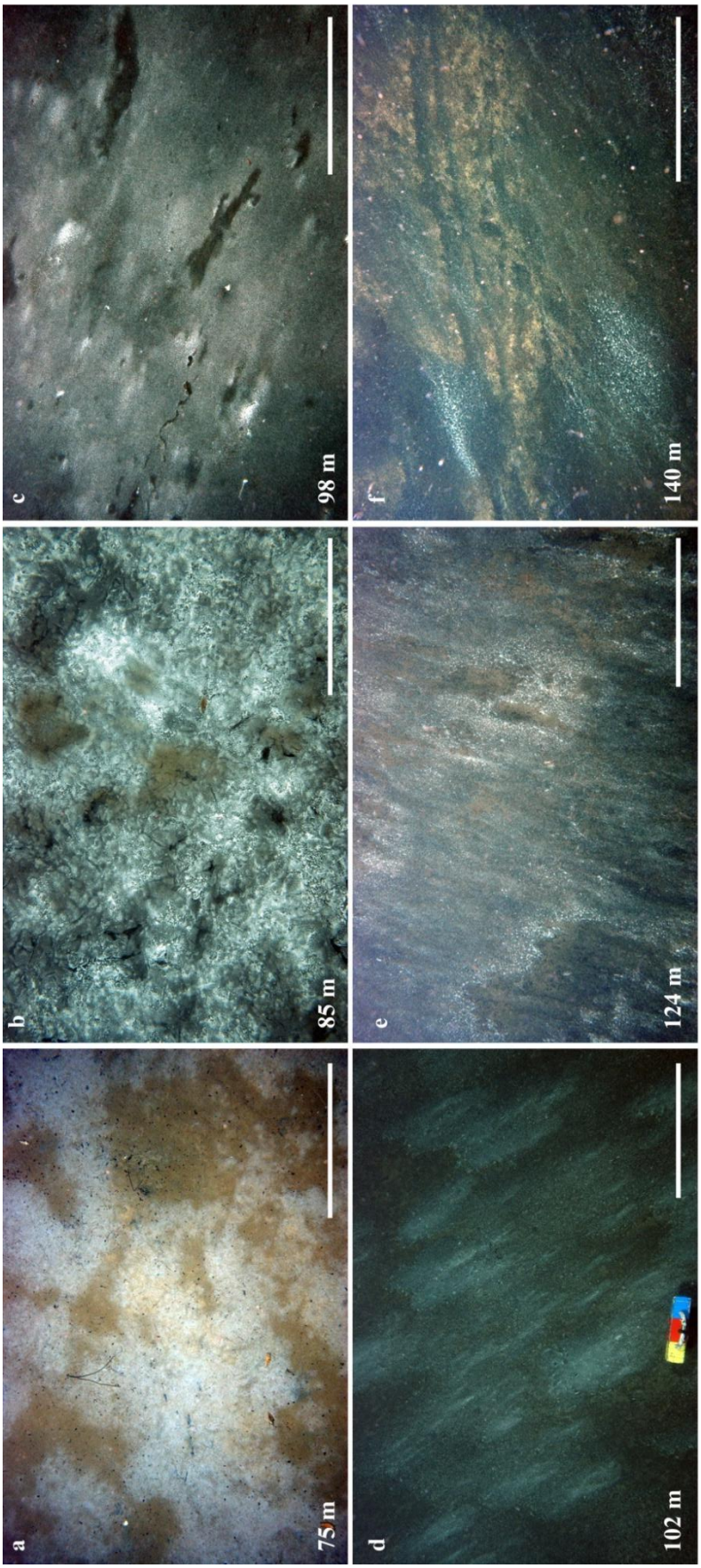


**Fig. 4.3:** Distribution of microbial mats on the sediment surface. Sea-floor images were obtained at water depths ranging from 75 m (panel a) to 140 m (panel f) using the towed camera system OFOS. The scale bars denote a distance of 50 cm.

120 m water depth, three lander deployments were carried out (BIGO-II-2, 124 m; BIGO I-4, 150 m; BIGO-II-3, 173 m). During all lander deployments the sediment surface was recovered intact and undisturbed, except BIGO-II-3. At this site, the sediments were laminated with a fabric comparable to flaky pastry. Upon retrieval of this lander on board of the ship, the sediments close to the chamber wall were disturbed. We do not know, whether this disturbance was caused during insertion of the chambers into the sediment or during lander retrieval. Nevertheless, concentration data did not indicate any disturbance during the flux measurements. Initial concentrations inside the chamber were close to the bottom-water concentrations.

*4.3.3.1 Bottom-water $O_2$ conditions*

Particularly in the oxycline environment but also in the hypoxic transition zone, $O_2$ time series that were conducted during the different BIGO deployments revealed strong fluctuations (Sommer et al. unpubl., the different time series will be published elsewhere). During the deployment of BIGO-I-1 at 66 m water depth the average bottom-water $O_2$ concentration was 55 $\mu$mol $L^{-1}$, with minimum and maximum values of 4 $\mu$mol $L^{-1}$ and 330 $\mu$mol $L^{-1}$. Only a few days later, during the deployment of BIGO-I-2, $O_2$ fluctuations were minor, resulting in an average bottom-water $O_2$ level of 159 $\mu$mol $L^{-1}$. At the upper boundary of the hypoxic transition zone, at the 80 m site (BIGO-II-4), the average bottom-water $O_2$ level was still elevated with 52 $\mu$mol $L^{-1}$. Deeper in the hypoxic transition zone, the $O_2$ fluctuations became strongly reduced, resulting in average bottom-water $O_2$ levels of 3.4 $\mu$mol $L^{-1}$, 2.4 $\mu$mol $L^{-1}$, and 0.4 $\mu$mol $L^{-1}$ at 96 m, 97 m, and 110 m water depth, respectively. At 124 m water depth, bottom-water $O_2$ concentrations during the entire time course of the BIGO-II-2 deployment were below 2 $\mu$mol $L^{-1}$. In the deep basin, at 150 m (BIGO-I-4) and at 173 m (BIGO-II-3) water depth, the bottom water was sulfidic with average $HS^-$ concentrations of 17 $\mu$mol $L^{-1}$ and 44 $\mu$mol $L^{-1}$, respectively. Hence, the $O_2$ levels were assumed to be zero.

*4.3.3.2 In situ fluxes of N species, $TPO_4$, and $HS^-$*

The depth distribution of $NH_4^+$ fluxes showed a distinct maximum of 1.1 mmol $m^{-2}$ $d^{-1}$ at 110 m water depth in the hypoxic transition zone that was associated with the occurrence of microbial mats (Table 4.2; Fig. 4.4). In the deep basin at the 173 m site, there was a

**Table 4.2:** Benthic fluxes of different N-species and $TPO_4$ measured during R/V *Alkor* cruise 355. Fluxes for both benthic chambers of each lander deployment are provided (CH1, CH2). All fluxes are in mmol $m^{-2}$ $d^{-1}$; positive fluxes are directed out of the sediment. Cases where fluxes were not determined are listed as "n.d."; cases where concentration time series inside the chamber did not allow clear interpretation are listed as "n.i.". Empty cells for DIN indicate that, due to the missing of one of the N species, this flux could not be calculated. Due to the accumulation of sulfide in the flux chamber, the $NO_2^-$ flux given in brackets is assumed to be zero.

| Gear no./ Chamber no. | | Water depth (m) | Incubation time (h) | $NH_4^+$ | $NO_3^-$ | $NO_2^-$ | DIN (= ∑ $NH_4^+$ + $NO_3^-$ + $NO_2^-$) | $TPO_4$ |
|---|---|---|---|---|---|---|---|---|
| BIGO-I-2 | CH1 | 65 | 35 | 0.13 | 0.12 | 0.002 | 0.25 | -0.01 |
| | CH2 | | | 0.21 | 0.26 | 0.003 | 0.47 | -0.01 |
| BIGO-I-1 | CH1 | 66 | 33 | 0.28 | 0.16 | 0.012 | 0.45 | 0.05 |
| | CH2 | | | 0.31 | 0.33 | 0.021 | 0.66 | 0.13 |
| BIGO-II-4 | CH1 | 80 | 35 | 0.50 | -0.24 | -0.001 | 0.26 | -0.03 |
| | CH2 | | | 0.30 | -0.27 | -0.001 | 0.03 | -0.06 |
| BIGO-I-3 | CH1 | 96 | 50.8 | 1.00 | -0.70 | n.i. | | 0.17 |
| | CH2 | | | 1.10 | -1.21 | n.i. | | 0.22 |
| BIGO-II-1 | CH1 | 97 | 33 | 0.95 | n.d. | 0.008 | | 0.23 |
| | CH2 | | | 0.68 | n.d. | 0.005 | | 0.17 |
| BIGO-II-5 | CH1 | 110 | 36.9 | 1.05 | -1.13 | n.i. | | 0.22 |
| | CH2 | | | 1.06 | -0.92 | 0.028 | 0.17 | 0.22 |
| BIGO-II-2 | CH1 | 124 | 38.5 | 0.30 | -0.44 | 0 | -0.14 | 0.07 |
| | CH2 | | | 0.30 | -0.34 | (0.003) | -0.04 | 0.09 |
| BIGO-I-4 | CH1 | 150 | 61.3 | 0.10 | 0 | (0.002) | 0.10 | 0.09 |
| | CH2 | | | 0.30 | 0 | (0.001) | 0.30 | 0.05 |
| BIGO-II-3 | CH1 | 173 | 62 | 0.64 | 0 | 0 | 0.64 | 0.20 |
| | CH2 | | | 0.52 | 0 | 0 | 0.52 | 0.10 |

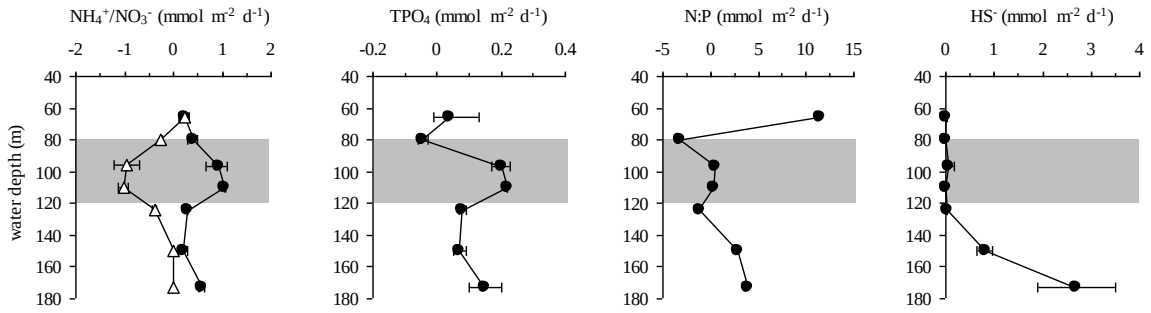


**Fig. 4.4:** Benthic fluxes of $NH_4^+$ (open triangles), $NO_3^-$ (filled circles), $TPO_4$, N:P (DIN:$TPO_4$), and $HS^-$ measured in benthic flux chambers along the oxic to anoxic gradient. Positive fluxes are directed out of the sediment. Average fluxes are given in mmol $m^{-2}$ $d^{-1}$. Error bars correspond to minimum and maximum values of the replicate flux measurements at the different sites (Table 4.2). The lander deployments at 64 m and 65 m as well as at 96 m and 97 m were each considered as one site. The gray panels represent the depth range where sediments were covered with extended mats of sulfide-oxidizing bacteria.

second maximum of 0.58 mmol $m^{-2}$ $d^{-1}$. There was a pronounced uptake of $NO_3^-$ in the hypoxic transition zone and at the upper boundary of the deep basin, mirroring the spatial pattern of $NH_4^+$ release, with a maximum uptake rate of 1.03 mmol $m^{-2}$ $d^{-1}$ at 110 m. At the sulfidic stations in the deep basin, $NO_3^-$ and $NO_2^-$ were no longer available from the bottom water (data not shown), resulting in zero fluxes of both species. In the oxycline environment, $NO_3^-$ was released with an average rate of 0.22 mmol $m^{-2}$ $d^{-1}$. $NO_2^-$ was released down to 110 m water depth, except the station at 80 m. Sea-bed release of DIN was elevated only in the deep basin with 0.58 mmol $m^{-2}$ $d^{-1}$ due to high $NH_4^+$ release, and at the shallowest site with 0.46 mmol $m^{-2}$ $d^{-1}$, where it was additionally caused by $NO_3^-$ and $NO_2^-$ release.

Similarly to $NH_4^+$, highest $TPO_4$ fluxes of up to 0.22 mmol $m^{-2}$ $d^{-1}$ were measured in the hypoxic transition zone. In the deep anoxic basin, $TPO_4$ fluxes were lower, but increased again towards the deepest studied site at 173 m water depth, with an average release of 0.15 mmol $m^{-2}$ $d^{-1}$. At the 80 m site $TPO_4$ was taken up by the sediment. At this site, the chamber incubations took place under oxic conditions (start concentration: 95 $\mu$mol $L^{-1}$, end: 19 $\mu$mol $L^{-1}$), hence $TPO_4$ can be assumed to have been immobilized. Despite oxic conditions inside the benthic chambers during the lander deployments at 65 m and 66 m, $TPO_4$ was released during deployment BIGO-I-1 (0.09 mmol $m^{-2}$ $d^{-1}$). Except for the 96 m site, N:P release ratios (DIN:$TPO_4$) indicate enhanced $TPO_4$ release over DIN in the hypoxic transition zone, whereas at the oxic sites and in the deep basin DIN release prevailed. $HS^-$ fluxes increased distinctively below 120 m water depth, reaching a

maximum of 2.7 mmol $m^{-2}$ $d^{-1}$ at 173 m water depth. Concentrations of the various solutes measured during the time course of the chamber incubations will be provided by the authors on demand.

## 4.4 Discussion

*4.4.1 N and P cycling across the oxic to anoxic gradient*

Changes in the N:P ratio are assumed to strongly control the alternating spring and summer blooms of phytoplankton and cyanobacteria in the Baltic Sea, which, via positive feedback loops with hypoxia and benthic nutrient release, causes an efficient internal nutrient recycling that might prevent the recovery of the central Baltic Sea from eutrophication. Our flux data that were obtained along a depth transect within one sampling period revealed two distinct depth zones, which were characterized by enhanced release of $NH_4^+$ and $TPO_4$. One major source was located in the deep permanently anoxic basin. The second one coincided with the hypoxic transition zone between 80 m and 120 m water depth. Although in situ flux data are nearly lacking, $NH_4^+$ and $TPO_4$ release from the deep anoxic basin has been generally considered to be the major source for nutrients to the water column. The significance of the hypoxic transition zone for nutrient release was not accounted for so far.

4.4.1.1 Deep Basin (> 120 m water depth)

In the deep basin, $NH_4^+$ release was predominantly driven by ammonification during the degradation of organic matter. Other processes that could release $NH_4^+$, such as DNRA or nitrification, can be ruled out as no electron acceptors except $SO_4^{2-}$ were available from the bottom water. The deep basin is almost permanently anoxic, however, on annual timescales intermittent $O_2$ supply occurs during inflows of saline waters across the sills in the Danish Straits (Stigebrandt 2001; Gustafsson and Stigebrandt 2007). The last major inflow prior to our sampling campaign occurred in winter 2003. In 2005, $NO_3^-$ was measured for the last time in the deep water of the Gotland Basin, and by the end of this year sulfidic conditions had returned to depths > 150 m (Nausch et al. 2006). Since then, with a short interruption in 2007, sulfidic conditions continuously became worse (Nausch et al. 2012).

**Table 4.3:** Possible contributions to the $NH_4^+$ and $TPO_4$ fluxes. Total oxygen uptake (TOU), sulfate reduction (SR) and organic carbon degradation rate ($R_{Corg}$) are also listed. All rates are in units of mmol $m^{-2}$ $d^{-1}$.

| Gear no./ chamber no. | | Water depth (m) | TOU | SR [a] | $R_{Corg}$ [b] | $NH_4^+{}_{RCorg}$ [c] | $NH_4^+{}_{DEN}$ [d] | $NH_4^+{}_{N2\text{-}fix}$ [f] | $TPO_4{}_{RCorg}$ [c] | $TPO_4{}_{RCorg,10}$ [h] |
|---|---|---|---|---|---|---|---|---|---|---|
| BIGO I-2 | CH1 | 65 | 8.3 | 0 | 5.73 | 0.86 | | 0.034 | 0.05 | |
| | CH2 | | 5.8 | 0 | 4.00 | 0.60 | | | 0.04 | |
| BIGO I-1 | CH1 | 66 | 16.3 | 0 | 11.25 | 1.70 | | 0.034 | 0.11 | |
| | CH2 | | 20.9 | 0 | 14.42 | 2.18 | | | 0.14 | |
| BIGO II-4 | CH1 | 80 | 9.9 | 0.62 | 8.07 | 1.22 | 0.05 | 0.091 [g] | 0.08 | |
| | CH2 | | 6.0 | 0.55 | 5.24 | 0.79 | 0.05 | | 0.05 | |
| BIGO I-3 | CH1 | 96 | 0 | 2.36 | 4.72 | 0.71 | 0.13 | 0.091 | 0.05 | 0.45 |
| | CH2 | | 0 | 2.11 | 4.22 | 0.64 | 0.23 | | 0.04 | 0.40 |
| BIGO II-1 | CH1 | 97 | 0 | 2.24 | 4.48 | 0.68 | n.d. [e] | 0.091 | 0.04 | 0.42 |
| | CH2 | | 0 | 2.55 | 5.10 | 0.77 | n.d. | | 0.05 | 0.48 |
| BIGO II-5 | CH1 | 110 | 0 | 1.25 | 2.50 | 0.38 | 0.21 | 0.065 | 0.02 | 0.24 |
| | CH2 | | 0 | 1.02 | 2.04 | 0.31 | 0.17 | | 0.02 | 0.19 |
| BIGO II-2 | CH1 | 124 | 0 | 0.58 | 1.16 | 0.18 | 0.08 | 0.099 | 0.01 | 0.11 |
| | CH2 | | 0 | 0.61 | 1.22 | 0.18 | 0.06 | | 0.01 | 0.12 |
| BIGO I-4 | CH1 | 150 | 0 | 0.19 | 0.38 | 0.06 | 0 | 0.047 [g] | 0.004 | 0.04 |
| | CH2 | | 0 | 0.23 | 0.46 | 0.07 | 0 | | 0.004 | 0.04 |
| BIGO II-3 | CH1 | 173 | 0 | 0.58 | 1.16 | 0.18 | 0 | 0.047 [g] | 0.01 | 0.11 |
| | CH2 | | 0 | 0.53 | 1.06 | 0.16 | 0 | | 0.01 | 0.01 |

[a] SR was calculated from sulfate pore-water gradients.

[b] $R_{Corg}$ was deduced from TOU in combination with sulfate reduction.

[c] Rates of $NH_4^+$ ($NH_4^+{}_{RCorg}$) and $TPO_4$ ($TPO_4{}_{RCorg}$) release during organic matter degradation were calculated from $R_{Corg}$ using Redfield C:N and C:P stoichiometries.

[d] $NH_4^+$ release during $C_{org}$ degradation by maximum potential denitrification ($NH_4^+{}_{DEN}$); considers the stoichiometry of complete denitrification where for 2 moles of $NO_3^-$ 40/106 moles of $NH_4^+$ are released.

[e] Since $NO_3^-$ fluxes were not determined for this site, only the $NO_3^-$ fluxes measured for BIGO-I-3 were included in the calculation of the theoretical $NH_4^+$ release shown in Fig. 4.5.

[f] $NH_4^+$ release due to benthic $N_2$-fixation ($NH_4^+{}_{N2\text{-}fix}$) was set to be the same as the actual $N_2$-fixation rates measured for the MUC stations indicated in Table 4.1, assuming that all fixed N is released into the environment.

[g] Direct rate measurements were not available for this water depth, hence rates from the adjacent MUC 12 and MUC 14 were used.

[h] Potential preferential $TPO_4$ release ($TPO_4{}_{RCorg,10}$) was estimated from the $R_{Corg}$ expanding the Redfield C:P stoichiometry by a factor of 10. This factor was derived from the deep basin (*see* text for details). For the oxic stations, it was assumed that no preferential $TPO_4$ release takes place.

In order to assess $NH_4^+$ release during ammonification, we calculated $C_{org}$ degradation rates ($R_{Corg}$ in Table 4.3) from the $SO_4^{2-}$ pore-water gradients, assuming that the contribution of anaerobic methane oxidation to the $SO_4^{2-}$ removal is negligible (Piker et al. 1998). For the deepest station (173 m, BIGO-II-3), the $C_{org}$ degradation rate was 1.4 mmol $m^{-2}$ $d^{-1}$. Assuming a Redfield C:N stoichiometry, this $C_{org}$ degradation liberates 0.2 mmol $m^{-2}$ $d^{-1}$ of $NH_4^+$, which is less than the actual flux measurement of 0.58 mmol $m^{-2}$ $d^{-1}$. Similar $NH_4^+$ release of 0.34 mmol $m^{-2}$ $d^{-1}$ and 0.55 mmol $m^{-2}$ $d^{-1}$ was derived from pore-water gradients for sites in water depths of 123 m and 238 m (Jilbert et al. 2011). We can only speculate about the processes generating this excess $NH_4^+$. Benthic $N_2$-fixation, which recently has been reported to occur in a variety of benthic habitats, including anoxic cold seep environments as well as coastal sediments (Fulweiler et al. 2007; Dekas et al. 2009; Bertics et al. 2010), only provides 0.05 mmol $m^{-2}$ $d^{-1}$ of $NH_4^+$ ($NH_4^+{}_{N2\text{-}fix}$ in Table 4.3), assuming that all fixed N is released as $NH_4^+$ into the environment. For benthic environments, to the best of our knowledge, the ratio between the fixed N that subsequently is released into the pore water and the fraction that is incorporated into biomass is not known. From culture studies with the pelagic nitrogen fixer *Trichodesmium* spp. it is known that only a small proportion of up to 20% of recently fixed N is released into the water column as $NH_4^+$ (Mulholland et al. 2004). Hence, the above assertion on $NH_4^+$ release by benthic $N_2$-fixers represents a maximum estimate, and there is a high probability that $N_2$-fixation is even less important for our measured $NH_4^+$ fluxes than discussed above.

Apparently, due to anoxia and, hence, impeded nitrification, $NH_4^+$ is efficiently returned into the bottom water and retained in the system. Due to the absence of $NO_3^-$ and $NO_2^-$ that could drive denitrification and anammox, it follows that the deep basin is insignificant for the removal of reactive N.

High $TPO_4$ release was measured in the deep basin. Recently, for our site at 124 m Viktorsson et al. (2013) provided a $TPO_4$ flux of 0.2 mmol $m^{-2}$ $d^{-1}$, which is even higher than the $TPO_4$ release of 0.08 mmol $m^{-2}$ $d^{-1}$ determined during this study. Previous studies attributed such enhanced $TPO_4$ fluxes under low-$O_2$ conditions mainly to the release of P associated with Fe oxyhydroxides when these are reductively dissolved (Sundby et al. 1992; McManus et al. 1997) and the preferential regeneration of P from organic matter

(Ingall et al. 1993; Wallmann 2003). Reductive Fe dissolution can be considered negligible as a mechanism for P release in the deep basin, as our data show that in the deep basin $HS^-$ accumulates in the surface sediments as well as in the water column below the redoxcline. Under such conditions, Fe is bound to sulfides and removed into the solid phase (Carman and Rahm 1997).

In order to determine whether $C_{org}$ degradation could support the measured $TPO_4$ release, we calculated the $C_{org}$ degradation rate for the deep basin sites using the Redfield C:P ratio. The use of the Redfield C:P ratio is justified, as a sediment trap study, conducted in the eastern Gotland Basin over a full seasonal cycle, showed that organic material intercepting 230 m water depth has an average C:P molar ratio of 99 (Emeis et al. 2000). At the 150 m and 173 m sites the $C_{org}$-driven $TPO_4$ release ($TPO_{4\ Corg}$ in Table 4.3) was 0.004 mmol $m^{-2}$ $d^{-1}$ and 0.01 mmol $m^{-2}$ $d^{-1}$, respectively (Fig. 4.5). This is too low to explain the higher release rates determined in the benthic chambers, pointing towards preferential P release during $C_{org}$ degradation. Enhanced release of P relative to C under reducing conditions has been suggested in several studies (Ingall et al. 1993; Slomp et al.

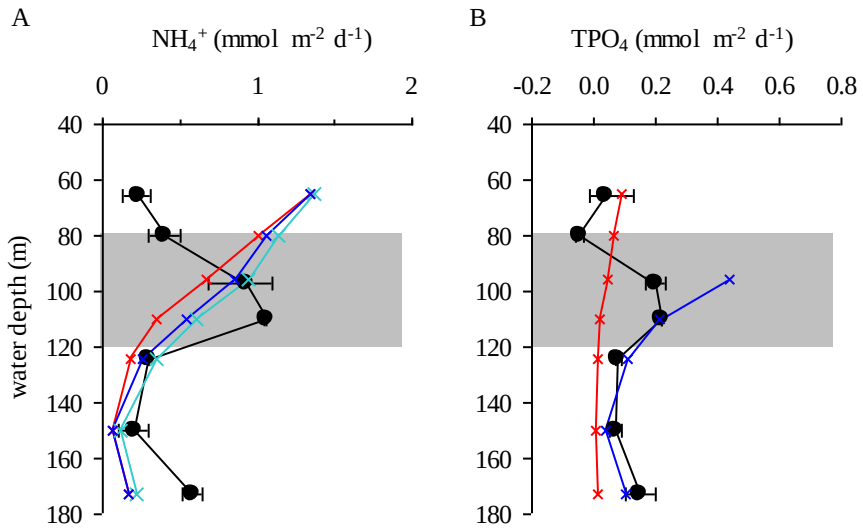


**Fig. 4.5:** (A) Assessment of the likelihood of dissimilatory nitrate reduction to ammonium (DNRA) contributing to the average $NH_4^+$ flux at the different sites (water depths 64 m and 65 m, as well as 96 m and 97 m each considered as one site). $NH_4^+$ release during ammonification is according to Redfield stoichiometry (red line). Organic matter degradation was calculated from total oxygen uptake and sulfate reduction rates (Table 4.3). The maximum potential contribution of $NO_3^-$ entering the denitrification pathway is indicated by the blue line. The contribution of benthic $N_2$-fixation to the $NH_4^+$ release is shown by the green line, assuming that all fixed $N_2$ is released into the environment. (B) Organic matter degradation according to Redfield stoichiometry (red line) is not sufficient to explain the measured $TPO_4$ fluxes. At the anoxic sites, preferential P regeneration during organic matter degradation (blue line) must be assumed to explain the high $TPO_4$ fluxes. Rates of different processes were calculated as described in the text (*see* "N and P cycling across the oxic to anoxic gradient").

2002; Jilbert et al. 2011), but the mechanism still is enigmatic. Recently, it has been demonstrated that carbon-limited bacteria preferentially remove P from organic matter in order to better access the remaining C (Steenbergh et al. 2011). As under anaerobic conditions the P cannot be retained within the cell, it is released into the pore water.
Lastly, biogenic calcium phosphate (Ca-P), i.e. fish debris, as has been suggested for the Peruvian and Arabian Sea oxygen minimum zones (Suess et al. 1981; Schenau et al. 2001), can be ruled out as an additional P source, since previous measurements at almost permanently hypoxic and anoxic sites in the Baltic Proper have shown no evidence for biogenic Ca-P burial (Mort et al. 2010).

4.4.1.2 Hypoxic transition zone (80 m to 120 m water depth)

The hypoxic transition zone was identified as a second major site for $NH_4^+$ and $TPO_4$ release. Here, we define the hypoxic transition zone as the depth range between the lower boundary of the oxycline at ~ 80 m and the redoxcline at ~ 120 m, with $O_2$ concentrations < 30 $\mu$mol $L^{-1}$ as derived from CTD casts. However, it should be noted that at the 80 m station bottom-water levels can fluctuate between 2 $\mu$mol $L^{-1}$ and 218 $\mu$mol $L^{-1}$ (Sommer et al. in prep.). Whereas down to 110 m water depth, only weak $O_2$ oscillations with maxima of up to 10 $\mu$mol $L^{-1}$ were recorded.
The coincidence between the occurrence of microbial mats and the consistently elevated release rates of $NH_4^+$ and $TPO_4$ led us to the assumption, that these sulfide-oxidizing organisms were involved in the cycling of N and P. Previous studies assign these filamentous bacteria in surface sediments from the eastern Gotland Basin to the genus *Beggiatoa* spp. (Piker et al. 1998; Emeis et al. 2000), which is known to release $NH_4^+$ during DNRA (Jørgensen and Nelson 2004). When $O_2$ availability becomes reduced, these organisms use $NO_3^-$ for $HS^-$ oxidation according to the following stoichiometry:

$$NO_3^- + HS^- + CO_2 + 2\ H_2O \rightarrow SO_4^{2-} + NH_4^+ + HCO_3^- \quad (4.1)$$

For example, the organic–rich sediments in the hypoxic Bay of Concepción, central Chile, are characterized by high rates of DNRA, which result in a marked $NH_4^+$ release to the bottom water, in addition to the $NH_4^+$ that originates from the degradation of organic matter (Farías et al. 1996; Graco et al. 2001). High release rates of $NH_4^+$ related to DNRA

have been also shown for the Peruvian upwelling region (Bohlen et al. 2011). DNRA is of high ecological significance since the $NO_3^-$, and possibly $NO_2^-$ (Zopfi et al. 2001), is converted into $NH_4^+$, thus conserving DIN within the ecosystem and opposing the removal of DIN by denitrification and anammox.

Although the presence of extended microbial mats implies the occurrence of DNRA in the hypoxic transition zone, we cannot provide direct evidence for this process. However, the feasibility of DNRA can be explored by estimating the $NH_4^+$ release that is only driven by the degradation of organic matter assuming Redfield C:N composition. Excess $NH_4^+$ release measured by the benthic landers would then indicate $NH_4^+$ generated during DNRA but also by $N_2$-fixation. For the stations except the 80 m site organic matter degradation was calculated from $SO_4^{2-}$ pore-water gradients assuming sulfate reduction (SR) as the major $C_{org}$ degradation pathway. For the 80 m site $C_{org}$ degradation was calculated from the TOU in addition to SR. TOU was converted into $C_{org}$ degradation rates using a molar ratio between $O_2$ consumption and $C_{org}$ degradation of 1.45 (Hedges et al. 2002).

Except for the 80 m station in the hypoxic transition zone, $NH_4^+$ release measured in benthic chambers was about 3-fold higher than that derived from organic matter degradation (Fig. 4.5). When all $NO_3^-$ that was taken up by the sediments would be channeled into $C_{org}$ degradation by complete denitrification instead of DNRA, where for two moles of $NO_3^-$ 40/106 moles of $NH_4^+$ are released, additional gain of $NH_4^+$ ($NH_4^+{}_{DEN}$ in Table 4.3) can explain the measured $NH_4^+$ release rates at 96/ 97 m and 124 m, but not at 110 m water depth (Fig. 4.5, blue line). $N_2$-fixation as a major source of additional $NH_4^+$ can be neglected as $N_2$-fixation at this site only amounted to 0.065 mmol $m^{-2}$ $d^{-1}$. Still another 0.5 mmol $NH_4^+$ $m^{-2}$ $d^{-1}$ are required to match the measured $NH_4^+$ release, strongly pointing towards the presence of DNRA at least at this particular site. Except for the 80 m site, the diffusive $HS^-$ flux towards the sediment surface as well as $NO_3^-$ uptake was high enough to support DNRA.

At the 80 m site, ammonification released much more $NH_4^+$ compared to the benthic chamber $NH_4^+$ flux. The flux chamber incubations at the 80 m site were conducted under oxic conditions, allowing for $NH_4^+$ oxidation during nitrification. Although the presence of microbial mats would potentially allow for DNRA, our data do not allow discerning whether DNRA took place at this site.

$TPO_4$ release was very high with up to 0.23 mmol $m^{-2}$ $d^{-1}$. In situ fluxes from the Swedish side of the eastern Gotland Basin as well as diffusive fluxes from the central Baltic Sea that were measured at similar water depths are much lower and range from -0.03 mmol $m^{-2}$ $d^{-1}$ to 0.08 mmol $m^{-2}$ $d^{-1}$ (Koop et al. 1990; Matthiesen et al. 1998; Jilbert et al. 2011; Viktorsson et al. 2013). As already described above, there are several mechanisms that might contribute to the high $TPO_4$ fluxes. Reductive Fe dissolution releasing high amounts of P has been proposed for hypoxic sites in water depths shallower than 90 m at several locations in the Baltic Sea (Jilbert et al. 2011, their group 1 sites). However, $TPO_4$ pore-water peaks indicating pronounced P release during Fe dissolution were not detected during our study (data not shown). Except the 80 m site, the color of the surface sediments retrieved by the benthic flux chambers was black, implying that Fe had precipitated as Fe sulfides and, hence, was not available any more for this process.

Again, as already shown for the deep basin preferential P release during $C_{org}$ degradation might explain the high release rates. In the deep basin, preferential P release can be assumed to be the sole process that contributes to the elevated $TPO_4$ flux. There, the measured $TPO_4$ flux was on average about 10-fold higher than the flux that could be derived from $C_{org}$ degradation according to Redfield C:P stoichiometry. When this factor of 10 is applied to the Redfield C:P stoichiometry to estimate the potential preferential P release from the $C_{org}$ degradation rates in the hypoxic transition zone (Fig. 4.5, blue line), the measured $TPO_4$ release rates can be fully explained.

Another option to explain the high $TPO_4$ release rates is the transient P storage and release of microbial mats, almost completely covering the sediment surface in this zone. Besides performing DNRA, certain genera of large filamentous sulfide-oxidizers may play an important role in benthic P cycling, carrying out luxurious uptake of $TPO_4$ from the pore water under oxic conditions, subsequently stored as polyphosphates. Under anoxic conditions, these polyphosphates are decomposed to gain energy, whereby $TPO_4$ is released again. Evidence for this metabolic mechanism has been provided for the genera *Thiomargarita* spp. and *Beggiatoa* spp. in sediments from the Namibian upwelling system (Schulz and Schulz 2005; Goldhammer et al. 2010). Noffke et al. (2012) speculated that microbial P uptake and release may also contribute to elevated benthic $TPO_4$ fluxes in shelf sediments from the Peruvian oxygen minimum zone, where large

occurrences of the sulfur bacteria *Beggiatoa* spp. and *Thioploca* spp. have been reported (Mosch et al. 2012). Although we cannot provide direct evidence for the transient microbial P cycling, the presence of *Beggiatoa* spp. in the hypoxic transition zone at least indicates that this process is possible.

4.4.1.3 Oxycline environment (60 m to < 80 m water depth)

In order to assess the function of sediments in the oxycline environment to act as a sink or source for reactive N, theoretical $NH_4^+$ release during $C_{org}$ degradation (calculated from the TOU) is compared to the measured $NH_4^+$ fluxes. The measured release of $NH_4^+$ was only moderate (0.13-0.30 mmol $m^{-2}$ $d^{-1}$), whereas the calculated $NH_4^+$ release during $C_{org}$ degradation is in the range of 0.60 mmol $m^{-2}$ $d^{-1}$ to 2.18 mmol $m^{-2}$ $d^{-1}$. This rather broad range is due to high variability of the TOU of 5.8 mmol $m^{-2}$ $d^{-1}$ to 20.9 mmol $m^{-2}$ $d^{-1}$. The difference of 0.39 mmol $m^{-2}$ $d^{-1}$ to 1.87 mmol $m^{-2}$ $d^{-1}$ between the calculated and the measured $NH_4^+$ release must have been oxidized during nitrification, as indicated by $NO_3^-$ and $NO_2^-$ release inside the flux chambers. However, during the chamber flux measurements the sum of $NO_3^-$ and $NO_2^-$ fluxes ranged only between 0.12 mmol $m^{-2}$ $d^{-1}$ to 0.35 mmol $m^{-2}$ $d^{-1}$. This implies that 0.13 mmol $m^{-2}$ $d^{-1}$ to 1.52 mmol $m^{-2}$ $d^{-1}$ must have been consumed during denitrification that is coupled to nitrification. Coupled denitrification to nitrification has been observed in a variety of different habitats including the northern Baltic Proper, playing a significant role in N removal (Seitzinger 1988; Tuominen et al. 1998; Devol and Christensen 1993). From two 75 m and 80 m deep oxic sites in the southeastern Gotland Basin, low denitrification rates of 0.15 mol $m^{-2}$ $d^{-1}$ and 0.16 mmol $m^{-2}$ $d^{-1}$ were reported (Deutsch et al. 2010). A denitrification rate of 1.2 mmol $m^{-2}$ $d^{-1}$ that was measured under oxic conditions was provided for water depths between 47 m and 82 m in the western Gotland Basin (Koop et al. 1990).

Despite the sink character of the oxycline environment, still large amounts of DIN were released in this shallow zone that were directly available for the primary producers in the euphotic zone. This is in strong contrast to the $NH_4^+$ that was released from the deep basin and oxidized at the redoxcline (*see* “Eastern Gotland Basin – Potential capability for recovery from eutrophication”).

Due to efficient scavenging of P by Fe oxyhydroxides (Sundby et al. 1992; Slomp et al. 1998) and P storage by microorganisms (Steenbergh et al. 2011) under oxic conditions, one would expect low rates of $TPO_4$ release in the oxic zone. Indeed, during deployment of BIGO-I-2 slight $TPO_4$ uptake of -0.01 mmol $m^{-2}$ $d^{-1}$ was measured. However, during the deployment of BIGO-I-1 $TPO_4$ release was elevated (0.05 mmol $m^{-2}$ $d^{-1}$ and 0.13 mmol $m^{-2}$ $d^{-1}$). This elevated $TPO_4$ release likely was due to enhanced levels of $C_{org}$ degradation (derived from TOU) of 11.25 mmol $m^{-2}$ $d^{-1}$ and 14.42 mmol $m^{-2}$ $d^{-1}$, compared to only 5.7 mmol $m^{-2}$ $d^{-1}$ and 4.0 mmol $m^{-2}$ $d^{-1}$ measured in BIGO-I-2 that was deployed at the same water depth. Assuming Redfield C:P ratio, a $TPO_4$ release of 0.11 mmol $m^{-2}$ $d^{-1}$ and 0.14 mmol $m^{-2}$ $d^{-1}$ can be calculated from these $C_{org}$ degradation rates, almost matching the measured P release, which indicates that despite the oxic bottom water P retention failed. About the reasons for this can be only speculated, but we hypothesize that the differences in the $TPO_4$ release between either lander deployment were not only due to differences in the $C_{org}$ degradation, but also to strong fluctuations of the bottom-water $O_2$. Time series of bottom-water $O_2$ levels recorded during the deployment of BIGO-I-1 revealed a distinct drop of the $O_2$ concentration from 300 $\mu$mol $L^{-1}$ to 50 $\mu$mol $L^{-1}$ within only 1 min, and a further drop to anoxic conditions in the following about 4 h that endured more than 20 h, before $O_2$ levels started to increase again. Such drastic changes in the bottom-water $O_2$ affect the redox-state of the sediment, especially at the surface where built up of Fe oxyhydroxides takes place. Hence, we assume that the BIGO-I-1 deployment was conducted at a redox-state, where the retention capacity of the surface sediment for P was exhausted, which could explain the elevated $TPO_4$ flux measured at the 66 m site.

### *4.4.2 Baltic Proper internal loading of $TPO_4$, $NH_4^+$, and $NO_3^-$*

It became apparent that, in addition to the deep basin, the hypoxic transition zone represents an important region for nutrient release that was not identified so far. In order to asses the significance of internal nutrient release during the time of our cruise in comparison to the external loading via the catchment area and atmospheric deposition, we made an approximation of the entire benthic nutrient load for the Baltic Proper, but excluding the Arkona basin. As flux measurements were only conducted in water depths below 60 m, the shallower coastal region was excluded from this extrapolation.

Moreover, the boundary of 60 m water depth approximately separates deeper muddy from sandy sediments in the Baltic Proper (www.helcom.fi/GIS/en_GB/HelcomGIS/). We are aware that this extrapolation bears uncertainties due to local and seasonal variability of particle deposition (Pohl et al. 2004; Hille et al. 2006), as well as with regard to the continuity of the bacterial mat features.

In order to extrapolate the flux measurements of $TPO_4$ and $NH_4^+$, the Baltic Proper was subdivided into three depth zones according to the vertical $O_2$ distribution in the water column (Fig. 4.2). The deep anoxic and sulfidic basin was classified as the depth zone below 120 m water depth, covering an area of 18,954 $km^2$ (Fig. 6). The 80 m and 120 m depth contour was taken as the upper and lower boundary of the hypoxic transition zone, covering an area of 47,230 $km^2$. The 80 m depth contour coincides well with the extension of hypoxic water masses ($O_2$ < 2 ml $L^{-1}$ = 89 $\mu$mol $L^{-1}$) in 2010 (Hansson et al. 2011; Fig. 6). Water depths between 60 m and < 80 m, where oxic conditions prevail, were defined as the oxycline environment, with an area of 26,088 $km^2$. To arrive at regional nutrient loads, these areas were multiplied with the averages of the benthic $TPO_4$ and $NH_4^+$ fluxes measured in each depth zone. In the oxycline environment, in addition to $NH_4^+$, $NO_3^-$ release was also taken into account.

The total $TPO_4$ load of the considered area (92,272 $km^2$) was 109.4 ktons $TPO_4$ $yr^{-1}$. As much as 70% (76.2 ktons $TPO_4$ $yr^{-1}$) was released from the hypoxic transition zone, whose area is 51% of the total area. For comparison the $TPO_4$ release of the deep basin whose area covers 21% of the entire investigated area was only 20% (21.4 ktons $TPO_4$ $yr^{-1}$). As to expect, due to the higher retention capacity of sediments underlying oxygenated bottom waters, $TPO_4$ release of the oxycline environment was low with 11% (11.8 ktons $TPO_4$ $yr^{-1}$). A study that was conducted in parallel to this investigation, also using benthic landers, revealed an internal $TPO_4$ load for the Baltic Proper (considered area: 206,000 $km^2$) of 146 kt $TPO_4$ $yr^{-1}$, based on pooled measurements for August and September during the years 2008 to 2010 (Viktorsson et al. 2013). Although the total area considered by Viktorsson et al. (2013) is 2.2 times bigger than that considered in this study, the overall $TPO_4$ load was similar. This is due to the large oxic area taken into account by these authors, but which can be almost neglected with regard to the $TPO_4$ release.

Overall, this and the study of Viktorsson et al. (2013) arrived at regional estimates of $TPO_4$ release that are much higher than the total external P load of 14 kt $yr^{-1}$ reported for the year 2006 (HELCOM 2009*b*). It is remarkable that our finding of enhanced $TPO_4$ release in the hypoxic transition zone is in contrast to the study of Viktorsson et al. (2013), where still anoxic sites in the deeper basin were the prominent sites for $TPO_4$ release, which hints towards seasonal and inter-annual regime shifts. Our study implies that this zone, which is particularly susceptible to $O_2$ fluctuations and to date was hardly consistently investigated, needs particular attention in Baltic Sea management plans.

Similarly to the $TPO_4$ release, $NH_4^+$ release from the hypoxic transition zone was extremely high and constituted 75% (200.3 ktons $yr^{-1}$) of the total $NH_4^+$ release, compared to 13% (34.9 ktons $yr^{-1}$) in the deep basin and 12% (31 ktons $yr^{-1}$) in the oxycline environment. From the latter, in addition to $NH_4^+$, 29 ktons $yr^{-1}$ $NO_3^-$ was released due to nitrification. This renders the oxycline environment an important zone for reactive N release and feedbacks with primary productivity since the $NO_3^-$ becomes directly accessible in the euphotic zone. The total internal DIN load of 295.2 kt $yr^{-1}$ of our considered area is about twice as much as the external DIN load of 140 kt $yr^{-1}$ for the year 2006 (HELCOM 2009*b*).

### *4.4.3 Eastern Gotland Basin - Potential capability for recovery from eutrophication*

The above described high internal nutrient load from the sediments in comparison to the external loading via the catchment area and atmospheric deposition raises the question, to what extent the Baltic Proper has the capability to break the vicious cycle of efficient internal nutrient cycling and to recover from eutrophication. In the following, an assessment of the sediments inside the different zones with regard to their function to act as a sink, recycling site or source for $TPO_4$ and DIN will be conducted. However, we are aware that the scope of our flux data is limited regionally as well as temporally, and might be applicable only for the summer situation. At least for $TPO_4$ it has been shown that high release rates were also present in August and September (Viktorsson et al. 2013). Otherwise, in situ flux data for the spring, fall, and winter are still urgently missing.

*4.4.3.1 Nitrogen*

A simple budget calculation is used to assess the function of the sediments in the different depth zones to act as sinks, sources or recycling sites for DIN. The input side includes uptake of $NO_3^-$ and $NO_2^-$ from the bottom water as well as $NH_4^+$ release to the pore water during organic matter degradation. The output side includes $NO_3^-$, $NO_2^-$, and $NH_4^+$ release into the bottom water. Organic matter degradation is the only $NH_4^+$-releasing process that is considered here. Benthic $N_2$ fixation as an additional $NH_4^+$ source is included in the total $NH_4^+$ release rates measured by the benthic landers. Since the budget only considers the active N turnover processes, burial is not accounted for. If the sum between input and output is zero ($DIN_{in} + DIN_{out} = 0$), the investigated environment represents a recycling site for DIN. When the sum of $DIN_{in} + DIN_{out}$ becomes negative, the sediments act as a sink for DIN, with the absolute value of this sum representing the $N_2$ release. Is the sum $DIN_{in} + DIN_{out}$ positive, the sediments act as a source for DIN. According to this budget calculation, sediments from the oxycline environment represented a sink for DIN, potentially opposing eutrophication (Table 4.4; Fig. 4.6). Moving across the hypoxic transition zone, this sink function gradually declined, until the redoxcline at about 120 m water depth was reached. In contrast, in the deep basin, where electron acceptors except $SO_4^{2-}$ were absent, the DIN budgets suggest that the sediments acted as a source for DIN. However, we do not know the processes causing this excess DIN. As mentioned above, $N_2$-fixation is one possibility.

**Table 4.4:** Balance of average DIN fluxes in and out across the sediment-water interface at the different sites (mmol $m^{-2}$ $d^{-1}$). $NH_4^+$ release during ammonification ($NH_4^+$ $_{RCorg}$) was taken from Table 4.3.

| | **$DIN_{in}$** | | | **$DIN_{out}$** | | | **$DIN_{in} + DIN_{out}$** |
|---|---|---|---|---|---|---|---|
| Water depth (m) | $NH_4^+$ $_{RCorg}$ | $NO_3^-$ | $NO_2^-$ | $NH_4^+$ | $NO_3^-$ | $NO_2^-$ | |
| 65.5 | 1.34 | 0 | 0 | 0.24 | 0.22 | 0.01 | -0.87 |
| 80 | 1.01 | 0.26 | 0.001 | 0.40 | 0 | 0 | -0.87 |
| 96.5 | 0.71 | 0.96 | 0 | 0.94 | 0 | 0 | -0.73 |
| 110 | 0.35 | 1.03 | 0 | 1.06 | 0 | 0.03 | -0.29 |
| 124 | 0.18 | 0.39 | 0 | 0.30 | 0 | 0 | -0.27 |
| 150 | 0.07 | 0 | 0 | 0.20 | 0 | 0 | 0.13 |
| 173 | 0.17 | 0 | 0 | 0.58 | 0 | 0 | 0.41 |

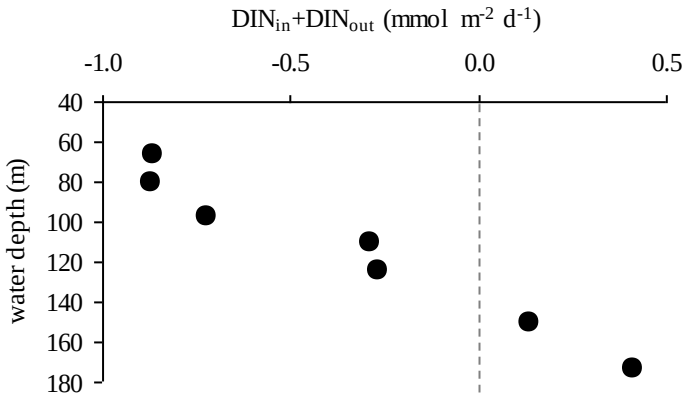


**Fig. 4.6:** Balance fluxes of $DIN_{in}$ and $DIN_{out}$ versus water depth (Table 4.5). Explanations on the mass balance are given in the text ("N and P cycling across the oxic to anoxic gradient"). All rates in the mass balance represent averages for each site (water depths 64 m and 65 m, as well as 96 m and 97 m each considered as one site).

The high $NH_4^+$ release from the sediments was also indicated by high $NH_4^+$ levels in the deep basin water (Fig. 4.2). However, only minor $NH_4^+$ amounts reached the surface, as the major part was oxidized at the lower boundary of the hypoxic transition (Fig. 4.2). Although there was an even higher $NH_4^+$ release from the sediments in the hypoxic transition zone, water-column $NH_4^+$ levels in this depth zone were only slightly elevated, indicating its oxidation. The oxycline environment is particular, since on the one hand, likewise to the hypoxic transition zone, it generally removes DIN from the environment. On the other hand, presence of bottom-water $O_2$ allows for nitrification, whereby $NO_3^-$ is released. Due to the shallow water depths, $NO_3^-$ is directly transported into the euphotic zone, having a positive feedback on surface-water primary productivity. Part of the $NH_4^+$ will probably also escape oxidation and contribute to the reactive N pool in the euphotic zone.

*4.4.3.2 Phosphorus*

The retention capacity of the sediment for P is evaluated for all sites by calculating their respective P burial efficiencies. The burial efficiency can be calculated from the rain rate of P to the sediment and the P burial rate. Assuming steady state conditions, the rain rate of P is equal to the sum of the P burial rate and the benthic release of $TPO_4$. Total sediment P needed to calculate P burial was not measured at the different sites, hence P burial rates determined in previous studies are applied.

For the anoxic part of the eastern Gotland Basin, Viktorsson et al. (2013) calculated a burial efficiency of 5%, using a P burial rate of 0.018 mmol $m^{-2}$ $d^{-1}$ and an average benthic $TPO_4$ release rate of 0.38 mmol $m^{-2}$ $d^{-1}$. Applying this burial rate and our mean $TPO_4$ release rate of 0.1 mmol $m^{-2}$ $d^{-1}$, a burial efficiency of 15% is calculated for the deep basin. Obviously, the deep basin sediments were highly efficient in returning incoming P back into the water column. This was also indicated by high $TPO_4$ concentrations in the deep basin water (Fig. 4.2). The average $TPO_4$ release rate of 0.21 mmol $m^{-2}$ $d^{-1}$ in the hypoxic transition zone was about 8-fold higher than the average P burial rate of 0.025 mmol $m^{-2}$ $d^{-1}$ determined previously for hypoxic sites in the Baltic Proper (Koop et al. 1990; Mort et al. 2010). This results in a burial efficiency of 11%, again indicating efficient recycling of the imported P back into the water column. This high benthic $TPO_4$ release became even expressed in the water-column P distribution (*see* Results, Fig. 4.2). For a 47 m deep oxic site in the western Gotland Basin, Koop et al. (1990) estimated a burial rate of 0.017 mmol $m^{-2}$ $d^{-1}$. These authors measured an average $TPO_4$ uptake of 0.03 mmol $m^{-2}$ $d^{-1}$ from the sediments, even exceeding the burial and indicating that some $TPO_4$ from the bottom water must have been captured by Fe oxyhydroxides at the oxic sediment surface. Under such conditions, an oxic environment acts as a sink for P. This was also the case for the 65 m site during deployment of BIGO I-2, where a $TPO_4$ uptake of 0.01 $m^{-2}$ $d^{-1}$ was measured. However, as mentioned above, due to the proximity of the 65 m/66 m stations to the oxycline, this environment is subjected to very dynamic bottom-water $O_2$ conditions, resulting in distinct fluctuations of the benthic $TPO_4$ release and uptake. About the reasons we can only speculate. It appears that due to the bottom-water $O_2$ fluctuations the redox state of these sediments is strongly affected, and that there exist periods, where the P retention capacity of the sediment is exhausted, so that despite oxic bottom-water conditions $TPO_4$ can be released. It is difficult to assess the overall sink or recycling function of these sediments for P, as $TPO_4$ flux time series spanning months to years would be urgently needed.

In summary, our study revealed high internal loading of $TPO_4$ as well as DIN that exceeded the external nutrient loading by a factor of 7.8 and 2.1, respectively. However, in contrast to $TPO_4$, the released DIN from the sediments apparently does not reach the euphotic zone, except at the shallower sites. This in combination with P and N turnover in the water column results in the supply of low N:P ratio water from the anoxic water

column to the euphotic zone. During summertime, when N-limited phytoplankton ceases, such low N:P ratios trigger cyanobacterial blooms (e.g. Niemi et al. 1979; Kononen et al. 2001). During this study, cyanobacteria were indeed observed to form dense brownish fluffy layers on the sea surface. Their $N_2$-fixing activity was clearly revealed by $N_2$:Ar equilibrium ratios < 1. By these mechanisms, the benthic release of $TPO_4$ and to a lesser extent DIN provides a positive feedback on the new generation of organic matter and thereby contributes to maintain the "vicious cycle", as has been described by Vahtera et al. (2007). Beside the long-time suspected relevance of the deep basin sediments for the internal $TPO_4$ and $NH_4^+$ loading, this study highlights the importance of the hypoxic transition zone, whose sediments were almost entirely covered with mats of sulfide-oxidizing bacteria, for the release of $TPO_4$ and $NH_4^+$. Strong bottom-water $O_2$ fluctuations were recorded in the hypoxic transition zone that were apparently related to wind forcing (Sommer et al. in prep.), hence nutrient release in this zone can be expected to strongly vary on a seasonal scale. $TPO_4$ release can be assumed to be less efficient during winter, where bottom water oxygenation is more likely than during summer conditions. Furthermore, under such conditions, sulfide-oxidizing bacteria might switch to aerobic sulfide oxidation, not releasing $NH_4^+$ anymore. Such seasonal regime shifts in the nutrient release introduce large uncertainties in the nutrient budget calculations. Hence, data on nutrient release with a seasonal coverage are urgently required, especially for the hypoxic transition zone, which needs particular attention in future Baltic Sea action plans for the mitigation of eutrophication.

## Acknowledgements

We thank the officers and crew of R/V *Alkor* for their support duing cruise AL355. Many thanks are due to B. Bannert, S. Cherednichenko, S. Kriwanek, and M. Türk for technical support deploying the benthic landers, the Ocean Floor Observation System (OFOS), and for taking care of water and sediment samples retrieved by the landers. We thank A. Bodenbinder, A. Bleyer, M. Dibbern, B. Domeyer, D. Lippke, T. Schorp, and S. Walter for taking care of the biogeochemical analyses onboard and in the home laboratory. We are grateful for technical support by H. Cordt with the membrane inlet mass spectrometry. This study was funded by the European Union project "HYPOX-In situ monitoring of oxygen depletion in hypoxic ecosystems of coastal and open seas and land-locked water

bodies" (EC grant 226213) and partly by the Sonderforschungsbereich 754 "Climate-Biogeochemistry Interactions in the Tropical Ocean" supported by the Deutsche Forschungsgemeinschaft.

## References

Bertics, V. J., J. A. Sohm, T. Treude, C.-E. T. Chow, D. G. Capone, J. A. Fuhrmann, and W. Ziebis. 2010. Burrowing deeper into benthic nitrogen cycling: The impact of bioturbation on nitrogen fixation coupled to sulfate reduction. Mar. Ecol. Prog. Ser. **409:** 1-15.

Bohlen, L., A. W. Dale, S. Sommer, T. Mosch, C. Hensen, A. Noffke, F. Scholz, and K. Wallmann. 2011. Benthic nitrogen cycling traversing the Peruvian oxygen minimum zone. Geochim. Cosmochim. Acta **75:** 6094-6111.

Carman, R., and L. Rahm. 1997. Early diagenesis and chemical characteristics of interstitial water and sediments in the deep deposition bottoms of the Baltic proper. J. Sea Res. **37:** 25-47.

Conley, D. J., C. Humborg, L. Rahm, O. P. Savchuk, and F. Wulff. 2002. Hypoxia in the Baltic Sea and basin-scale changes in phosphorus biogeochemistry. Environ. Sci. Technol. **36:** 5315-5320.

Conley, D. J., S. Björck, E. Bonsdorff, J. Carstensen, G. Destouni, B. G. Gustafsson, S. Hietanen, M. Kortekaas, H. Kuosa, H. E. M. Meier, B. Müller-Karulis, K. Nordberg, A. Norkko, G. Nürnberg, H. Pitkänen, N. N. Rabalais, R. Rosenberg, O. P. Savchuk, C. P. Slomp, M. Voss, F. Wulff, and L. Zillén. 2009. Hypoxia related processes in the Baltic Sea. Environ. Sci. Technol. **43:** 3412-3420.

Dale, A. W., V. Bertics, T. Treude, S. Sommer, and K. Wallmann. 2013. Modeling benthic-pelagic nutrient exchange processes and porewater distributions in a seasonally hypoxic sediment: Evidence for massive phosphate release by *Beggiatoa*? Biogeosciences **10:** 629-651.

Dekas, A. E., R. S. Poretsky, and V. J. Orphan. 2009. Deep-sea archaea fix and share nitrogen in methane consuming microbial consortia. Science **326:** 422-426.

Devol, A. H., and J. P. Christensen. 1993. Benthic fluxes and nitrogen cycling in sediments of the continental margin of the eastern North Pacific. J. Mar. Res. **51:** 345-372.

Diaz, R. J., and R. Rosenberg. 2008. Spreading dead zones and consequences for marine ecosystems. Science **321:** 926-929.

Deutsch, B., S. Forster, M. Wilhelm, J. W. Dippner, and M. Voss. 2010. Denitrification in sediments as a major nitrogen sink in the Baltic Sea: An extrapolation using sediment characteristics. Biogeosciences **7:** 3259-3271.

Emeis, K.-C., U. Struck, T. Leipe, F. Pohllehne, H. Kunzendorf, and C. Christiansen. 2000. Changes in the C, N, P burial rates in some Baltic Sea sediments over the last 150 years — relevance for P regeneration rates and the phosphorus cycle. Mar. Geol. **167:** 43-59.

Farías, L., L. A. Cuechas, and M. A. Salamanca. 1996. Effect of coastal upwelling on nitrogen regeneration and ammonium supply to the water column in Concepcion Bay, Chile. Est. Coast. Shelf Sci. **43:** 137-155.

Fulweiler, R. W., S. W. Nixon, B. A. Buckley, and S. L. Ranger. 2007. Reversal of the net dinitrogen gas flux in coastal marine sediments. Nature **448:** 180-182.

Gallardo, V. A. 1977. Large benthic microbial communities in sulfide biota under Peru-Chile subsurface countercurrent. Nature **268:** 331-332.

Goldhammer, T., V. Brüchert, T. G. Ferdelman, and M. Zabel. 2010. Microbial sequestration of phosphorus in anoxic upwelling sediments. Nat. Geosci. **3:** 557-561.

Grasshoff, K., M. Erhardt, and K. Kremling. 1999. Methods of seawater analysis. 3rd ed., Wiley-VCH.

Graco, M., L. Farías, V. Molina, D. Gutiérrez, and L. P. Nielsen. 2001. Massive developments of microbial mats following phytoplankton blooms in a naturally eutrophic bay: Implications for nitrogen cycling. Limnol. Oceanogr. **46:** 821-832.

Gustafsson, B. G., and A. Stigebrandt. 2007. Dynamics of nutrients and oxygen/hydrogen sulphide in the Baltic Sea deep water. J. Geophys. Res. **112:** G02023, doi: 10.1029/2006JG000304

Gutiérrez, D., E. Enríquez, S. Purca, L. Quipúzcoa, R. Marquina, G. Flores, and M. Graco. 2008. Oxygenation episodes on the continental shelf of central Peru: Remote forcing and benthic ecosystem response. Prog. Oceanogr. **79:** 177-189.

Hamme, R. C., and S. R. Emerson. 2004. The solubility of neon, nitrogen and argon in distilled water and seawater. Deep-Sea Res. I **51:** 1517-1528.

Hansson, M., L. Andersson, and P. Axe. 2011. Areal extent and volume of anoxia and hypoxia in the Baltic Sea, 1960-2011. SMHI Rep. Oceanogr. No. 42.

Hedges, J. I., J. A. Baldock, Y. Gélinas, C. Lee, M. L. Peterson, and S. G. Wakeham. 2002. The biochemical and elemental compositions of marine plankton: A NMR perspective. Mar. Chem. **78:** 47-63.

HELCOM. 2009*a*. Eutrophication in the Baltic Sea — an integrated thematic assessment of the effects of nutrient enrichment in the Baltic Sea region: Executive summary. Balt. Sea Environ. Proc., no. 115A. Helsinki Comission.

HELCOM. 2009*b*. Eutrophication in the Baltic Sea — an integrated thematic assessment of the effects of nutrient enrichment and eutrophication in the Baltic Sea region. Balt. Sea Environ. Proc., no. 115B. Helsinki Comission.

Hietanen, S., and K. Lukkari. 2007. Effects of short-term anoxia on benthic denitrifcation, nutrient fluxes and phosphorus forms in coastal Baltic sediment. Aquat. Microb. Ecol. **49:** 293-302.

Hietanen, S., and J. Kuparinen. 2008. Seasonal and short-term variation of denitrification and anammox at a coastal station on the Gulf of Finland, Baltic Sea. Hydrobiologia **596:** 67-77.

Hille, S., G. Nausch, and T. Leipe. 2005. Sedimentary deposition and reflux of phosphorus (P) in the eastern Gotland Basin and their coupling with P concentrations in the water column. Oceanologia **47:** 663-679.

Hille, S., T. Leipe, and T. Seifert. 2006. Spatial variability of recent sedimentation rates in the Eastern Gotland Basin (Baltic Sea). Oceanologia **48:** 297-317.

Ingall, E. D., R. M. Bustin, and P. Van Cappellen. 1993. Influence of water column anoxia on the burial and preservation of carbon and phosphorus in marine shales. Geochim. Cosmochim. Acta **57:** 303-316.

Jäntti, H., F. Stange, E. Leskinen, and S. Hietanen. 2011. Seasonal variation in nitrification and nitrate-reduction pathways in coastal sediments in the Gulf of Finland, Baltic Sea. Aquat. Microb. Ecol. **63:** 171-181.

Jäntti, H., and S. Hietanen. 2012. The effects of hypoxia on sediment nitrogen cycling in the Baltic Sea. Ambio **41:** 161-169.

Jilbert, T., C. P. Slomp, B. G. Gustafsson, and W. Boer. 2011. Beyond the Fe-P redox connection: Preferential regeneration of phosphorus from organic matter as a key control on Baltic Sea nutrient cycles. Biogeosciences. **8:** 1699-1720.

Jonsson, P., R. Carman, and F. Wulff. 1990. Laminated sediments in the Baltic: A tool for evaluating nutrient mass balances. Ambio **19:** 152-158.

Jørgensen, B. B., and D. C. Nelson. 2004. Sulfide oxidation in marine sediments: Geochemistry meets microbiology. GSA Spec. Pap. **379:** 63-81.

Kana, T. M., M. B. Sullivan, J. C. Cornwell, and K. M. Groszkowski. 1994. Denitrification in marine sediments determined by membrane inlet mass spectrometry. Limnol. Oceanogr. **3:** 334-339.

Karlson, K., R. Rosenberg, and E. Bonsdorff. 2002. Temporal and spatial large scale effects of eutrophication and oxygen deficiency on benthic fauna in Scandinavian and Baltic waters — a review. Oceanogr. Mar. Biol. Annu. Rev. **40:** 427-489.

Kononen, K. 2001. Eutrophication, harmful algal blooms and species diversity in phytoplankton communities: Examples from the Baltic Sea. Ambio **30:** 184-189.

Koop, K., W. R. Boynton, F. Wulff, and R. Carman. 1990. Sediment water oxygen and nutrient exchanges along a depth gradient in the Baltic Sea. Mar. Ecol. Progr. Ser. **63:** 65-67.

Kuparinen, J., and L. Tuominen. 2001. Eutrophication and self-purification: Counteractions forced by large-scale cycles and hydrodynamic processes. Ambio **30:** 190-194.

Matthäus, W., and H. Franck. 1992. Characteristics of major Baltic inflows — a statistical analysis. Cont. Shelf Res. **12:** 1375-1400.

Matthiesen, H. 1998. Phosphate release from marine sediments: by diffusion, advection and resuspension. Ph.D. thesis, Univ. of Aarhus.

McManus, J., W. M. Berelson, K. H. Coale, K. S. Johnson, and T. E. Kilgore. 1997. Phosphorus regeneration in continental margin sediments. Geochim. Cosmochim. Acta **61:** 2891-2907.

Mort, H. P., C. P. Slomp, B. G. Gustafsson, and T. J. Andersen. 2010. Phosphorus recycling and burial in Baltic Sea sediments with contrasting redox conditions. Geochim. Cosmochim Acta **74:** 1350-1362.

Mosch, T., S. Sommer, M. Dengler, A. Noffke, L. Bohlen, O. Pfannkuche, V. Liebetrau, and K. Wallmann. 2012. Factors influencing the distribution of epibenthic megafauna across the Peruvian oxygen minimum zone. Deep-Sea Res. I **68:** 123-135.

Mulholland, M. R., D. A. Bronk, and D. G. Capone. 2004. Dinitrogen fixation and release of ammonium and dissolved organic nitrogen by *Trichodesmium* ISM101. Aquat. Microb. Ecol. **37:** 85-94.

Nausch, G., R. Feistel, H. U. Lass, K. Nagel, and H. Siegel. 2006. Hydrographisch-chemische Zustandseinschätzung der Ostsee 2005, Meereswiss. Ber. Warnemünde **66:** 3-82.

Nausch, G., R. Feistel, and V. Mohrholz. 2012. Water exchange between the Baltic Sea and the North Sea, and conditions in the deep basins. HELCOM Baltic Sea Environment Fact Sheets. 2012. Online.
(10.08.2013), http://www.helcom.fi/BSAP_assessment/ifs/ifs2012/en_GB/WaterExchange/

Nehring, D. 1987. Temporal variations of phosphorus and inorganic nitrogen compounds in central Baltic Sea deep waters. Limnol. Oceanogr. **32:** 494-499.

Niemi, Å. 1979. Blue-green algal blooms and N:P ratio in the Baltic Sea. Acta Bot Fenn. **110:** 57-61.

Noffke, A., C. Hensen, S. Sommer, F. Scholz, L. Bohlen, T. Mosch, M. Graco, and K. Wallmann. 2012. Benthic iron and phosphorus fluxes across the Peruvian oxygen minimum zone. Limnol. Oceanogr. **57:** 851-867.

Piker, L., R. Schmaljohann, and J. F. Imhoff. 1998. Dissimilatory sulfate reduction and methane production in Gotland deep sediments (Baltic Sea) during a transition period from oxic to anoxic bottom water (1993-1996). Aquat. Microb. Ecol. **14:** 183-193.

Pohl, C., A. Löffler, and U. Hennings. 2004. A sediment trap flux study for trace metals under seasonal aspects in the stratified Baltic Sea (Gotland Basin; 57°19.20'N, 20°03.00'E). Mar. Chem. **84:** 143-160.

Rheinheimer, G., K. Gocke, H.-G. Hoppe. 1989. Vertical distribution of microbial and hydrographic-chemical parameters in different areas of the Baltic Sea. Mar. Ecol. Prog. Ser. **52:** 55-70.

Savchuk, O. P. 2005. Resolving the Baltic Sea into seven subbasins: N and P budgets for 1991-1999. J. Mar. Syst. **56:** 1-15.

Schenau, S. J., and G. J. De Lange. 2001. Phosphorus regeneration vs. burial in sediments of the Arabian Sea. Mar. Chem. **75:** 201-217.

Schincke, H., and W. Matthäus. 1998. On the causes of major Baltic inflows — an analysis of long time series. Cont. Shelf. Res. **18:** 67-97.

Schmaljohann, R., M. Drews, S. Walter, P. Linke, U. von Rad, and J. F. Imhoff. 2001. Oxygen minimum zone sediments in the northeastern Arabian Sea off Pakistan: a habitat for the bacterium *Thioploca*. Mar. Ecol. Prog. Ser. **211:** 27-42.

Schulz, H. N., and H. D. Schulz. 2005. Large sulfur bacteria and the formation of phosphorite. Science **21:** 416-418.

Slomp, C. P., J. F. P. Malschaert, and W. Van Raaphorst. 1998. The role of adsorption in sediment-water exchange of phosphate in North Sea continental margin sediments. Limnol. Oceanogr. **43:** 832-846.

Slomp, C. P., J. Thomson, and G. J. De Lange. 2002. Enahnced regeneration of phosphorus during formation of the most recent Mediterranean sapropel (S1). Geochim. Cosmochim. Acta **66:** 1171-1184.

Seitzinger, S. P. 1988. Denitrification in freshwater and coastal marine ecosystems: Ecological and geochemical significance. Limnol. Oceanogr. **33:** 702-724.

Sommer, S., P. Linke, O. Pfannkuche, T. Schleicher, J. Schneider v. Deimling, A. Reitz, M. Haeckel, S. Flögel, and C. Hensen. 2009. Seabed methane emissions and the habitat of frenulate tube worms on the Captain Arutyunov mud volcano (Gulf of Cadiz). Mar. Ecol. Prog. Ser. **382:** 69-86.

Steenberg, A. K., P. L. E. Bodelier, H. L. Hoogveld, C. P. Slomp, and H. J. Laanbroek. 2011. Phosphatases relieve carbon limitation of microbial activity in Baltic Sea sediments along a redox-gradient. Limnol. Oceanogr. **56:** 2018-2026.

Stigebrandt, A. 2001. Physical oceanography of the Baltic Sea, p. 19-74. *In* F. Wulff, L. Rahm and P. Larsson [eds.], A systems analysis of the Baltic Sea. Springer.

Stigebrandt, A. 2003. Regulation of the vertical stratification, length of stagnation periods and oxygen conditions in the deeper deepwater of the Baltic proper. *In* W. Fennel and B. Hensch [eds.], Meereswiss. Ber. Warnemünde **54:** 69-80.

Suess, E. 1981. Phosphate regeneration from sediments of the Peru continental margin by dissolution of fish debris. Geochim. Cosmochim. Acta **45:** 577-588.

Sundby, B., C. Gobeil, N. Silverberg, and A. Mucci. 1992. The phosphorus cycle in coastal marine sediments. Limnol. Oceanogr. **37:** 1129-1145.

Tengberg, A., J. Hovdenes, H. J. Andersson, O. Brocandel, R. Diaz, D. Hebert, T. Arnerich, C. Huber, A. Körtzinger, A. Khripounoff, F. Rey, C. Rönning, J. Schimanski, S. Sommer, and A. Stangelmayer. 2006. Evaluation of a life-time based optode to measure oxygen in aquatic systems. Limnol. Oceanogr.: Methods **4:** 7-17.

Tuominen, L., A. Heinänen, J. Kuparinen, and L. P. Nielsen. 1998. Spatial and temporal variability of denitrification in the sediments of the northern Baltic Proper. Mar. Ecol. Prog. Ser. **172:** 13-24.

Viktorsson, L., E. Almroth-Rosell, A. Tengberg, R. Vankevich, I. Neelov, A. Isaev, V. Kravtsov, and P. O. J. Hall. 2012. Benthic phosphorus dynamics in the Gulf of Finland, Baltic Sea. Aquat. Geochem., doi: 10.1007/s10498-011-9155-y

Viktorsson, L., N. Ekeroth, M. Nilsson, M. Kononets, and P. O. J. Hall. 2013. Phosphorus recycling in sediments of the central Baltic Sea. Biogeosciences **10:** 3901-3916.

Voss, M., G. Nausch, and J. P. Montoya. 1997. Nitrogen stable isotope dynamics in the central Baltic Sea: Influences of deep-water renewal on the N cycle changes. Mar. Ecol. Prog. Ser. **158:** 11-21.

Vahtera, E., D. J. Conley, B. G. Gustafsson, H. Kuosa, H. Pitkänen, O. P. Savchuk, T. Tamminen, M. Viitasalo, M. Voss, N. Wasmund, and F. Wulff. 2007. Internal ecosystem feedbacks enhance nitrogen-fixing cyanobacteria blooms and complicate management in the Baltic Sea. Ambio **36:** 186-194.

Wallmann, K. 2003. Feedbacks between oceanic redox states and marine productivity: A model perspective focused on benthic phosphorus cycling. Glob. Biogeochem. Cycles **17:** 1084, doi: 10.1029/2002GB001968

Zillén, L., D. J. Conley, T. Andrén, E. Andrén, and S. Björck. 2008. Past occurrences of hypoxia in the Baltic Sea and the role of climate variability, environmental change and human impact Earth Sci. Rev. **91:** 77-92.

Zopfi, J., P. Kjær, L. P. Nielsen, and B. B. Jørgensen. 2004. Ecology of *Thioploca* spp.: Nitrate and sulfur storage in relation to chemical microgradients and influence of *Thioploca* spp. on the sedimentary nitrogen cycle. Appl. Environ. Microbiol. **67:** 5530-5537.

# 5 Synthesis

The three studies presented in this thesis investigated the benthic nutrient turnover in two different highly oxygen-deficient systems off Peru and in the Gotland Basin, Baltic Sea, focusing on P but also including associated cycles of Fe and N. The OMZ off Peru is the result of sluggish circulation, long residence time of water masses and decomposition of organic matter exported from the productive surface layer, where high productivity is sustained by coastal upwelling. Chapter 2 presents results on benthic P and Fe release in this region. Chapter 3 advances this flux study via an investigation of likely sources driving sea-bed P release. In contrast to the Peruvian OMZ, the land-locked Baltic Sea suffers from anthropogenically induced eutrophication, which is associated with extended hypoxia and anoxia. In addition to external nutrient input, such conditions are naturally exacerbated by impeded ventilation due to limited water exchange with the North Sea as well as intense stratification maintained by high levels of freshwater run-off. Major findings on the benthic P and N turnover along an oxic to anoxic gradient are presented in Chapter 4.

In order to elucidate potential benthic feedbacks on surface-water primary productivity off the coast of Peru, sedimentary fluxes of $TPO_4$ and $Fe^{2+}$ were quantified by in situ benthic chamber incubations and pore-water profiles across a latitudinal depth transect (80-1000 m) at 11°S, covering the full range of completely anoxic to oxic bottom-water conditions (chapter 2 of this thesis). The transect was divided into three different zones: the shelf that is subjected to periodically fluctuating bottom-water $O_2$ conditions (Gutiérrez et al. 2008), the core of the OMZ where anoxia was assumed to be permanent, and the depth range below 500 m where $O_2$ levels increased again.
Overall, highly enhanced nutrient release from the OMZ sediments was measured. $TPO_4$ fluxes were high (maximum 292 mmol $m^{-2}$ $yr^{-1}$) throughout the shelf and the core of the OMZ in association with high organic carbon degradation rates. In contrast, $Fe^{2+}$ fluxes were high on the shallow shelf (maximum 316 mmol $m^{-2}$ $yr^{-1}$) and persistent but moderately low (15.4 mmol $m^{-2}$ $yr^{-1}$) in water depths between 250 m and 600 m, which is attributed to the continuous reduction of Fe oxyhydroxides. With increasing $O_2$ concentrations, $Fe^{2+}$ fluxes became negligible due to the precipitation of $Fe^{2+}$ in the oxic

sediment surface. This process in combination with a general decrease of organic matter degradation further resulted in a strong decrease of $TPO_4$ fluxes with increasing water depth.

Ratios between organic carbon degradation and $TPO_4$ flux indicated excess release of P over C when compared to Redfield stoichiometry. Most likely, this was caused by preferential P release during organic matter degradation, dissolution of fish debris, and/or P release from sulfide-oxidizing microbial mat communities. Fe oxyhydroxides were of particular relevance as a P source only on the shallow shelf.

The benthic fluxes measured during this research are among the highest reported from similar oxygen-deficient continental margin systems, and highlight the efficiency of OMZ sediments returning $TPO_4$ and $Fe^{2+}$ to the bottom water, from where it might eventually be transported to the productive surface layer. Through this benthic-pelagic coupling, $TPO_4$ and $Fe^{2+}$ fluxes may provide important positive feedbacks allowing extensive phytoplankton blooms to develop and, in turn, an expansion of anoxia. The shelf region is particularly important in this regard, since $O_2$ fluctuations trigger a complex biogeochemical reaction network of Fe, P and sulfur turnover resulting in transient, high $Fe^{2+}$ and $TPO_4$ release under anoxia.

Chapter 3 advances the Chapter 2 flux study by considering the solid phase of P for a subset of sites from the 11°S transect, and also characterizing the entire depth range. This study aims to distinguish the contributions of different sources to the high benthic $TPO_4$ release by using a combined approach including solid phase P speciation measurements obtained by sequential extraction of sediment samples, a mass balance, and benthic modeling. Besides total sedimentary P, individual solid phase P species considered were Fe-bound P, a fraction of authigenic Ca-P (including carbonate flour apatite, biogenic apatite and calcium carbonate-bound P), detrital P and organic P. Biogenic apatite, referred to as fish-P, was further separated from the total pool of authigenic Ca-P.

P speciation measurements revealed that authigenic Ca-P was the major fraction along the transect. It accounted for 35% to 47% of the depth-averaged total extracted P on the shelf and upper slope, but for > 70% below 300 m water depth. Below 259 m water depth, fish-P dominated the authigenic Ca-P pool by 60% to 69%. Organic P was present in considerable amounts (18-37%) only at the shelf and the upper slope, whereas detrital P

and Fe-bound P were typically of minor importance at all sites. Organic matter in surface sediments was highly depleted in P relative to Redfield stoichiometry with C:P ratios of up to 516. Assuming the occurrence of preferential P mineralization in the water column and allowing for the deposition of highly P-depleted organic matter at the sea floor, mass balance calculations suggest that organic P only accounted for a small fraction (2-8%) of the total particulate P input to the sediments. In order to test the feasibility of enhanced P mineralization taking place in the water column, in contrast to preferential P release during organic matter degradation in the sediment surface, a diagenetic transport reaction model was used for one site within the core of the OMZ. Both the degradation of organic matter (which, on deposition, is already P-depleted) as well as preferential P release in the sediment were indeed found possible; however, these processes contributed only 2% and 13% to the total P release into the pore water, respectively. Remarkably, organic matter C:P ratios as low as 50 were measured in shallow waters at 10°S (Franz et al. 2012). Applying such low ratios for the shelf in our working area, it would become exceptional as the significance of the organic P input to the total would strongly increase from 8% to 49%.

According to the solid phase speciation, authigenic Ca-P (coming largely from fish debris) is a likely candidate for the missing source of P required to close the P budget in Peruvian OMZ sediments. Expanding upon the previous chapter, where high $TPO_4$ release rates were resolved, this study indeed identified these sediments as weak sinks for P, whereas more than 80% of P was recycled back into the water column and potentially contributing directly to surface water primary productivity.

In the Gotland Basin, $TPO_4$ and DIN fluxes were quantified in situ across an oxic to anoxic depth gradient using benthic landers (Chapter 4). In situ fluxes were complemented by CTD casts for water-column nutrient and $O_2$ measurements to investigate the benthic-pelagic coupling because of its significance for feedbacks on primary productivity and consequently the euthrophication state of the Baltic Proper. Based on bottom-water $O_2$ levels the study area was divided into three different zones: the oxic zone at 60 m to < 80 m water depth, the hypoxic transition zone between > 80 m to 120 m, and the deep anoxic and sulfidic basin at > 120 m. The hypoxic transition zone was characterized by fluctuating $O_2$ levels as well as the occurrence of extended mats of

vacuolated sulfur bacteria. One primary finding was that in addition to the deep anoxic basin, the hypoxic transition zone was was found to be a major release site for $TPO_4$ and $NH_4^+$ with rates of up to 0.2 mmol $m^{-2}$ $d^{-1}$ and 1 mmol $m^{-2}$ $d^{-1}$, respectively. There is circumstantial evidence that these bacterial mats, which covered the sediment surface almost entirely, were strongly involved in the turnover of N, converting $NO_3^-/NO_2^-$ into $NH_4^+$ during dissimilatory nitrate reduction to ammonium (DNRA). Thereby, these organisms retain reactive N in the ecosystem opposing the self-cleaning effect of denitrification and anammox. Beyond their involvement in the N cycle, transient release and uptake of $TPO_4$ during anoxic and oxic conditions have been described for these sulfide-oxidizers (Goldhammer et al. 2010). However, this process can only be speculated, as the entire $TPO_4$ release from the sediment could be potentially covered by preferential P release during organic matter degradation. Extrapolation of benthic fluxes to the entire Baltic Proper, excluding the Arkona basin and shallow sandy sites at < 60 m water depth, resulted in high internal $TPO_4$ and DIN loads of 109 kt $yr^{-1}$ and 295 kt $yr^{-1}$, respectively. This is ~ 8-fold higher than the total external P load of 14 kt $yr^{-1}$ and ~ 2-fold higher than the external DIN load of 140 kt $yr^{-1}$ for the year 2006 (HELCOM 2009). This up-scaling of fluxes revealed the importance of the hypoxic transition zone for internal nutrient loading as this zone only covered 51% of the total area, but released as much as 70% of the total $TPO_4$ load. Likewise, 75% of the internal $NH_4^+$ load (200 kt $yr^{-1}$) was released from this particular environment. In contrast to $TPO_4$, the released DIN from the sediments apparently does not reach the euphotic zone except at the shallower sites. This results in the supply of water with a low N:P ratio to the euphotic zone. In summertime, this favors the development of $N_2$-fixing cyanobacterial blooms which significantly counteract the Baltic Proper from recovering from eutrophication.

This is the first study that classified the hypoxic transition zone as a defined environment and revealed its significance for the benthic nutrient release. As $O_2$ availability in the hypoxic transition zone appears to be a function of wind forcing (Sommer et al. in prep.) this zone needs to be investigated over a full seasonal cycle to assess its importance for the nutrient budget of the central Baltic Sea. Seasonal resolution of internal nutrient loading is urgently required for the successful implementation of future Baltic Sea management plans.

*Concluding remarks and future perspectives*

Despite major differences in the hydrography and geomorphology of the Peruvian OMZ and the Gotland Basin, both environments share distinct commonalities. Firstly, as expected, elevated nutrient mobilization into the bottom water took place in zones where oxygen deficiency persists. Secondly, both regions possess depth zones where periodic $O_2$ intrusions occur. The upper boundary of the Peruvian OMZ is subjected to $O_2$ fluctuations related to the passage of Kelvin waves which, at a time series station on the shelf off Callao, were resolved to occur on monthly to inter-annual time scales (Gutiérrez et al. 2008). In the Gotland Basin, a hypoxic transition zone was identified between water depths of 80 m and 120 m, where strong $O_2$ fluctuations at time scales of hours to months were measured during lander deployments (Sommer et al. in prep.). Furthermore, the sediments within this particular depth zone in both regions were covered with extended mats of sulfide-oxidizing bacteria which, as indicated above and shown by other studies (e.g. Jørgensen and Nelson 2004; Goldhammer et al. 2010) can be strongly involved in the cycling of N and P. Both of these environments are unique as oscillating bottom-water $O_2$ conditions likely trigger a transient and complex biogeochemical reaction network of P, N, Fe and sulfur turnover, resulting in high $TPO_4$, $NH_4^+$ and $Fe^{2+}$ release under $O_2$-deficient conditions. This renders them as sensitive regions that over annual/interannual cycles strongly affect regional water-column nutrient budgets and consequently the maintenance or spread of hypoxia. Therefore, it is of great importance to understand the dynamics of these environments for extended time periods, e.g. for at least one year in the Gotland Basin and for up to several years in the Peruvian OMZ. Specific questions that need to be addressed in future research for both regions can be summarized as follows:

1. Repeated series of in situ flux measurements similar to those presented in this study are urgently required in regard to the above-mentioned time scales of $O_2$ oscillations.

2. It is of major importance to investigate how seasonal changes in the surface-water primary productivity and organic carbon deposition affect the magnitude of benthic fluxes.

3. With respect to phosphorus cycling off Peru, the following issues need to be addressed:
    i. In order to further constrain the role of organic phosphorus in benthic P turnover and release into the pore water, it is important to determine the C:P composition of the deposited particulate organic matter.
    ii. In order to unambiguously identify other sources contributing to P release, P speciation measurements of particles need to be determined across the benthic boundary layer. The potential contribution of authigenic apatite that might be formed within the water column should be investigated by extending these P speciation measurements to suspended particles in the water column.

4. The involvement of the microbial mats in the benthic P and N cycling needs to be studied during extended series of combined in situ and ex situ experiments under controlled conditions of $O_2$ as well as $NO_3^-/NO_2^-$. One major aspect is to investigate the transient release and uptake of P of these sulfide-oxidizing bacteria during fluctuating anoxic and oxic bottom- water conditions. The ratio between $NO_3^-$ and $NO_2^-$ that is channeled into DNRA or denitrification needs to be determined to assess the function of the sediments acting as recycling sites or sinks for reactive N. Environmental controls that might cause shifts in this ratio need to be identified.

# List of Abbreviations

In chapters 2 to 4 sometimes different abbreviations are used for the same parameter. The number given in brackets denotes the chapter where the respective abbreviation is used.

| | |
|---|---|
| ADP | adenosine diphosphate |
| AMP | adenosine monophosphate |
| anammox | anaerobic ammonium oxidation |
| ATP | adenosine triphosphate |
| $BE_{Corg}$ | burial efficiency of organic carbon |
| $BE_{Ptot}$ | burial efficiency of total particulate phosphorus |
| BIGO | Biogeochemical Observatory |
| BW | bottom water |
| C | carbon |
| $C_{Al}(10)$ | concentration of aluminum at 10 cm sediment depth |
| $C_{Corg}(10)$ | concentration of organic carbon at 10 cm sediment depth |
| $C_{ox}$ (2), $R_{Corg}$ (4) | organic carbon degradation rate |
| $C_{Porg}(10)$ | concentration of organic phosphorus at 10 cm sediment depth |
| CA | cellulose acetate |
| $CaCO_3$ | calcium carbonate |
| Ca-P | calcium phosphate minerals |
| $Ca_{10}(PO_4)_6(OH)_{10}$ | hydroxylapatite |
| CTD | conductivity, temperature, depth |
| $D_s$ | effective diffusion coefficient in the sediment |
| DIN | dissolved inorganic nitrogen (here including: ammonium, nitrate, and nitrite) |
| $DIN_{in}$ | total N uptake by the sediment excluding burial |
| $DIN_{out}$ | total N release from the sediment |
| DNA | deoxyribonucleic acid |
| DNRA | dissimilatory nitrate reduction to ammonium |
| ds | density of dry solids |
| ENSO | El Niño Southern Oscillation |
| ESSW | Equatorial Subsurface Water |

| | |
|---|---|
| Fe | iron |
| $Fe^{2+}$ | ferrous iron |
| $F_{Corg}$ | burial flux of organic carbon |
| $F_{Porg}$ | burial flux of organic phosphorus |
| $F_{sed}$ | sediment accumulation rate |
| $F_{TPO4}$ | benthic phosphate flux |
| $FeCl_3$ | ferric chloride |
| Fe oxyhydroxides | iron oxides and iron hydroxides |
| FeS | iron monosulfides |
| fish-P | phosphorus in biogenic apatite from fish remains |
| HCl | hydrochloric acid |
| HEPES | 4-(2-hydroxyethyl)-1-piperazineethanesulfonic acid |
| $HNO_3$ | nitric acid |
| ICP-OES | inductively coupled plasma-optical emission spectrometry |
| $k_{fit}$ | kinetic constant used to fit simulated phosphate pore-water concentrations to the measured values |
| $MgCl_2$ | magnesium chloride |
| Mn oxyhdroxides | manganese oxides and manganese hydroxides |
| MUC | multiple corer |
| N | nitrogen |
| $N_2$ | dinitrogen gas |
| $NH_4^+$ | ammonium |
| $NH_4^+{}_{DEN}$ | ammonium release during organic carbon degradation by maximum potential denitrification (for details see chapter 4) |
| $NH_4^+{}_{N2\text{-}fix}$ | ammonium release due to benthic $N_2$-fixation |
| $NH_4^+{}_{RCorg}$ | ammonium release during organic carbon degradation |
| $NO_3^-$ | nitrate |
| $NO_2^-$ | nitrite |
| $O_2$ | oxygen |
| OFOS | Ocean Floor Observation System |
| OMZ | oxygen minimum zone |
| P | phosphorus |
| $P_{excess}$ | excess phosphorus |
| $P_{tot}$ | total particulate phosphorus |

| | |
|---|---|
| PCU | Peru Chile Undercurrent |
| $\Phi_0$ | porosity at the sediment-water interface (0-1 cm) |
| φ | porosity of compacted sediment |
| $R_{Corg}$ | depth-integrated organic carbon decay rate |
| $r_{CP}$(0-1) | organic carbon to phosphorus ratio at 0-1 cm sediment depth |
| $r_{CP}$(flux) | carbon to phosphorus ratio of organic matter deposited at the sediment-water interface |
| $R_{Porg}$ (3), $TPO_{4\ Corg}$ (4) | phosphate release during organic matter degradation |
| RNA | ribonucleic acid |
| $RR_{auth}$ | rain rate of authigenic P phase |
| $RR_{Corg}$ | rain rate of organic carbon |
| $RR_{Porg}$ | rain rate of organic phosphorus |
| $RR_{Pterr}$ | phosphorus rain rate in terrigenous particles |
| $RR_{Ptot}$ | rain rate of total particulate phosphorus |
| RSD | relative standard deviation |
| S | sulfur |
| SEDEX | name of a method for the extraction of sediment phosphorus |
| $SO_4^{2-}$ | sulfate |
| SR | sulfate reduction |
| $\Sigma R_{PSS}$ | net uptake or release of phosphate required to fit the pore-water phosphate data, once phosphate release from organic phosphorus has been accounted for (for details see chapter 3) |
| $\Sigma R_{TPO4}$ | sum of biogeochemical reactions contributing to the dissolved phosphate pore-water pool |
| SWI | sediment-water interface |
| TA | total alkalinity |
| $TH_2S$ (2); $HS^-$ (4) | total dissolved sulfide |
| TOC (2); $C_{org}$ (3); $C_{org}$ (4) | organic carbon |
| TOU | total oxygen uptake |
| $TPO_4$ | phosphate (including all species of orthophosphoric acid dissociation) |
| $TPO_{4\ RCorg,10}$ | potential preferential phosphate release during organic matter degradation |
| $TPO_{4\text{-}SIM}$ | simulated phosphate pore-water concentration |

| | |
|---|---|
| w | burial velocity of compacted sediment |
| XRF | x-ray fluorescence |
| ζ | factor that converts $F_{sed}$ from g $cm^{-2}$ $yr^{-1}$ to g $m^{-2}$ $d^{-1}$ |

# Acknowledgements

Zuallererst möchte ich mich herzlichst bei Christian Hensen für die Betreuung meiner Doktorarbeit bedanken. Ich danke ihm für seinen Ansporn, seine verlässliche Unterstützung, sowie die vielen Diskussionen und Anregungen, die sehr zu dieser Arbeit beigetragen haben. Zudem möchte ich mich für die, auch unter eigenen zeitlichen Belastungen, gleichbleibend freundliche und entspannte Arbeitsatmosphäre bedanken.

Klaus Wallmann möchte ich dafür danken, dass er mich als Doktorandin in seiner Arbeitsgruppe aufgenommen hat, für sein Vertrauen und seine Ermunterung, sowie für viele gute und anregende Gespräche zu verschiedenen Themen der Biogeochemie.
Außerdem möchte ich Tina Treude herzlich für die Übernahme des Zweitgutachtens danken.

Desweiteren gilt mein besonderer Dank Stefan Sommer für die unerschöpflichen Diskussionen über Bakterienmatten und ihre biogeochemischen Kopplungen. Diese haben dieser Arbeit zu vielen, ganz eigenen Aspekten mitverholfen, worüber ich wirklich froh bin. Ich danke ihm zudem für die Möglichkeit, die Daten zu den Phosphor- und Stickstoffflüssen aus dem Gotlandbecken zu Veröffentlichung vorzubereiten, sowie für seine fortwährende Unterstützung während der ganzen Zeit.

Andy Dale danke ich für seinen Beitrag zum zweiten Manuskript zum Phosphorkreislauf vor Peru, für die gewonnenen Einblicke in die Modellierung sowie für seine jederzeit vorhandene Diskussionsbereitschaft.

Vielen Dank an die Technikerinnen der Arbeitsgruppe Marine Geosysteme, Anke Bleyer, Andrea Bodenbinder, Bettina Domeyer, Meike Dibbern, Renate Ebbinghaus, Sonja Kriwanek und Regina Surberg für die geochemische Analytik während der Ausfahrten mit R/V Meteor (M77), R/V Maria S. Merian (MSM 17-4) und R/V Alkor (AL 355) und in den Laboren des GEOMAR, sowie an Hans Cordt für die Unterstützung mit dem Massenspektrometer. Für die technische Unterstützung außerhalb der Labore danke ich Bernhardt Bannert, Asmus Petersen, Wolfang Queisser, Matthias Türk und Sergey Cherednichenko.
Renate Ebbinghaus sei zudem besonders für die langwierige Unterstützung bei der Durchführung der sequentiellen Phosphorextraktionen gedankt.

Florian Scholz danke ich für alle Diskussionen zum Eisen- und Phosphorkreislauf. Vielen Dank an Lee Bryant für ihre spontane Bereitschaft zum Korrekturlesen einzelner Passagen, und an Ulle für alle ablenkenden Momente.

Dem „Büro“ danke ich für eine gute Zeit, die meist entspannte Atmosphäre, für tägliche gemeinsame Mittagessen sowie die Abende außerhalb des Institutsgeschehens.
Thomas, du gehst hier ein bißchen unter, und ich denke, dass wir und hierüber ganz einig sind;

Ich glaube, es ist klar, welche Rolle du in meinem Leben einnimmst.